Late Holocene relative sea-level changes and earthquakes around the upper Cook Inlet, Alaska, USA

Hamilton, Sarah Louise

Late Holocene relative sea-level changes and earthquakes around the upper Cook Inlet, Alaska, USA

Volume Two

Figures and Appendices

by

Sarah Louise Hamilton

A thesis submitted in the fulfilment of the requirements for the degree of Doctor of Philosophy

Department of Geography

University of Durham

March 2003

Contents of Volume Two

List of figures	ii
Contents of Appendices	vii

List of Figures

Chapter 1		**Page**
1.1	Schematic diagrams of the EDC model	1
1.2	Schematic diagram of co-seismic submergence	2
1.3	The Cascadia subduction zone	3
1.4	Region affected by the 1964 Alaskan earthquake	4
Chapter 2		
2.1	Location of field sites around the upper Cook Inlet	5
2.2	Satellite image showing the location of the Kenai River Flats and Kenai City Pier transects	6
2.3	Oblique aerial photograph of Kenai River Flats	7
2.4	Altitude (m) of vegetation zones found at Kenai	8
2.5	Contemporary environments at Kenai River Flats	9
2.6	Oblique aerial photograph of Kenai City Pier	10
2.7	Contemporary environments at Kenai City Pier	11
2.8	Oblique aerial photograph of Kasilof	12
2.9	Bank section at Kasilof	13
2.10	Oblique aerial photograph of Girdwood	14
2.11	Cliff face at Girdwood	15
2.12	Winter conditions at Girdwood	16
2.13	Winter conditions at Kenai	17
Chapter 3		
3.1	Schematic diagram of organic content changes associated with the EDC model	18
3.2	Transfer function development	19

Chapter 4

4.1	Tidal observations for Kenai River Flats	20
4.2	High tide observations at Girdwood	21
4.3	Hours inundated per year for the Kenai contemporary samples	22
4.4	Kenai contemporary diatom data and cluster analysis using Euclidian distance	23
4.5	Altitude range of classes produced using Euclidian distance	24
4.6	Kenai contemporary diatom data and cluster analysis using Chord distance	25
4.7	Altitude range of classes produced using Chord distance	26
4.8	Diatom optima and tolerances based upon WA model	27
4.9	Regression results for the full contemporary data set (altitude (m) relative to MHHW)	28
4.10	Regression results using hours inundated per year for the full contemporary data set	29
4.11	Regression results for contemporary samples found below MHHW	30
4.12	Regression results using altitude (m) relative to MHHW for contemporary samples above +1.0 m MHHW	31
4.13	Regression results using hours inundated per year for contemporary samples above +1.0 m MHHW	32
4.14	Back calculation for hours inundated per year to altitude (m) relative to MHHW	33
4.15	Regression results using altitude (m) relative to MHHW for contemporary samples above -0.5 m MHHW	34
4.16	Observed against predicted altitude (m) relative to MHHW for contemporary Kenai data using MAT	35
4.17	Cumulative frequency distribution of MAT minimum dissimilarity coefficients	36

Chapter 5

5.1	Summary litho-stratigraphy at Kenai River Flats	37
5.2	Surface vegetation at Kenai 2000-7	38
5.3	Lithology of Kenai 2000-7 showing the upper peat-silt boundary	39
5.4	Detailed litho-stratigraphy of Kenai 2000-7	40
5.5	Loss on ignition values for Kenai 2000-7	41
5.6	(a) Kenai 2000-7 diatom data (polyhalobous, mesohalobous and	42

	oligohalobous-halophile salinity classes)	
	(b) Kenai 2000-7 diatom data (oligohalobous-indifferent and halophobous salinity classes)	43
5.7	Chrono-stratigraphy of Kenai 2000-7	44
5.8	Comparison of radiocarbon dates for Kenai	45
5.9	Calibration results for Kenai 2000-7 using different models	46
5.10	Minimum dissimilarity coefficient values from MAT for Kenai 2000-7	47
5.11	Reconstruction of relative sea-level change for Kenai 2000-7 using the best combination of models	48

Chapter 6

6.1	Summary litho-stratigraphy at Girdwood	49
6.2	Location of sampling sites at Girdwood	50
6.3	Chrono-stratigraphy of Girdwood	51
6.4	Comparison of radiocarbon dates for Girdwood	52
6.5	(a) Detailed litho-stratigraphy of Girdwood G-800	53
	(b) Girdwood G-02-2 showing increase in silt content within the upper peat	54
6.6	Girdwood G-800 diatom data	55
6.7	Calibration results for Girdwood G-800 using different models	56
6.8	Minimum dissimilarity coefficient values from MAT for Girdwood G-800	57
6.9	Reconstruction of relative sea-level change for Girdwood G-800 using the best combination of models	58
6.10	Detailed litho-stratigraphy of Girdwood G-01-1A	59
6.11	(a) Girdwood G-01-1A diatom data	60
	(b) Girdwood G-01-1A pollen data	61
6.12	Calibration results for Girdwood G-01-1A using different models	62
6.13	Minimum dissimilarity coefficient values from MAT for Girdwood G-01-1A	63
6.14	Reconstruction of relative sea-level change for Girdwood G-01-1A using the best combination of models	64
6.15	Detailed litho-stratigraphy of Girdwood G-01-1C	65
6.16	Girdwood G-01-1C diatom data	66
6.17	Calibration results for Girdwood G-01-1C using different models	67

6.18	Minimum dissimilarity coefficient values from MAT for Girdwood G-01-1C	68
6.19	Reconstruction of relative sea-level change for Girdwood G-01-1C using the best combination of models	69
6.20	Detailed litho-stratigraphy of Girdwood G-01-1E	70
6.21	Girdwood G-01-1E diatom data	71
6.22	Calibration results for Girdwood G-01-1E using different models	72
6.23	Minimum dissimilarity coefficient values from MAT for Girdwood G-01-1E	73
6.24	Reconstruction of relative sea-level change for Girdwood G-01-1E using the best combination of models	74
6.25	Detailed litho-stratigraphy of Girdwood G-01-1F	75
6.26	Girdwood G-01-1F diatom data	76
6.27	Calibration results for Girdwood G-01-1F using different models	77
6.28	Minimum dissimilarity coefficient values from MAT for Girdwood G-01-1F	78
6.29	Reconstruction of relative sea-level change for Girdwood G-01-1F using the best combination of models	79
6.30	Detailed litho-stratigraphy of Girdwood G-01-9	80
6.31	Girdwood G-01-9 diatom data	81
6.32	Calibration results for Girdwood G-01-9 using different models	82
6.33	Minimum dissimilarity coefficient values from MAT for Girdwood G-01-9	83
6.34	Reconstruction of relative sea-level change for Girdwood G-01-9 using the best combination of models	84

Chapter 7

7.1	(a) Detailed litho-stratigraphy of Kasilof KS-01-1	85
	(b) Detailed litho-stratigraphy of Kasilof KS-3	86
7.2	Chrono-stratigraphy of Kasilof	87
7.3	Comparison of radiocarbon dates for Kasilof	88
7.4	^{137}Cs results for the upper part of Kasilof KS-3	89
7.5	Kasilof KS-01-1 diatom data	90
7.6	Calibration results for Kasilof KS-01-1 using different models	91
7.7	Minimum dissimilarity coefficient values from MAT for Kasilof KS-01-1	92

7.8	Reconstruction of relative sea-level change for KS-01-1 using the best combination of models	93
7.9	Kasilof KS-3 diatom data	94
7.10	Calibration results for Kasilof KS-3 using different models	95
7.11	Minimum dissimilarity coefficient values from MAT for Kasilof KS-3	96
7.12	Reconstruction of relative sea-level change for Kasilof KS-3 using the best combination of models	97

Chapter 8

8.1	Models of reconstructed relative sea-level change showing effects of different types of reworked sediment following co-seismic submergence	98
8.2	Relationship between the magnitude of co-seismic and pre-seismic relative sea-level rise	99
8.3	Possible pre-1964 periods of co-seismic submergence using dates from this thesis	100
8.4	Radiocarbon dates from around the Cook Inlet comparing possible periods of co-seismic submergence from this thesis against those suggested by Combellick (1994)	101
8.5	Schematic models of co-seismic submergence, post- and inter-seismic uplift, sediment accumulation and marsh peat burial	102
8.6	Relationship between age of peat layers and depth below present marsh surface at different sites around the Cook Inlet compared to eustatic and GIA models	103

Contents of Appendices
Stored on CD

Appendix Number and File Name	Summary of contents
Appendix 1	
Optima & tol.doc	Optima and tolerance of contemporary diatom species
Appendix 2	
Graphs above -1.6.doc	Regression results using altitude (m) relative to MHHW for contemporary samples above -1.6 m MHHW
Graphs above -1.0.doc	Regression results using altitude (m) relative to MHHW for contemporary samples above -1.0 m MHHW
Graphs above -0.5.doc	Regression results using altitude (m) relative to MHHW for contemporary samples above -0.5 m MHHW
Graphs above 0.doc	Regression results using altitude (m) relative to MHHW for contemporary samples above 0 m MHHW
Graphs above +0.5.doc	Regression results using altitude (m) relative to MHHW for contemporary samples above +0.5 m MHHW
Graphs above +1.0 MHHW.doc	Regression results using altitude (m) relative to MHHW for contemporary samples above +1.0 m MHHW
Graphs above +1.0hrs.doc	Regression results hours inundated per year for contemporary samples above +1.0 m MHHW
Appendix 3	
14Cdates.xls	Radiocarbon dates from this study, Combellick (1991) and Combellick and Reger (1994)
Appendix 4	
Girdwood Troels Smith.doc	Troels Smith descriptions of sediment from Girdwood
Kasilof Troels Smith.doc	Troels Smith descriptions of sediment from Kasilof
Kenai Troels Smith.doc	Troels Smith descriptions of sediment from Kenai
Appendix 5	
Diatom count.doc	Information on diatom counts
Appendix 6	
KE 2000-7.xls	Transfer function results for Kenai 2000-7
G-800.xls	Transfer function results for Girdwood G-800

G-01-1A.xls	Transfer function results for Girdwood G-01-1A
G-01-1C.xls	Transfer function results for Girdwood G-01-1C
G-01-1E.xls	Transfer function results for Girdwood G-01-1E
G-01-1F.xls	Transfer function results for Girdwood G-01-1F
G-01-9.xls	Transfer function results for Girdwood G-01-9
KS-01-1.xls	Transfer function results for Kasilof KS-01-1
KS-3.xls	Transfer function results for Kasilof KS-3

Appendix 7

Contemp.xls	Altitude & vegetation description of contemporary samples

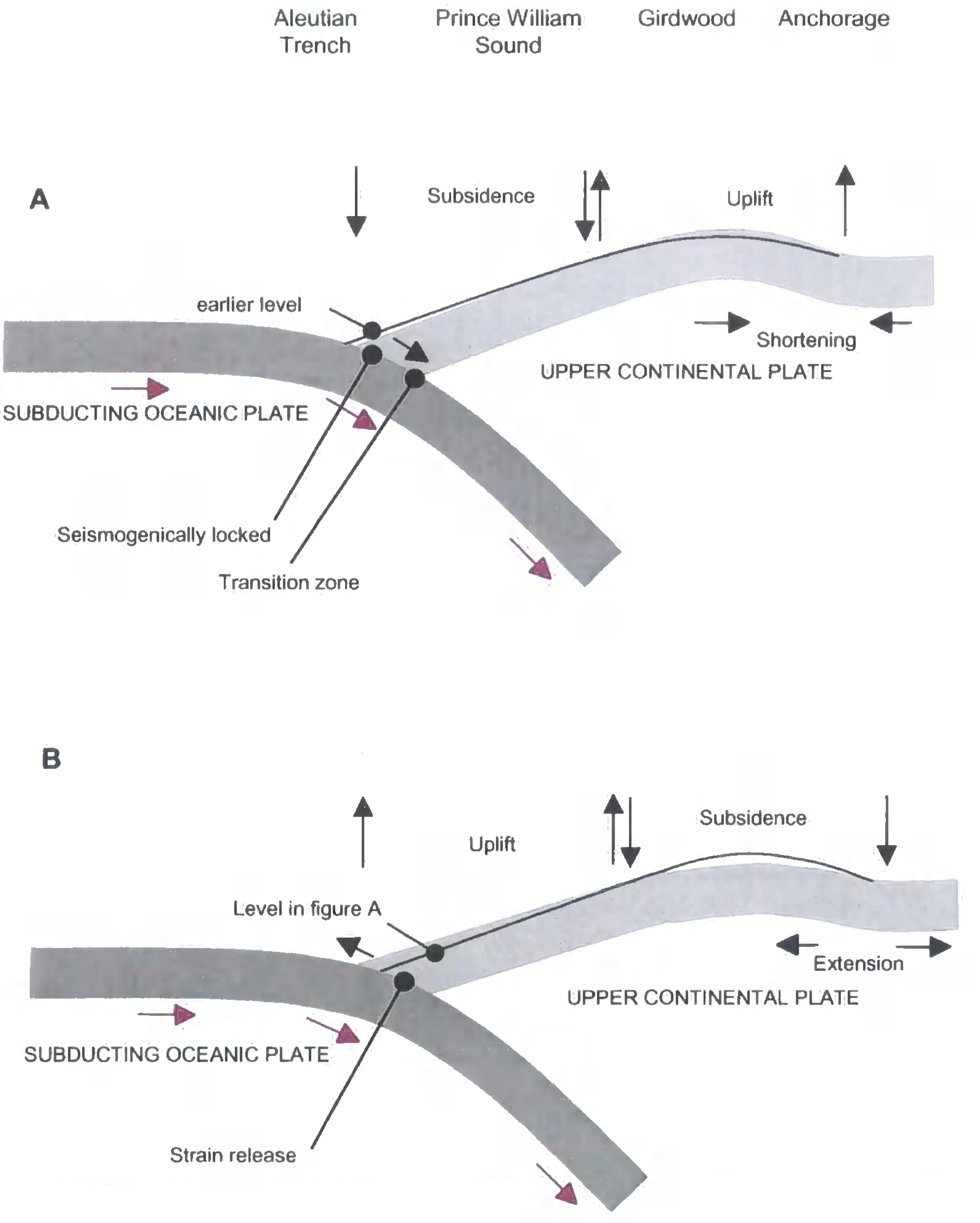

Figure 1.1

Schematic diagrams showing the pattern of (A) inter-seismic and (B) co-seismic deformation associated with a subduction zone earthquake during the earthquake deformation cycle. Adapted from Nelson *et al.* (1996) to reflect the spatial pattern of co-seismic deformation during the 1964 earthquake in Alaska. Site locations are shown in figure 1.4

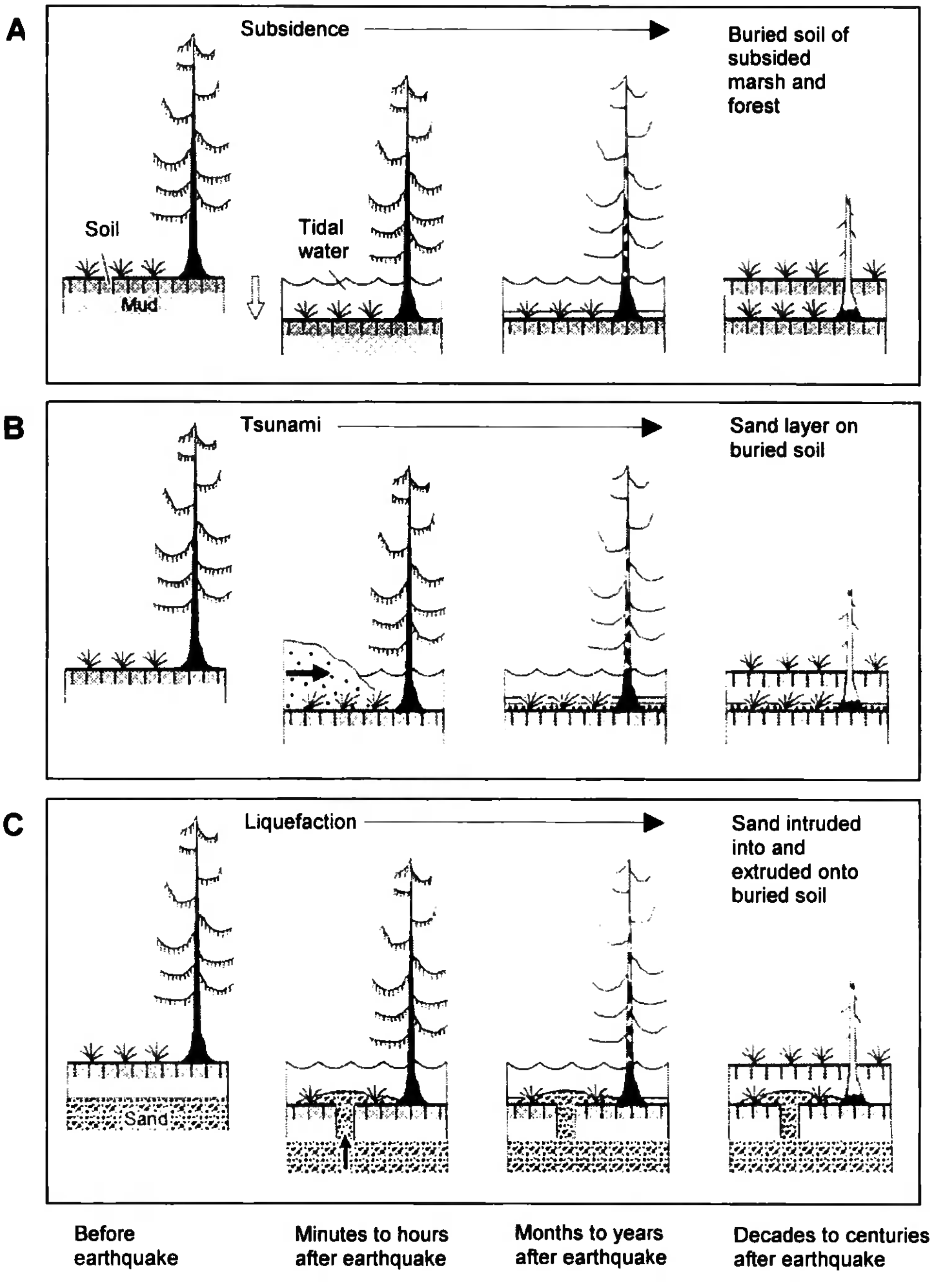

Figure 1.2

Schematic diagram showing the development of peat-silt couplets following co-seismic submergence together with associated possible tsunami deposits and liquefaction features (Atwater & Hemphill-Haley, 1997)

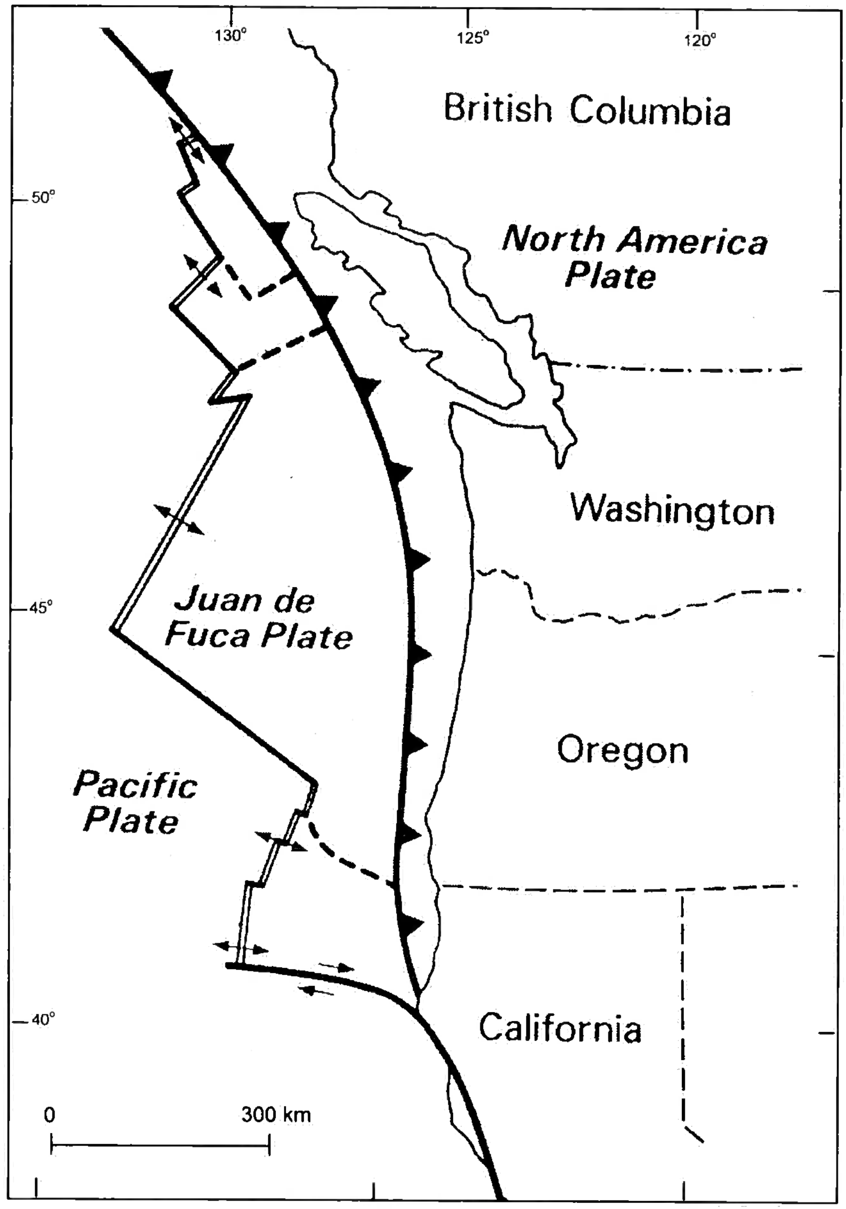

Figure 1.3

The Cascadia subduction zone off the coast of the Pacific Northwest of the USA and Canada (Long & Shennan, 1994)

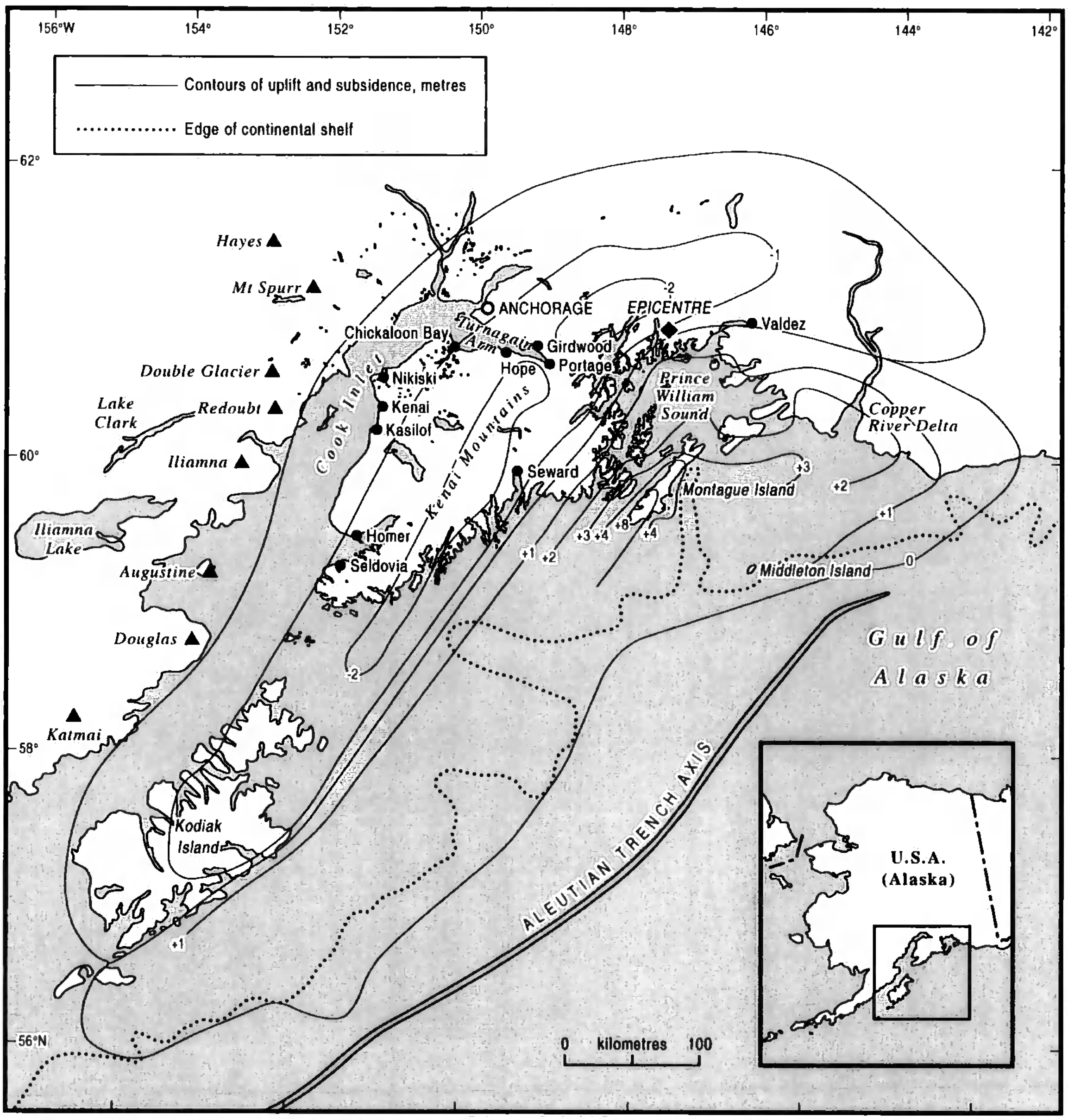

Figure 1.4

Region affected by the 1964 Alaskan earthquake showing location of sites studied, generalised contours of co-seismic uplift and subsidence (modified from Plafker, 1969) and eight volcanoes (solid triangles) marking the eastern end of the Aleutian volcanic arc

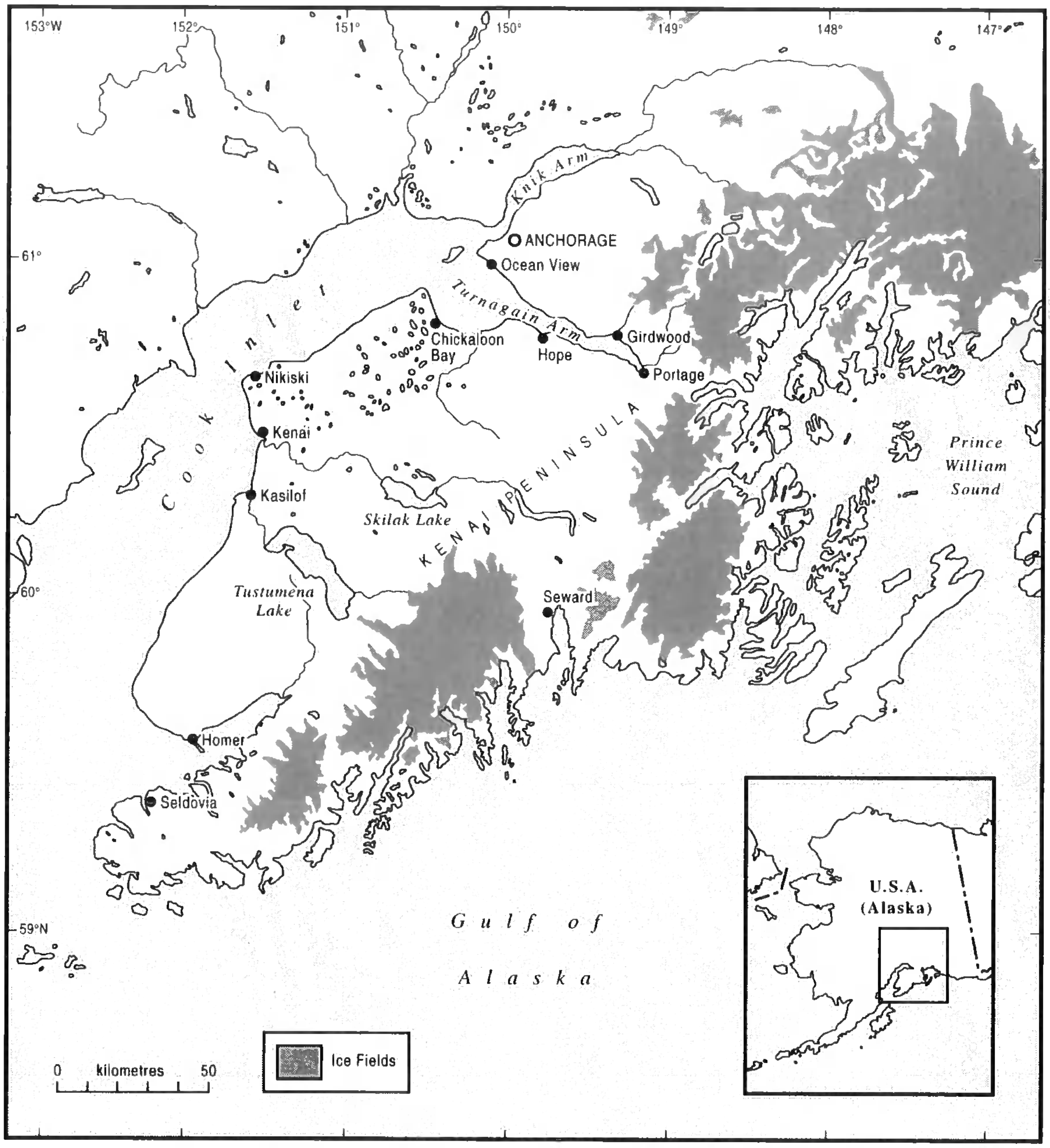

Figure 2.1

Location of field sites around the upper Cook Inlet and Turnagain Arm, major rivers and ice fields

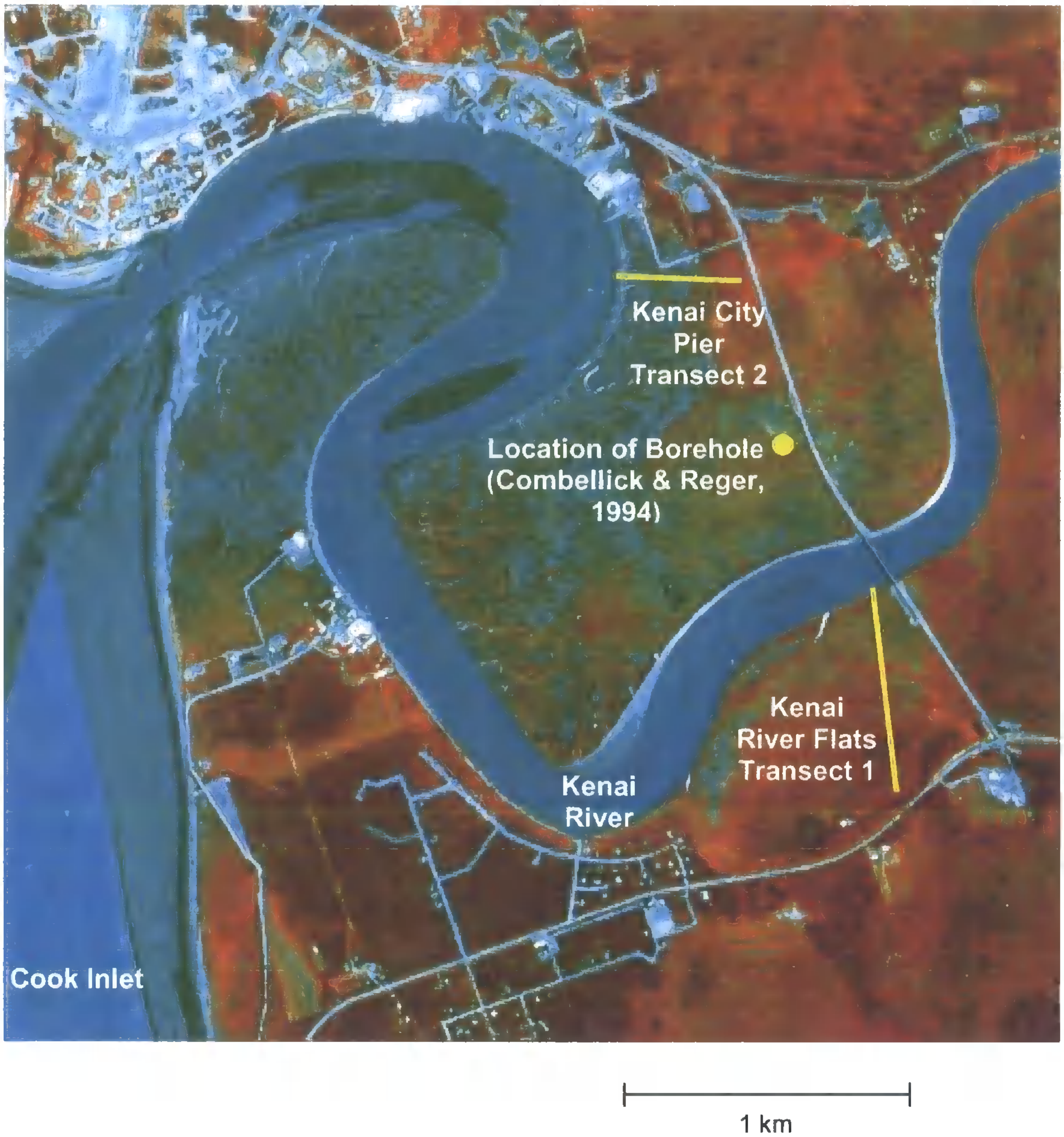

Figure 2.2

Satellite image showing the location of the Kenai River Flats and Kenai City Pier transects in relation to the Kenai River entrance (Rod Combellick, State of Alaska Geological and Geophysical Survey)

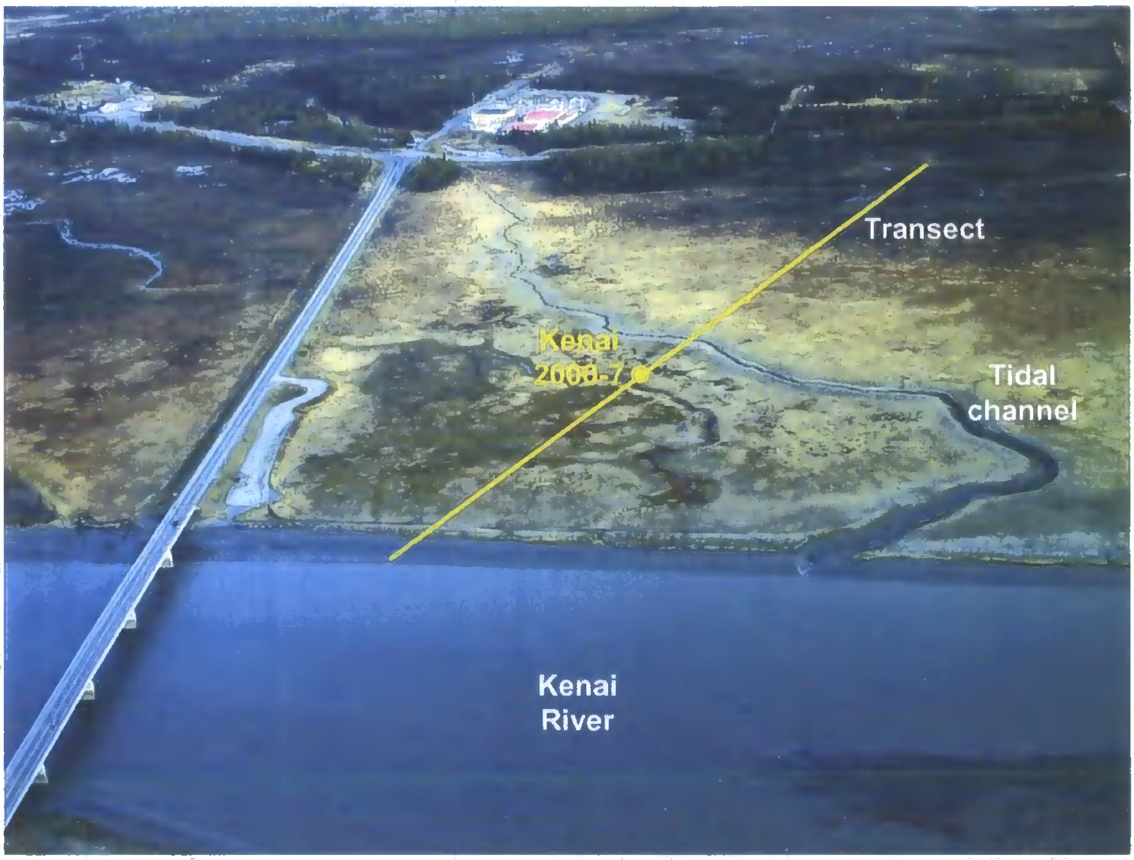

Figure 2.3

Oblique aerial photograph of Kenai River Flats showing the transect across the marsh, location of coring site Kenai 2000-7 and tidal channel. The contemporary transect incorporates all environments from unvegetated mudflat through to raised bog

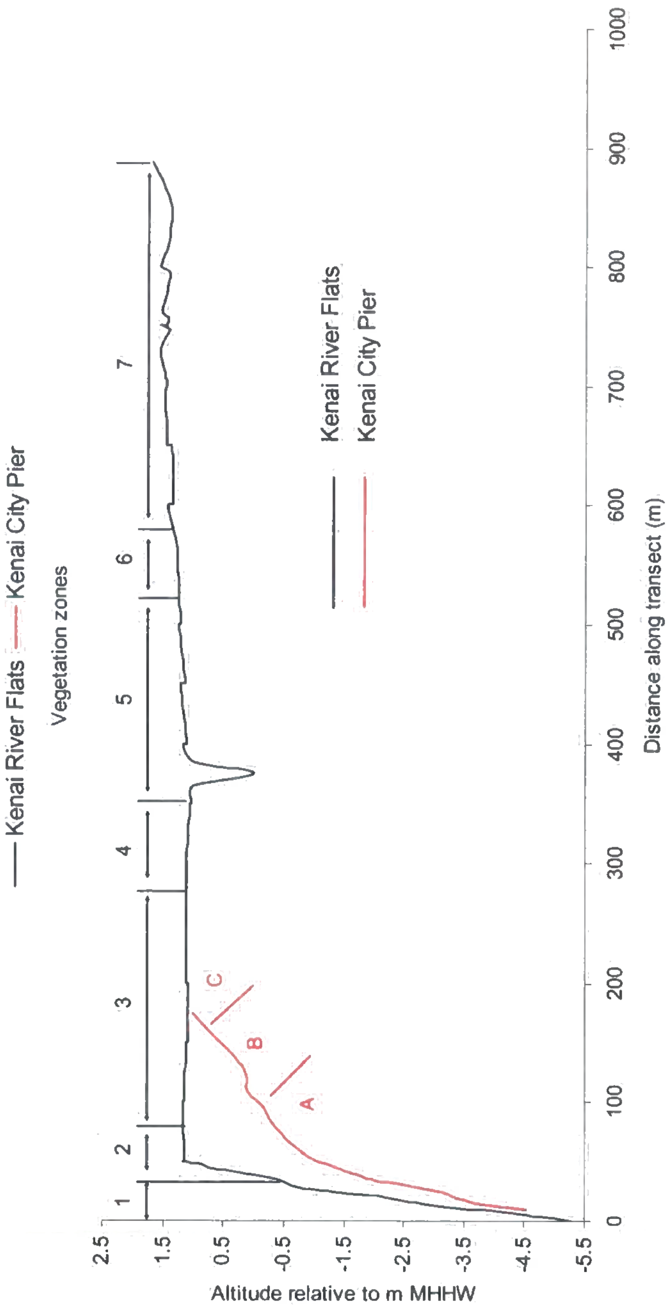

Figure 2.4

Altitude (m) of vegetation zones (described in table 2.1) found at Kenai River Flats and Kenai City Pier

Vegetation zone 7

Towards the landward limit of the transect, diverse raised bog communities develop comprising Poaceae, *Carex lyngbyei*, *Sphagnum* sp., *Vaccinium* sp., *Empetrum nigrum*, *Salix* sp., *Alnus* sp., *Picea* sp. and *Betula* sp. The ground at the most landward site is completely water logged with a floating mat of vegetation

Vegetation zones 4 and 5

Midway along the transect there is a transition from mid marsh to high marsh. Vegetation consists of Poaceae, *Juncus* sp., *Triglochin maritima*, *Carex lyngbyei* with rare *Potentilla egedii*, *Puccinellia* sp. and *Plantago maritima*

Vegetation zones 1, 2 and 3

Towards the river, a small levee separates the unvegetated mudflat from the marsh surface, and so there is a poor transition between the two. Vegetation at the marsh front consists of Poaceae, *Triglochin maritima*, *Potentilla egedii* and *Juncus* sp

Figure 2.5

Contemporary environments at Kenai River Flats

Figure 2.6

Oblique aerial photograph of Kenai City Pier. The contemporary marsh transect at this site has a more extensive tidal flat that gently grades into low marsh

Vegetation zone 7
At the landward limit of the transect diverse raised bog communities develop, similar to those found at Kenai River Flats

Vegetation zone 4
Along the transect, vegetation changes to mid marsh consisting of Poaceae, *Juncus* sp., *Triglochin maritima* with rare *Potentilla egedii*, *Puccinellia* sp. and *Plantago maritima* together with the introduction of *Carex lyngbyei*

Vegetation zones 1 and 2
At Kenai City Pier, the mudflat is more extensive and there is gentle transition into the upper tidal flat/marsh pioneer zone and then into low marsh

Figure 2.7

Contemporary environments at Kenai City Pier

Figure 2.8

Oblique aerial photograph (looking upstream) of the marsh and Kasilof River showing location of the bank section with the three laterally extensive peat layers. The sampling site lies 3.75 km from the river entrance into the Cook Inlet

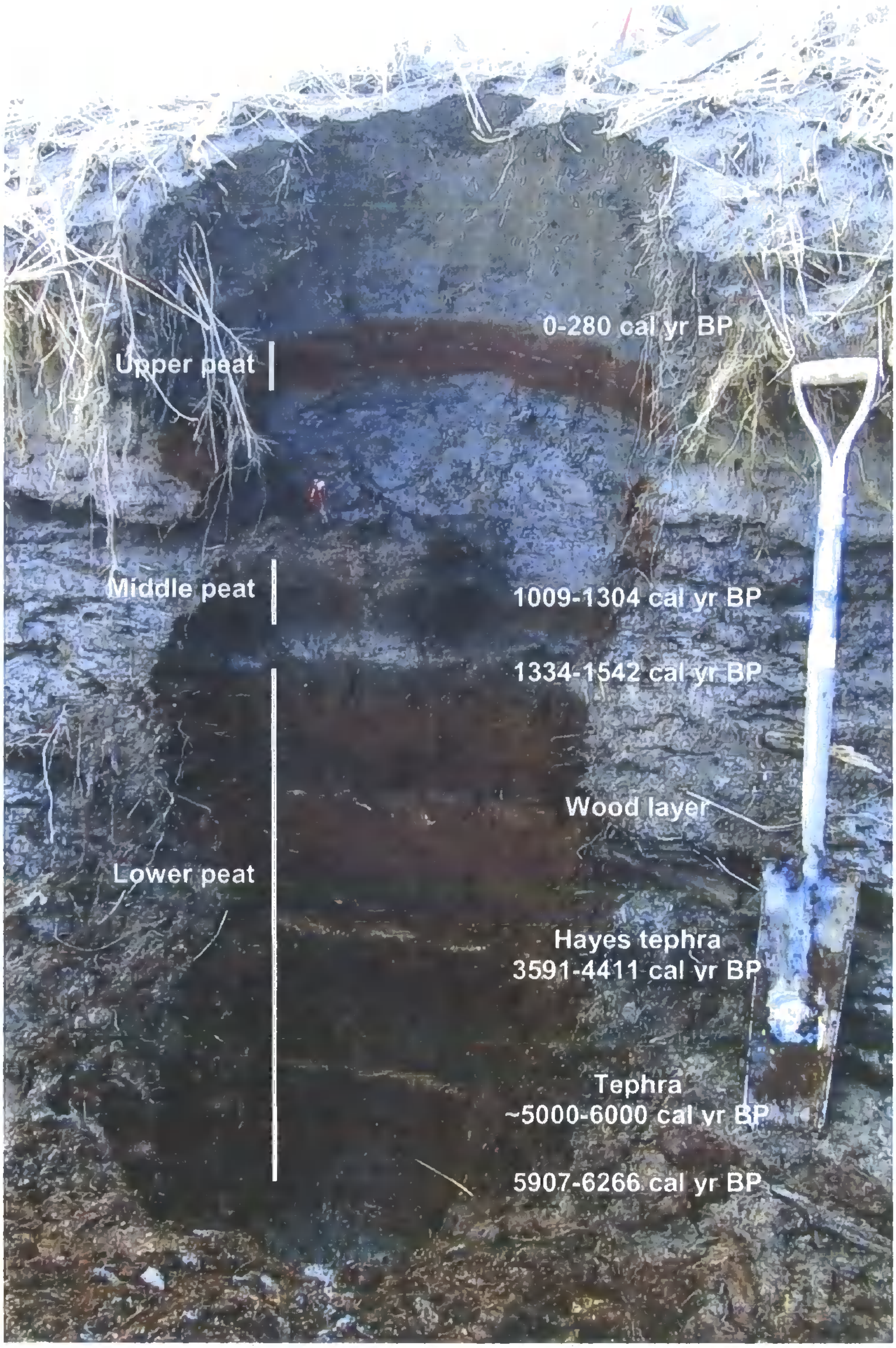

Figure 2.9

Bank section at Kasilof showing three buried peat layers. The lowest is approximately 1 m thick and contains distinctive wood layers and tephras. Ages shown are recalibrated radiocarbon dates from Combellick and Reger (1994)

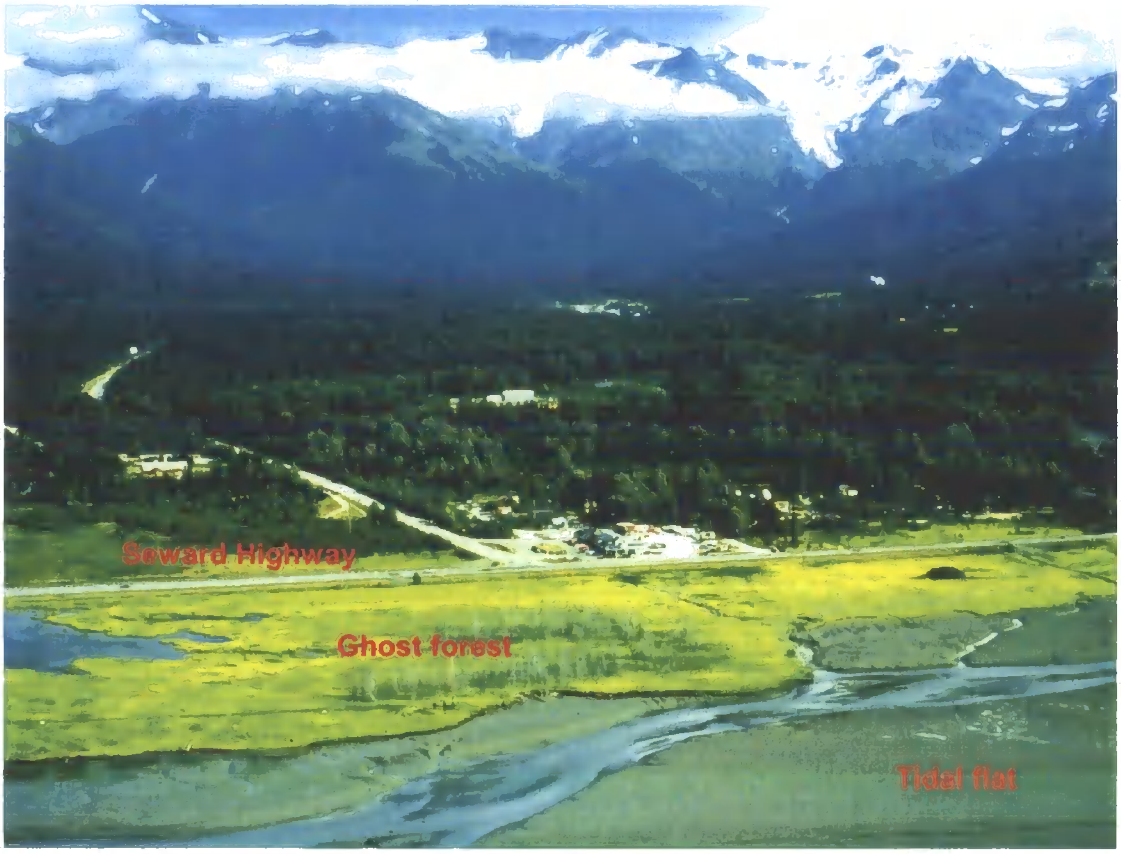

Figure 2.10

Oblique aerial photograph of Girdwood showing extensive tidal flat areas, a small cliff separating the tidal flat from the marsh surface and ghost forests rooted in the 1964 buried peat layer (Rod Combellick, State of Alaska Geological and Geophysical Survey)

Figure 2.11

Cliff face (~1 m) at Girdwood separating the contemporary tidal flat from the marsh surface exposing the 1964 peat in which the ghost forest is rooted

Snow covers the frozen marsh surface at Girdwood

The small cliff face separating the mudflat from the marsh surface is not visible due to the amount of ice in the Turnagain Arm. Highest tides deposit some ice blocks onto the marsh surface

Melting ice blocks on the marsh surface deposit a significant amount of sediment that becomes part of the annual sediment accumulation

Figure 2.12

Winter conditions at Girdwood, April 2002

Snow covers the frozen marsh surface at Kenai. The tidal channel that dissects the contemporary transect is not visible due to the amount of ice contained within it

The Kenai River (same location as figure 2.5) is frozen, with ice blocks pushed up the riverbank onto the contemporary marsh surface. No contemporary mudflats are visible

Further downstream at Kenai City Pier, the Kenai River is not frozen. Large ice blocks are deposited on the mudflat that is frozen down to a depth of approximately 0.5 m

Figure 2.13

Winter conditions at Kenai, April 2002

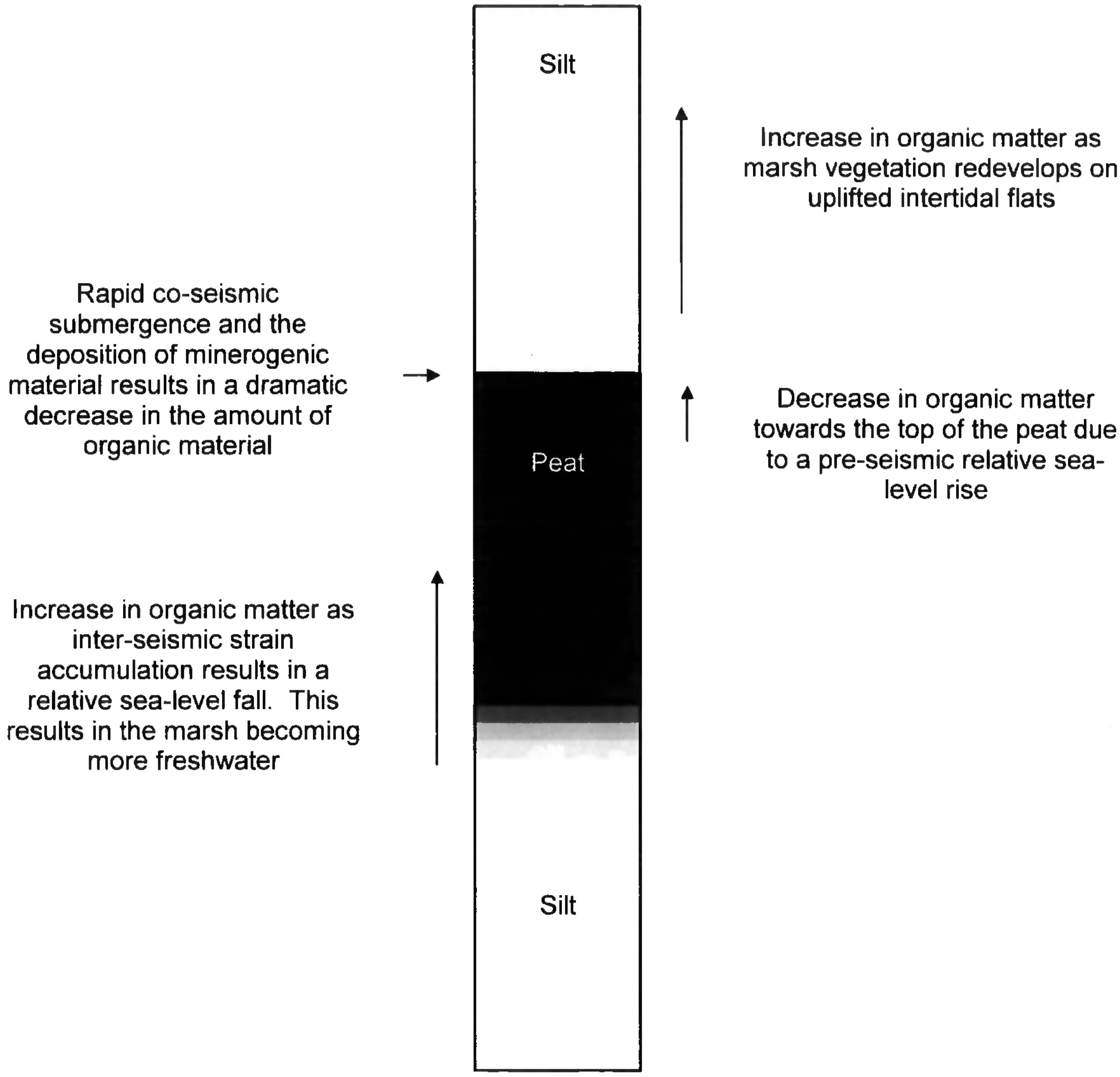

Figure 3.1

Schematic diagram of organic content changes (Hamilton, 1998) associated with the EDC model

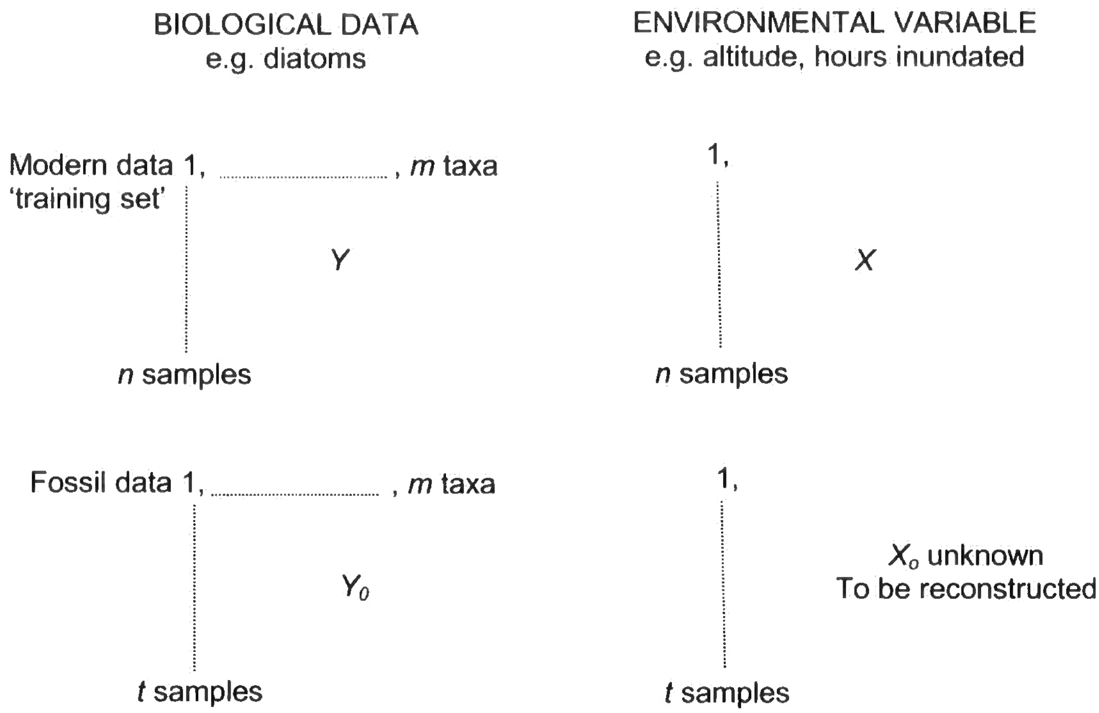

Figure 3.2

The primary aim of a transfer function is to predict the value of one or more environmental variables (*Xo*) from fossil biological data (*Yo*) consisting of *m* species in *t* samples. To estimate values of *Xo* the contemporary response of the same *m* species to the environmental variable(s) of interest is modelled. This involves a contemporary 'training set' of *m* species at *n* sites (*Y*) studied as surface assemblages with an associated set of contemporary environmental variables (*X*) for the same *n* sites. The modern relationships between Y and X are modelled and the resulting function is then used as a transfer function to transform the fossil data (*Yo*) into quantitative estimates of the past environmental variable(s) *Xo* (diagram and text from Birks, 1995)

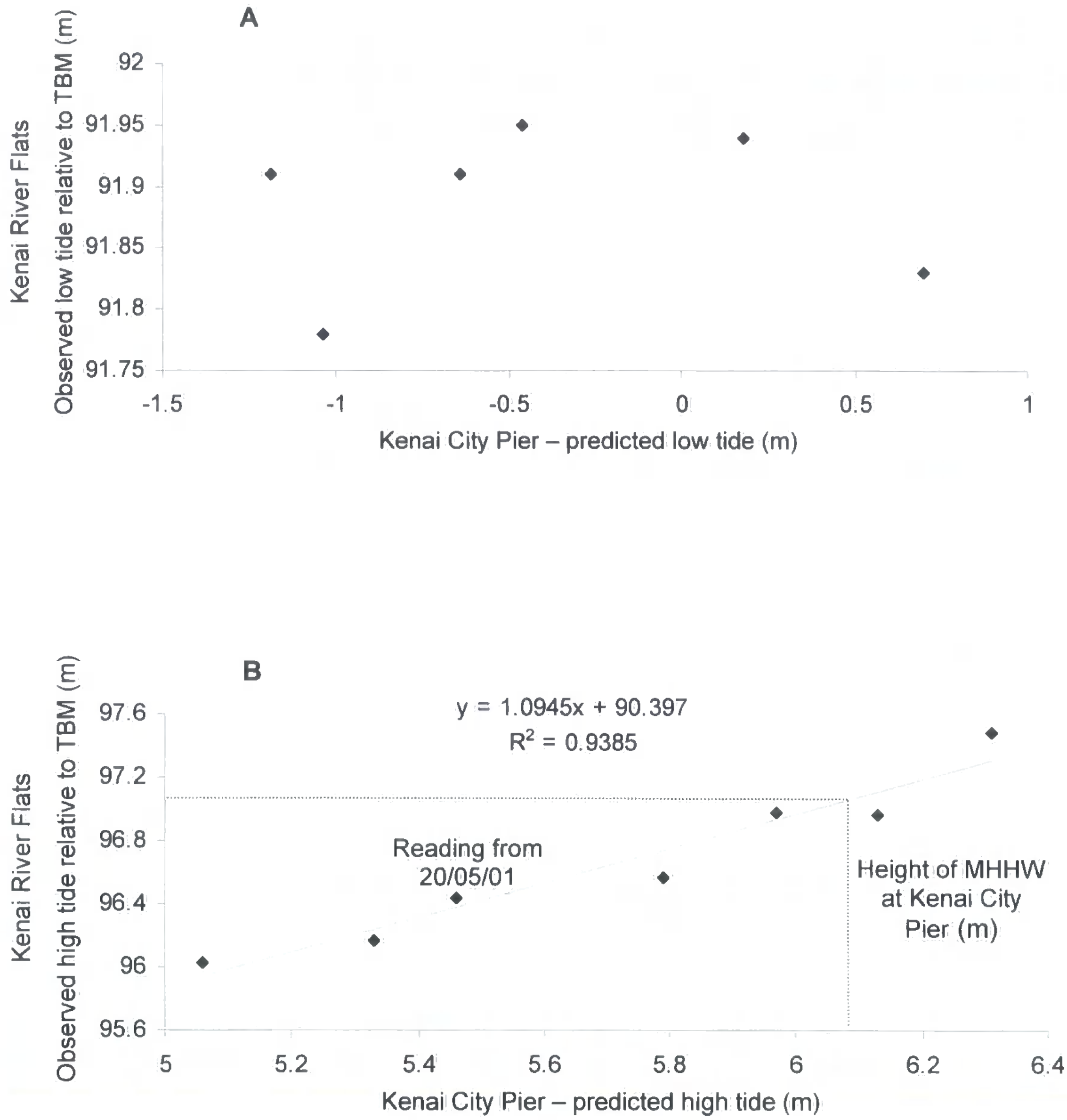

Figure 4.1

Tidal observations (m relative to TBM = 100) for Kenai River Flats. Figure 4.1(a) shows the relationship between observed low tide at Kenai River Flats (m TBM) and predicted low tide at Kenai City Pier (m MLLW) and figure 4.1(b) shows the same relationship for high tide

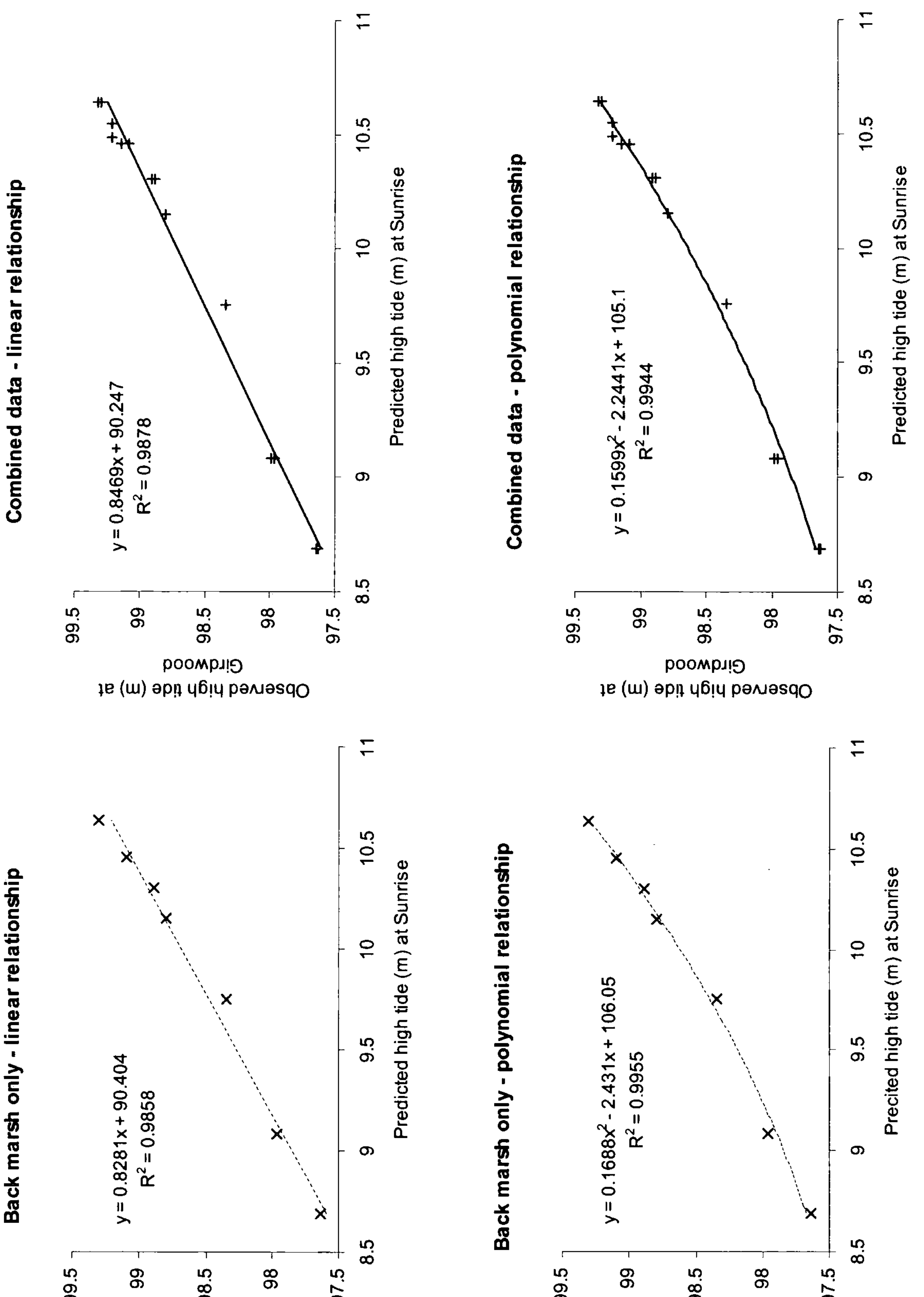

Figure 4.2

High tide observations at Girdwood against predicted at Sunrise

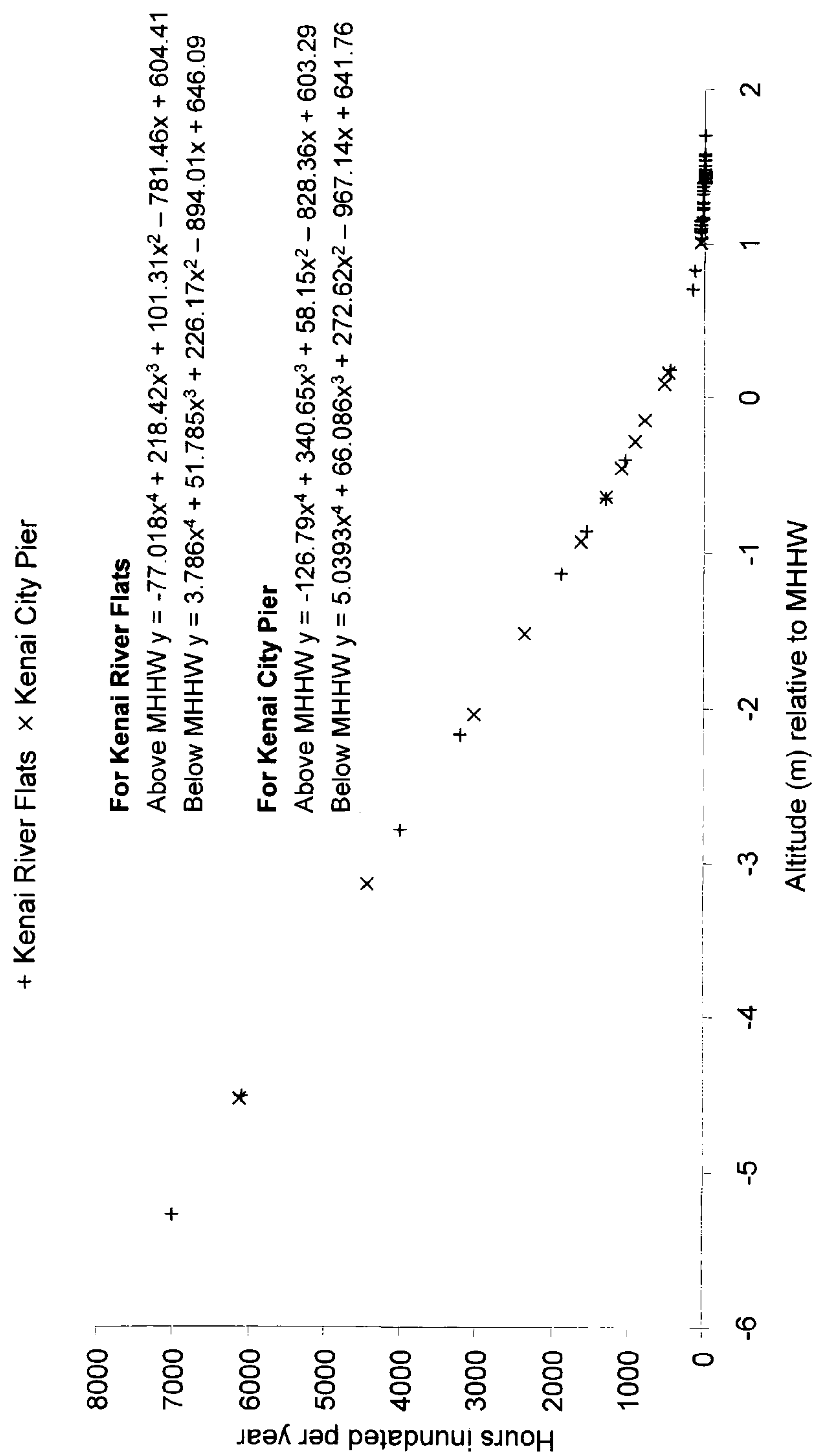

Figure 4.3

Hours inundated per year for the contemporary samples from Kenai River Flats and Kenai City Pier calculated using hourly water level data for Seldovia

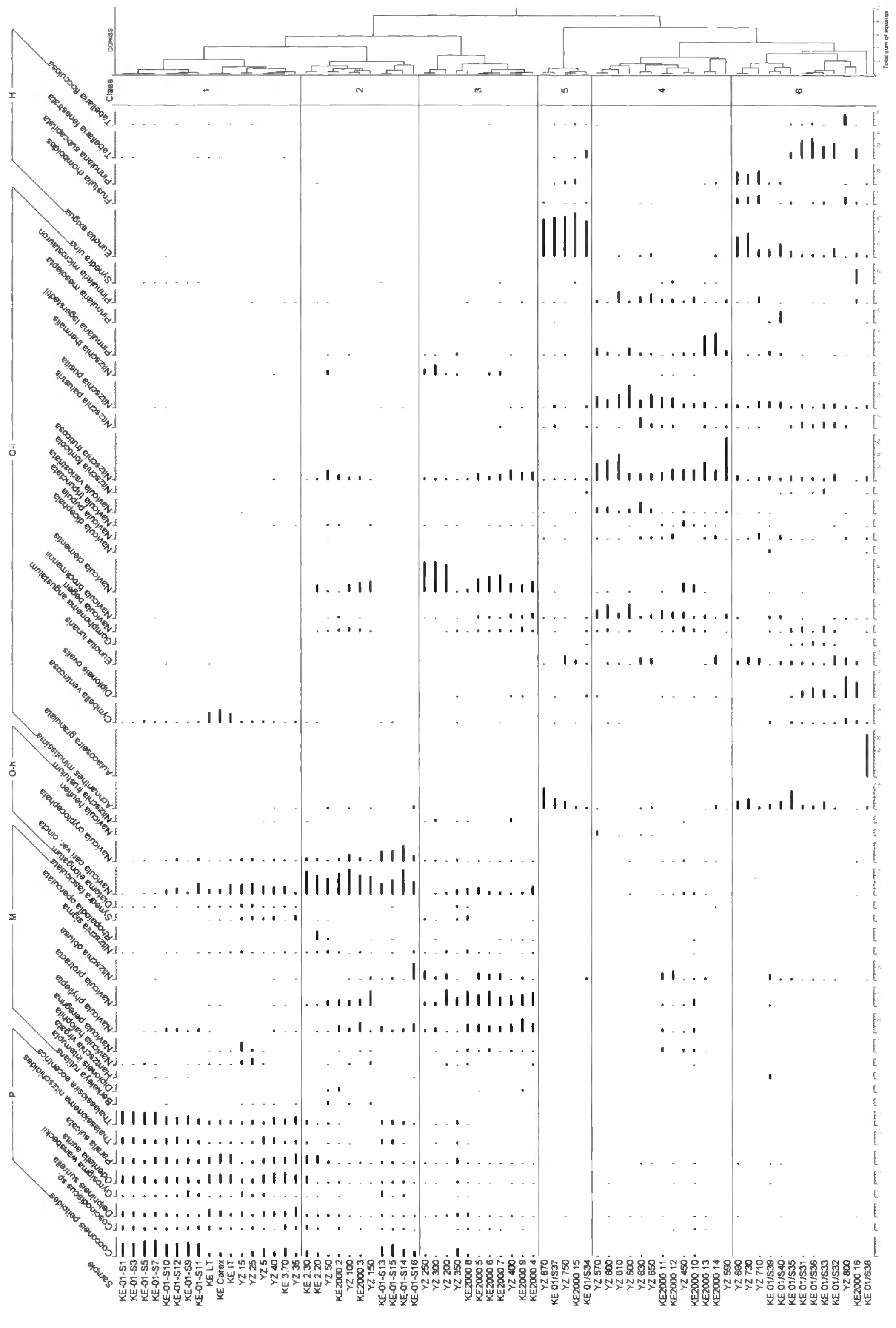

Figure 4.4

Kenai contemporary diatom data (>5% total diatom valves) and cluster analysis using Euclidian distance. Summary salinity classes: polyhalobian (P), mesohalobian (M), oligohalobian-halophile (O-h), oligohalobian-indifferent (O-i), halophobe (H)

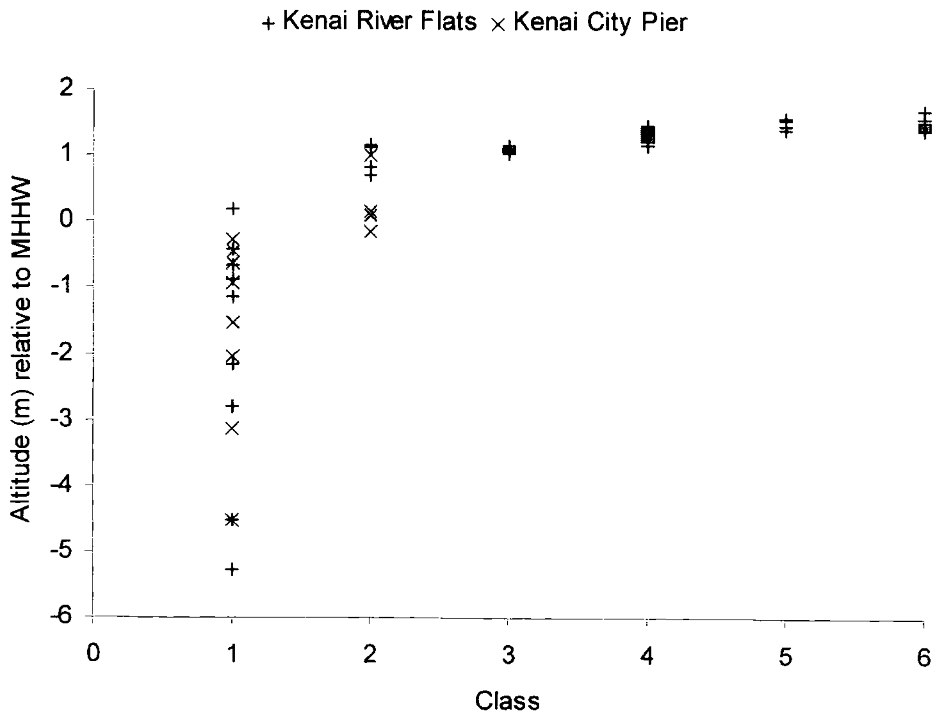

Figure 4.5

Altitude range of classes produced using Euclidian distance

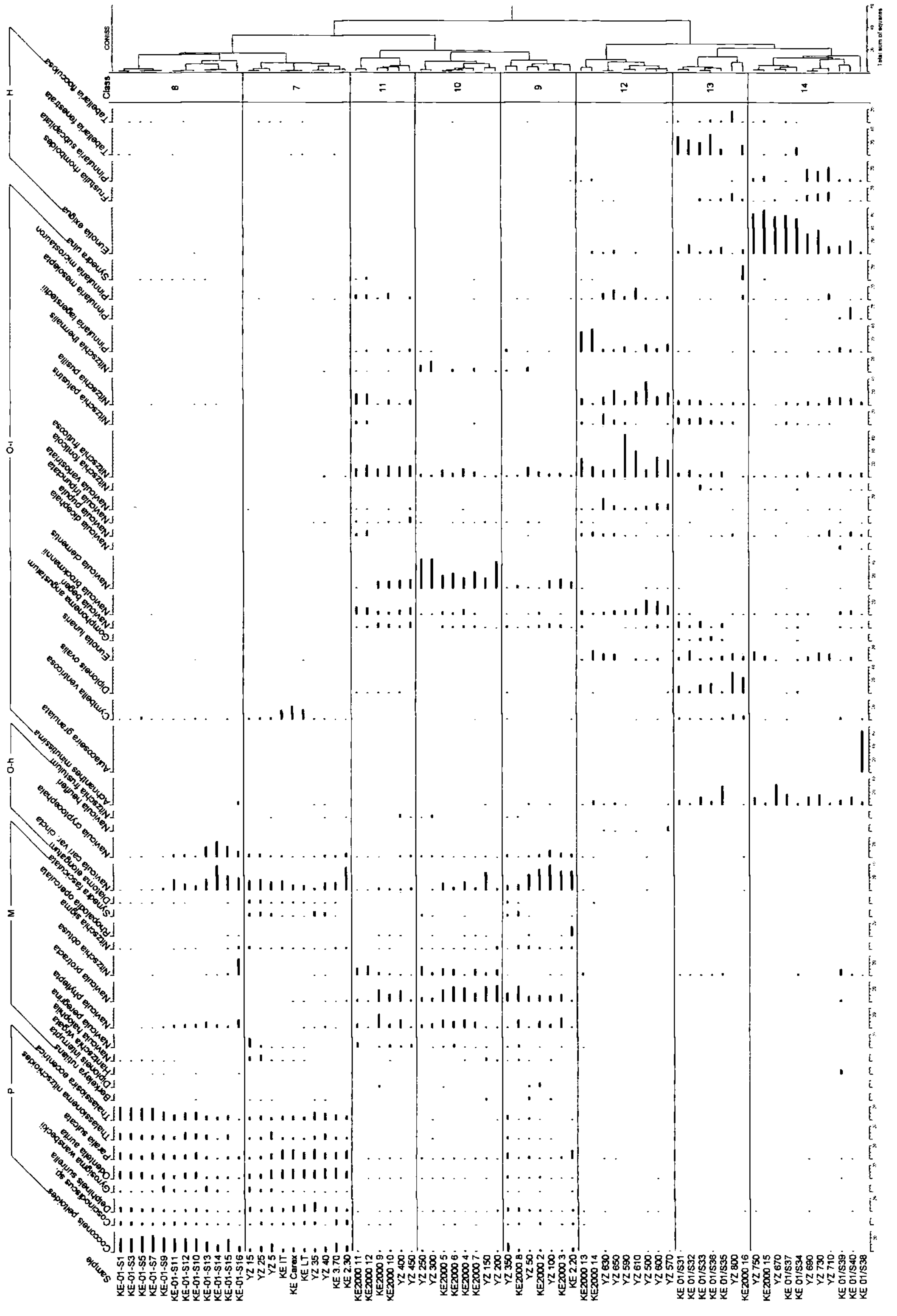

Figure 4.6

Kenai contemporary diatom data (>5% total diatom valves) and cluster analysis using Chord distance. Summary salinity classes: polyhalobian (P), mesohalobian (M), oligohalobian-halophile (O-h), oligohalobian-indifferent (O-i), halophobe (H)

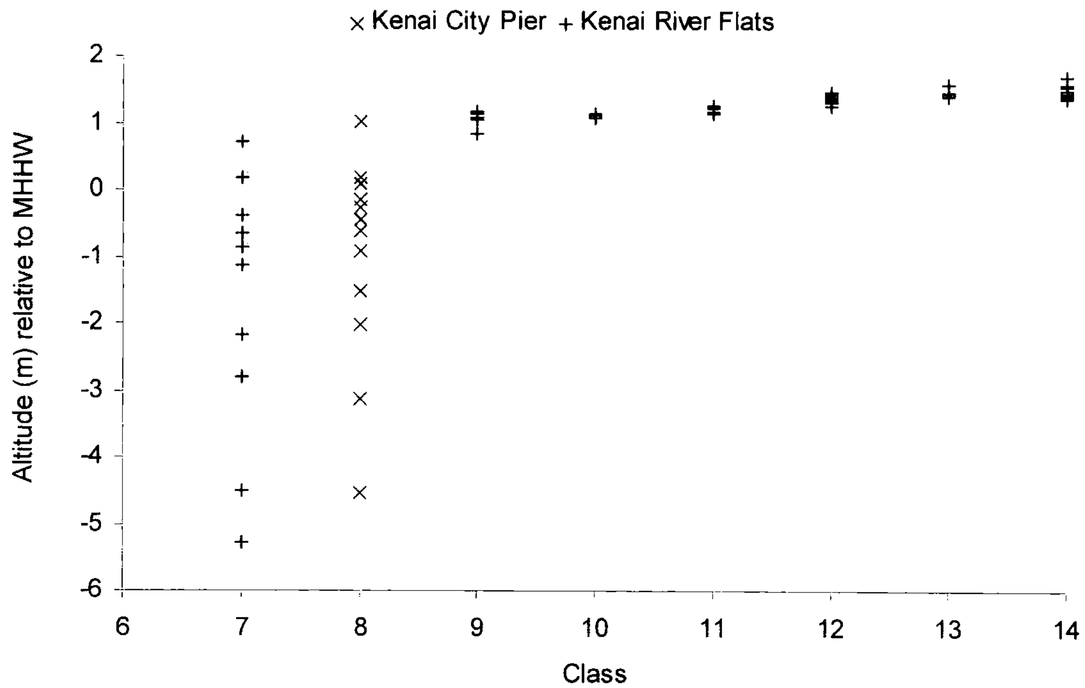

Figure 4.7

Altitude range of classes produced using Chord distance

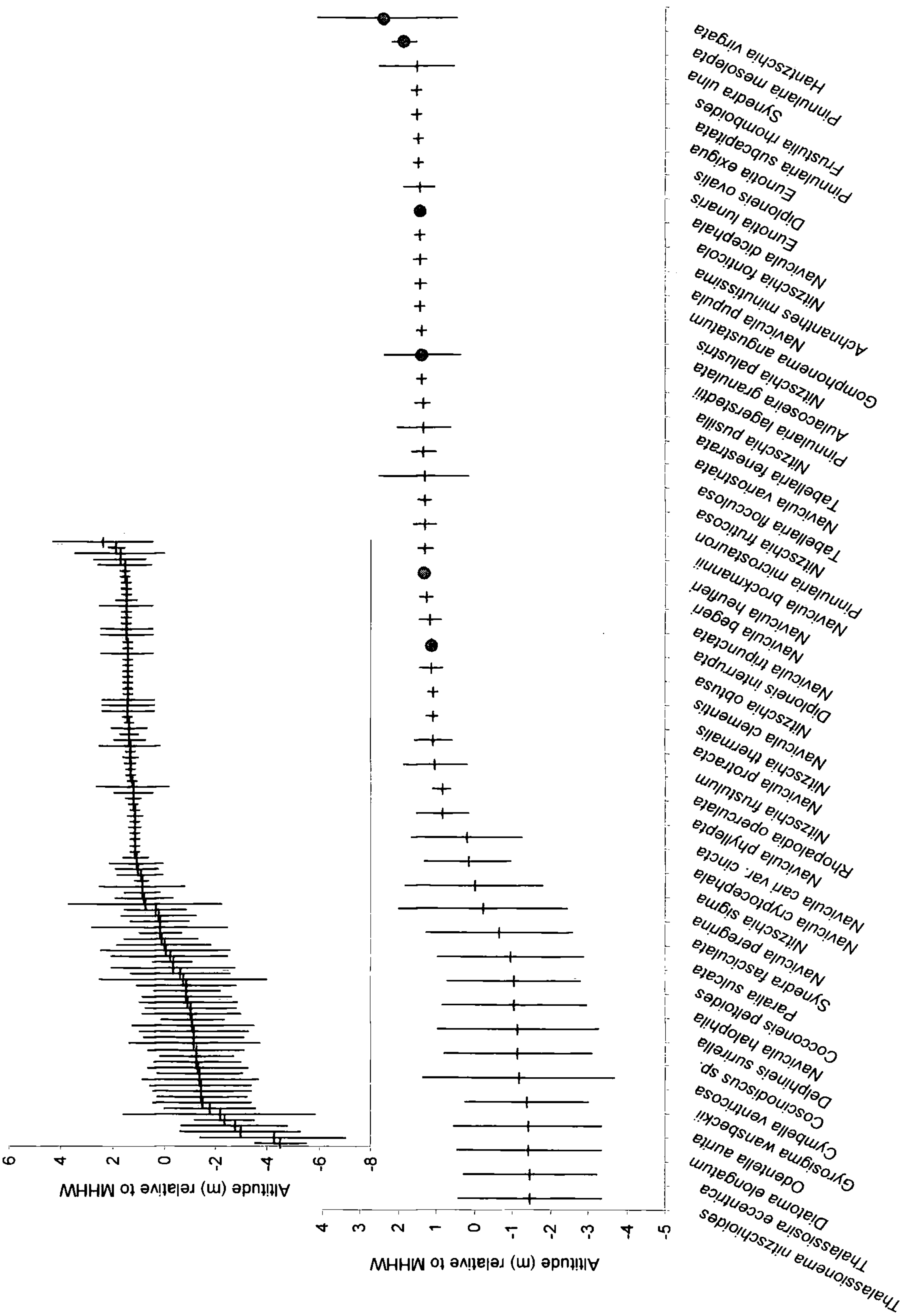

Figure 4.8

Diatom optima and tolerance based upon WA model. Main diagram shows species that account for over 5% total diatom valves counted in at least one sample and solid circles indicate those that occur in five or fewer. Inset shows the full data set (appendix 1)

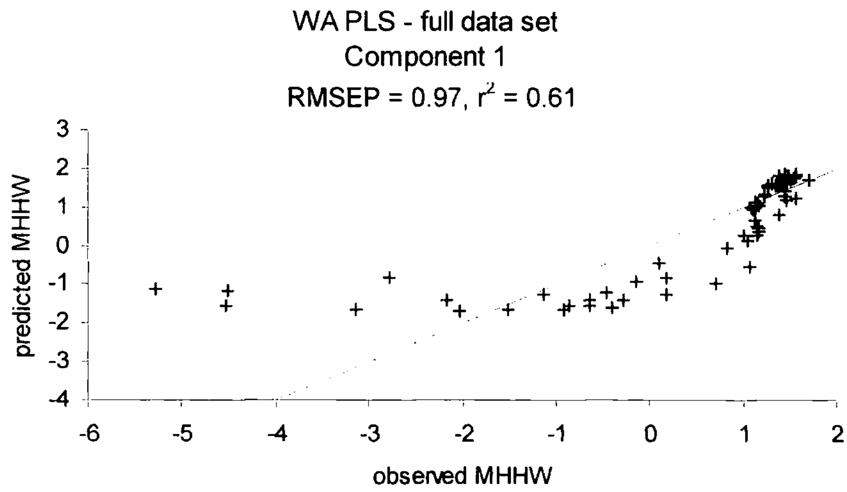

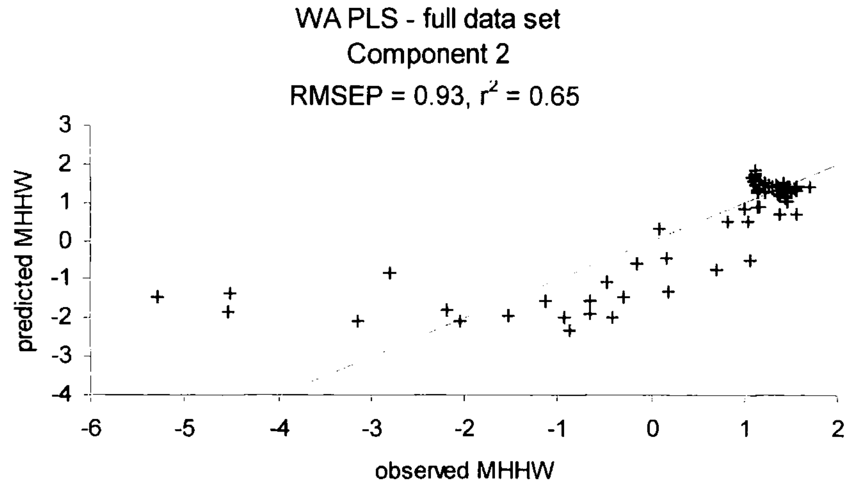

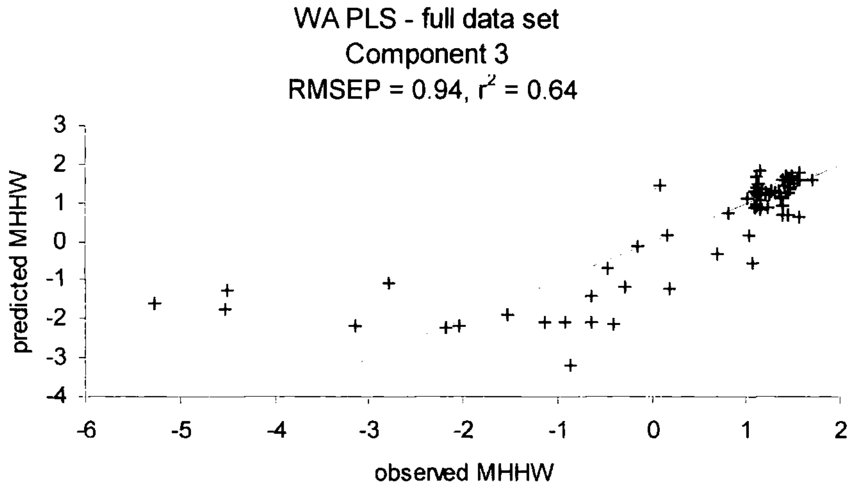

Figure 4.9

Regression results for the full contemporary data set using WA-PLS components 1, 2 and 3 (altitude (m) relative to MHHW)

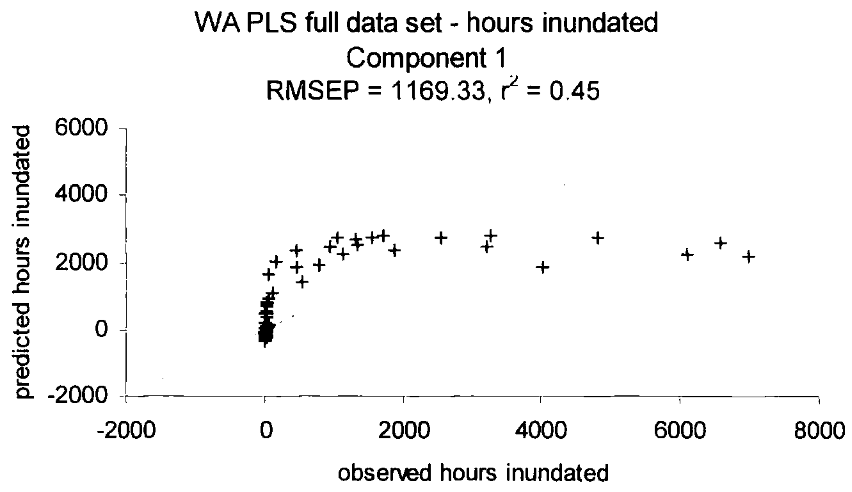

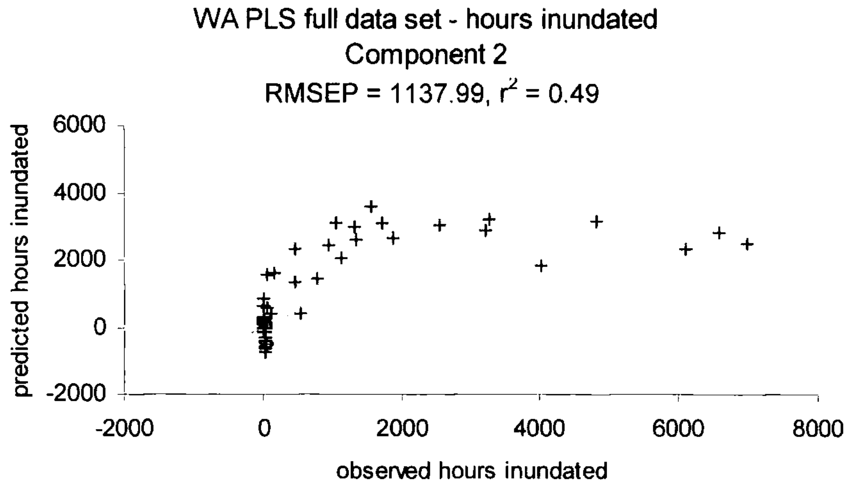

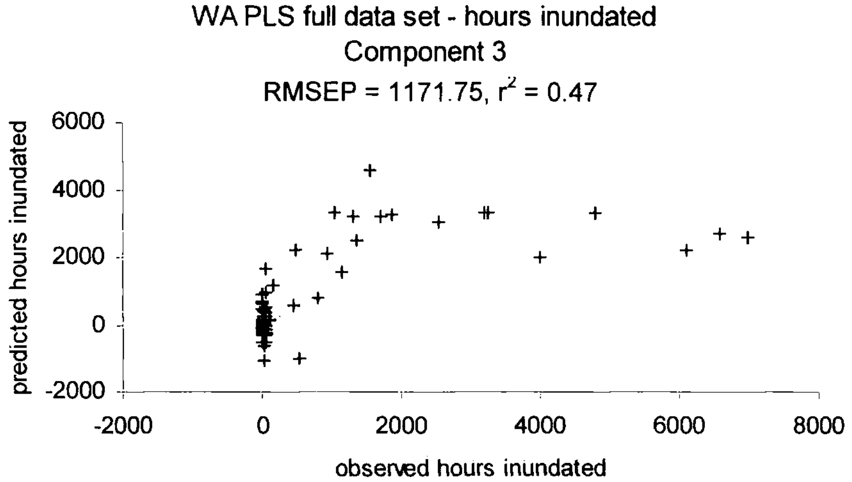

Figure 4.10

Regression results using hours inundated per year for the full contemporary data set (WA-PLS components 1, 2 and 3)

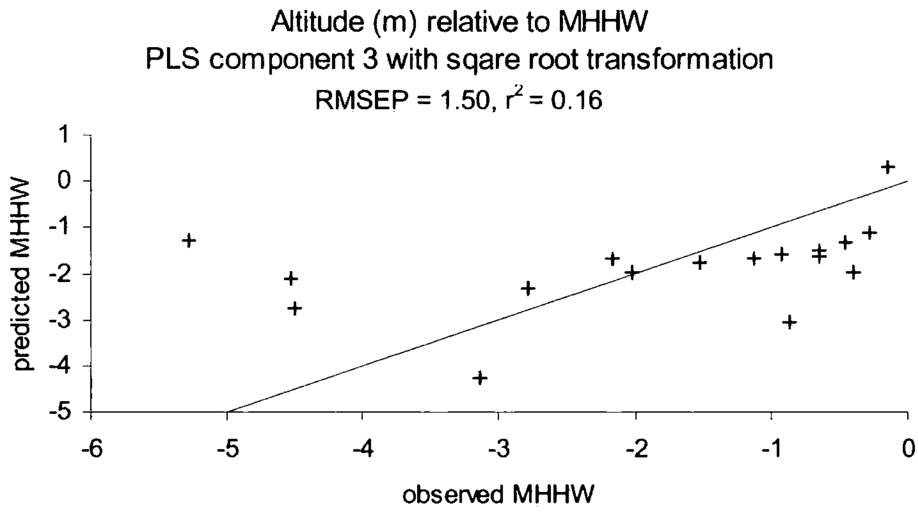

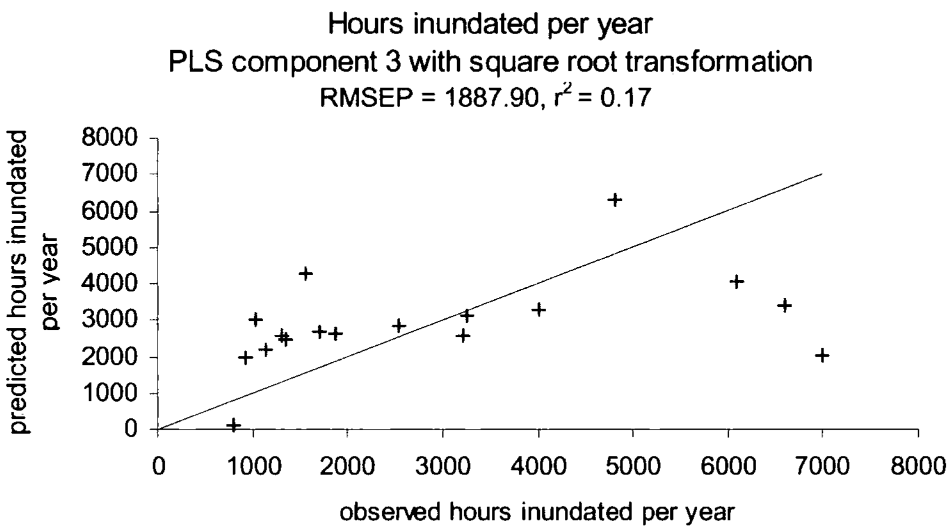

Figure 4.11

Regression results for contemporary samples found below MHHW using PLS component 3 with a square root transformation for both altitude (m) relative to MHHW and hours inundated per year

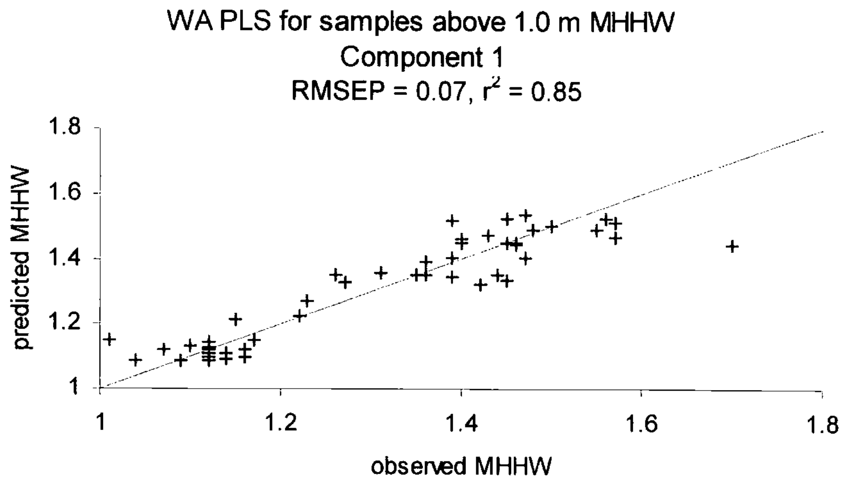

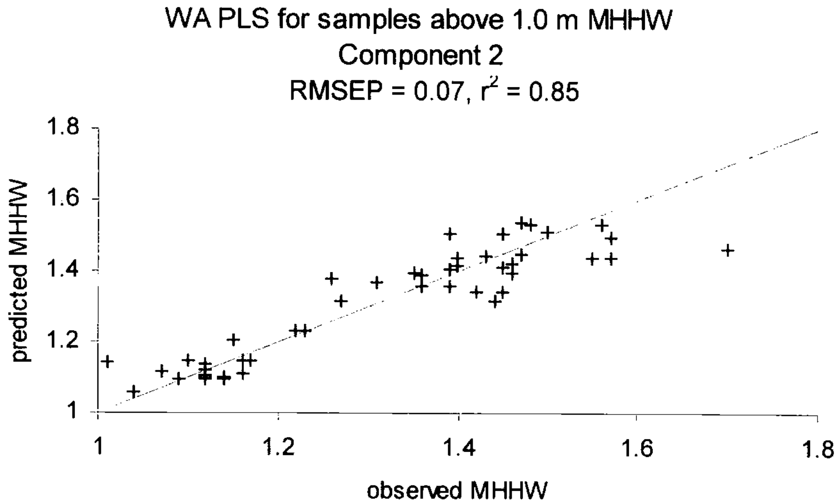

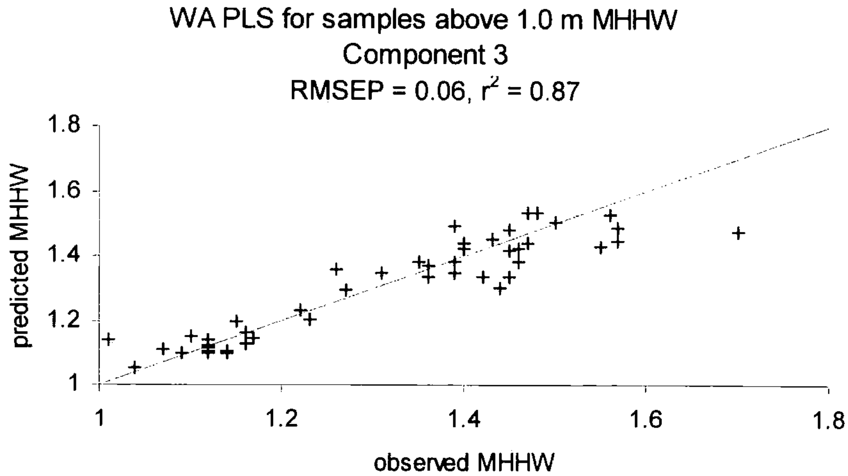

Figure 4.12

Regression results using altitude (m) relative to MHHW for contemporary samples above +1.0 m MHHW (WA-PLS components 1, 2 and 3)

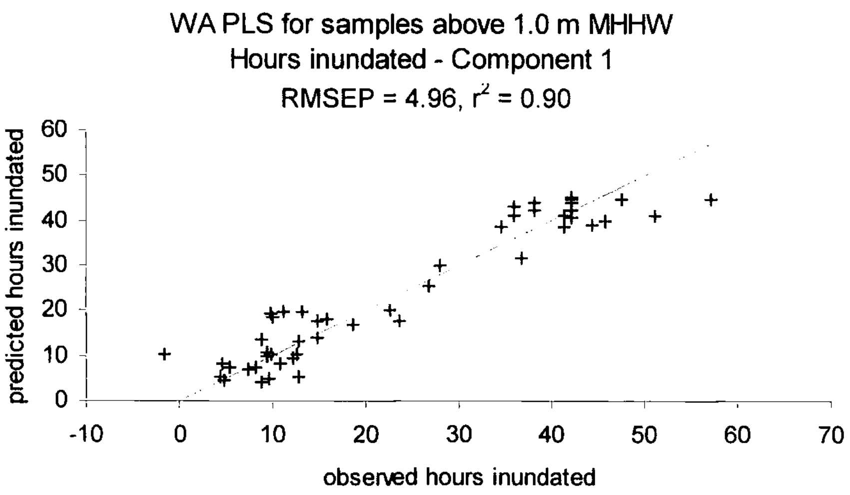

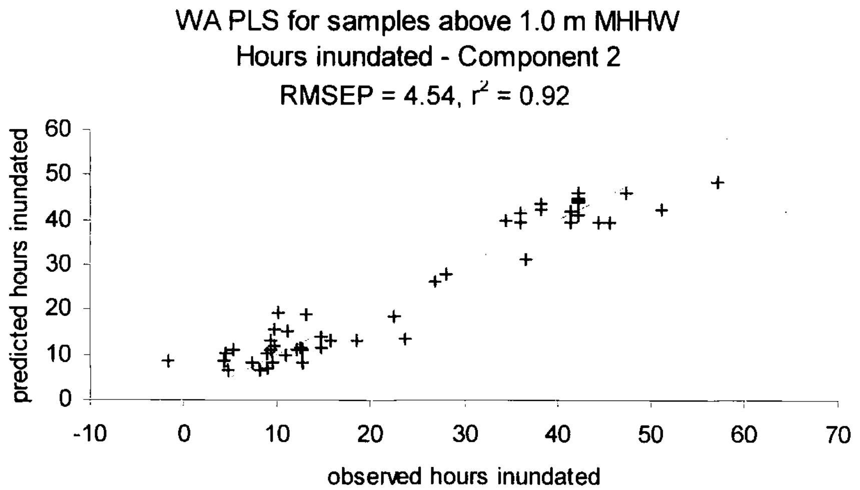

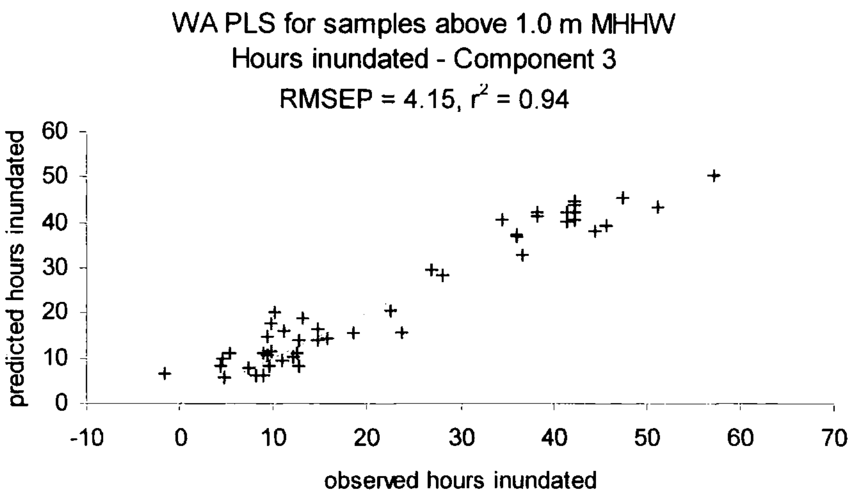

Figure 4.13

Regression results using hours inundated per year for contemporary samples above +1.0 m MHHW (WA-PLS components 1, 2 and 3)

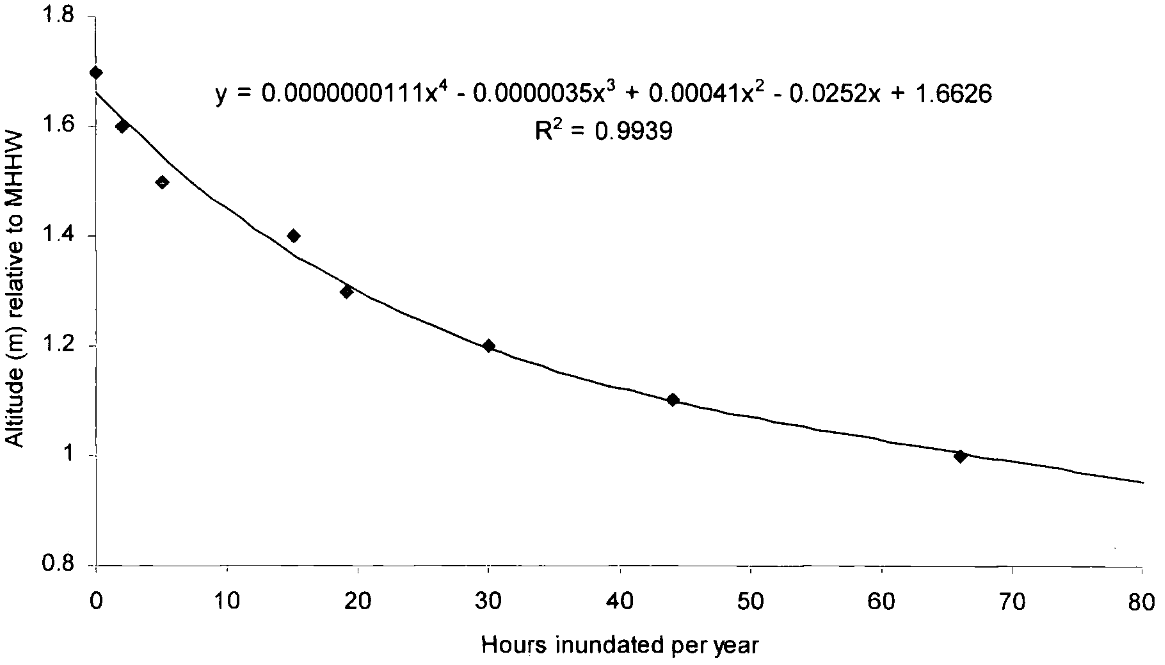

Figure 4.14

Hours inundated per year for sites above +0.8 m MHHW showing observations (solid symbols) and equation (solid line) used to back calculate predicted altitude (m) from regression models based on hours inundated data sets

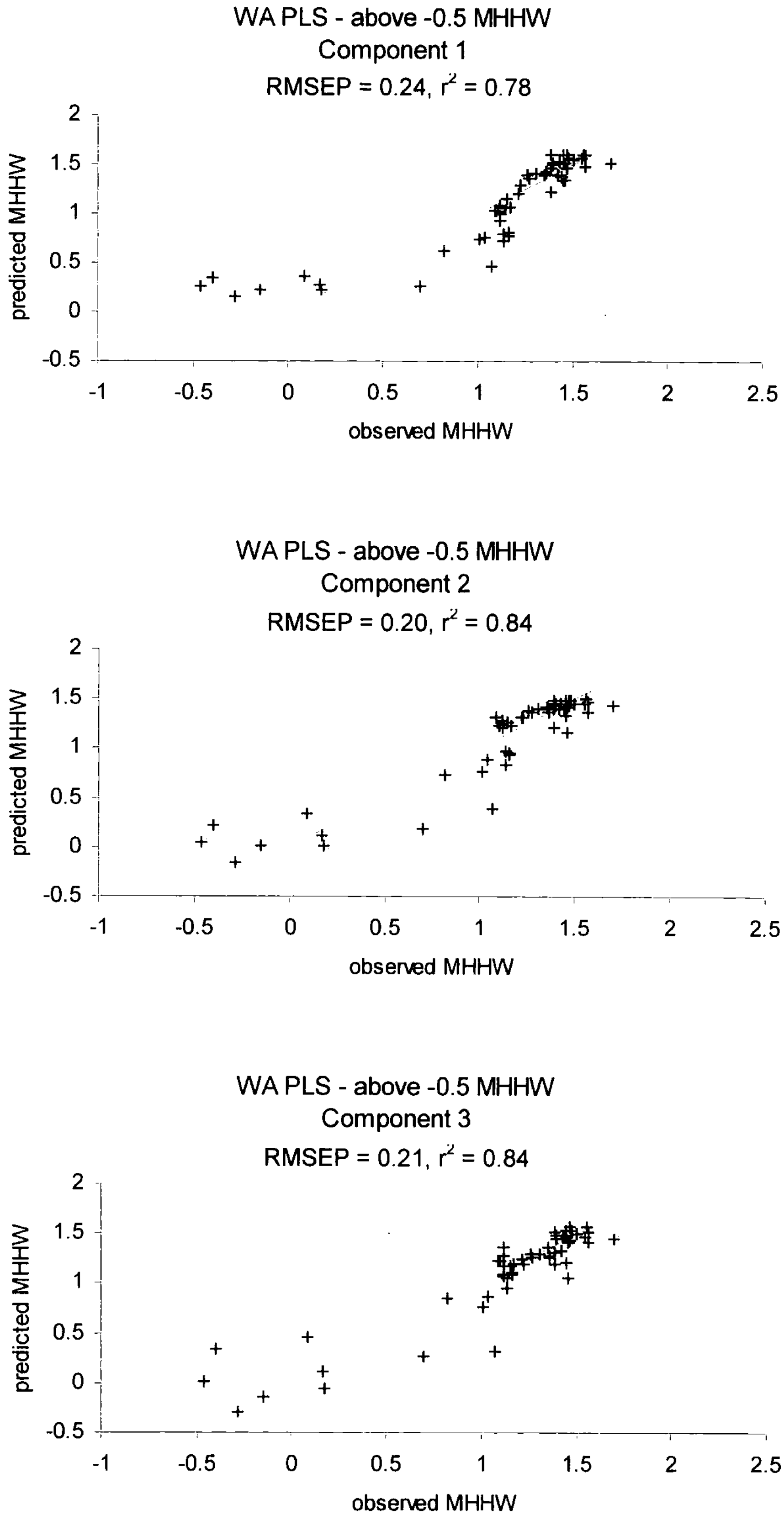

Figure 4.15

Regression results using altitude (m) relative to MHHW for contemporary samples above -0.5 m MHHW (WA-PLS components 1, 2 and 3)

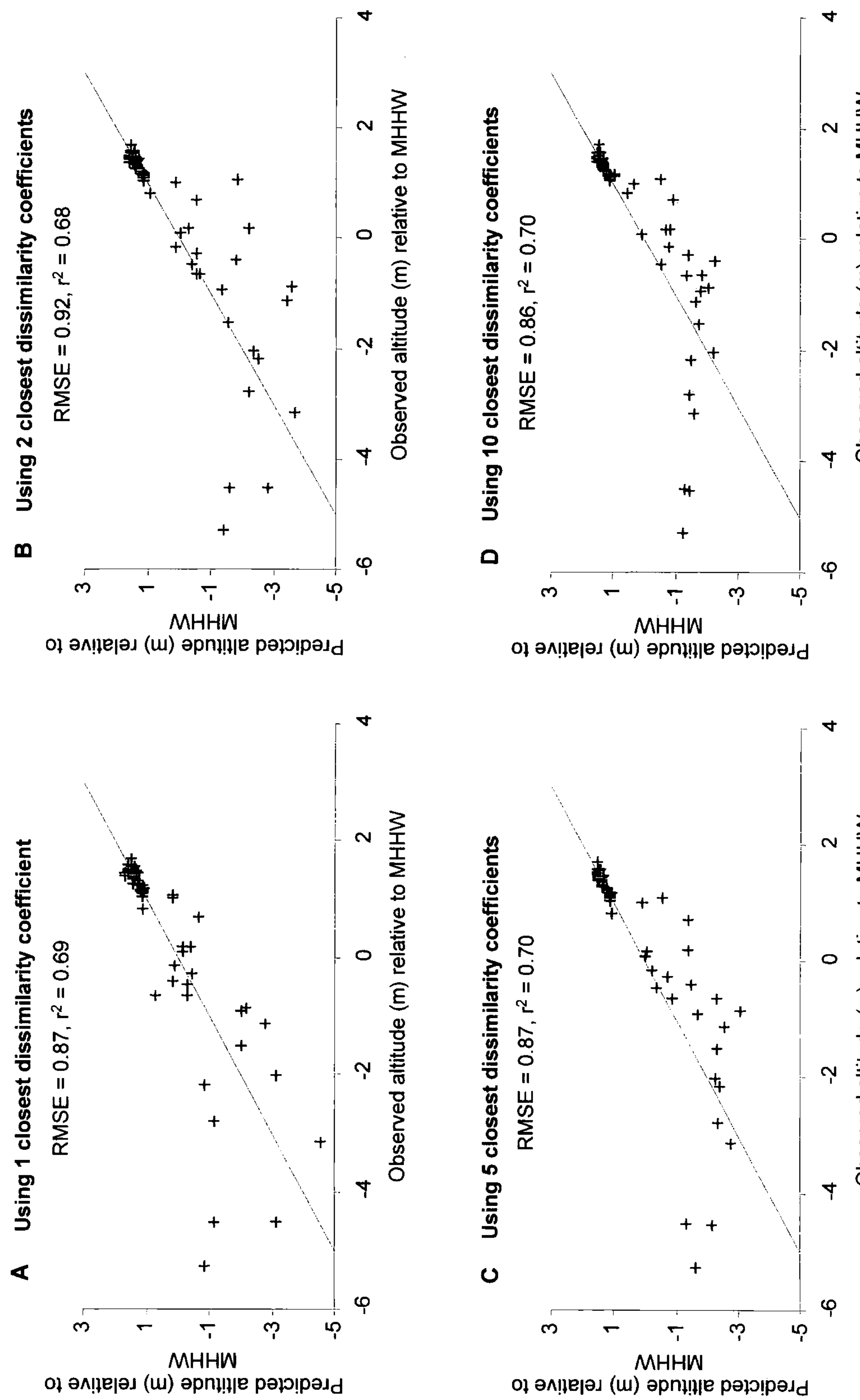

Figure 4.16

Observed against predicted altitude (m) relative to MHHW for contemporary Kenai data using MAT and 1, 2, 5 or 10 closest dissimilarity coefficients

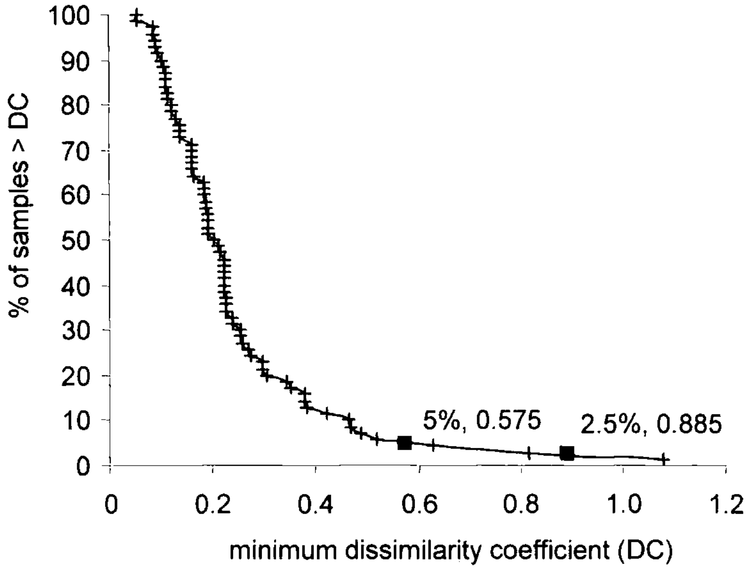

Figure 4.17

Cumulative frequency distribution of MAT minimum dissimilarity coefficients showing the extreme 2.5% and 5% thresholds used to define “good”, “close” and “poor” analogues

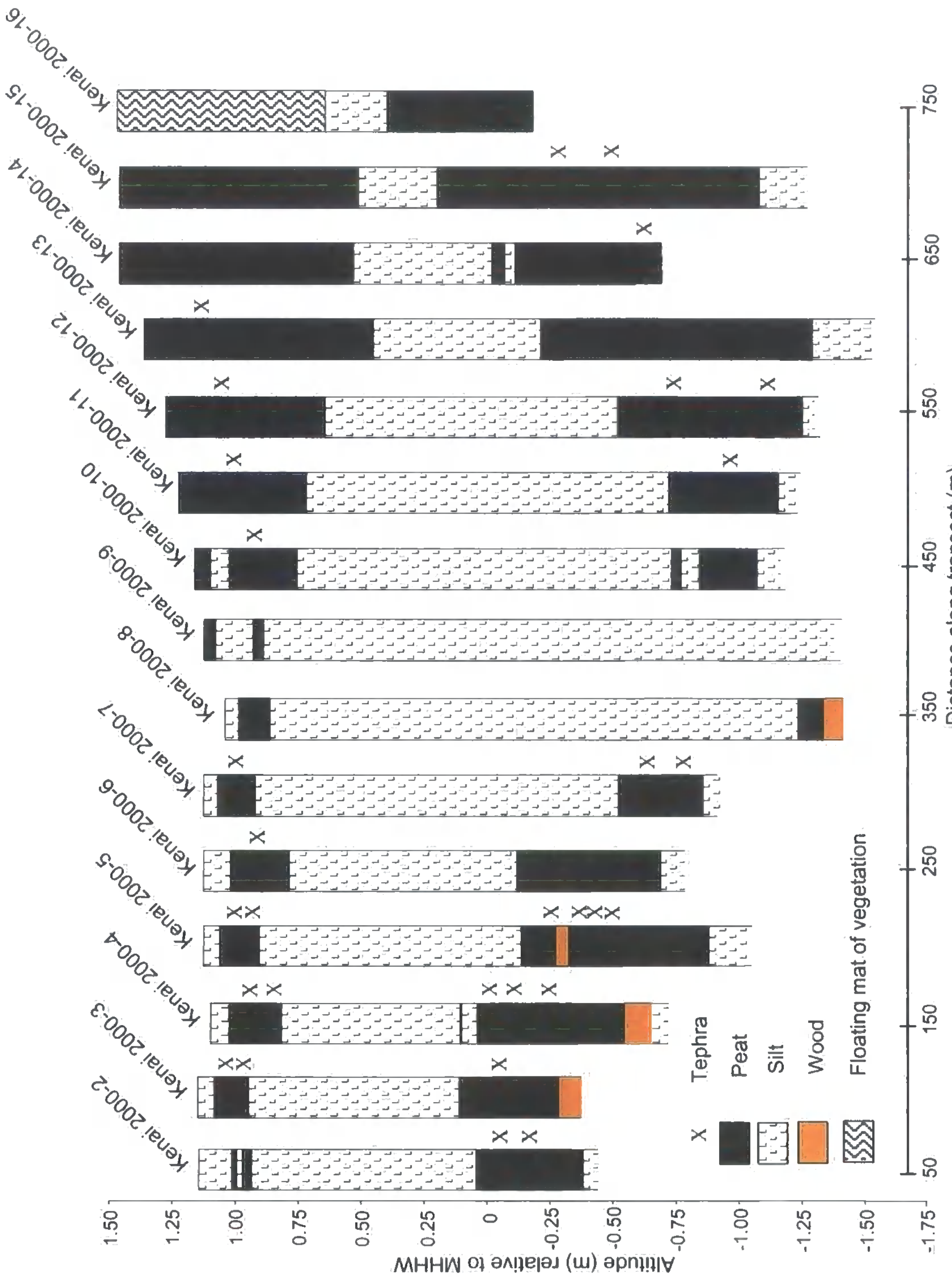

Figure 5.1

Summary litho-stratigraphy at Kenai River Flats

Figure 5.2

Surface vegetation at Kenai 2000-7 consisting of Poaceae, *Carex lyngbyei* and rare *Triglochin maritima*. Dead trees rooted in the uppermost peat layer (figure 5.1) were killed following submergence during the 1964 earthquake

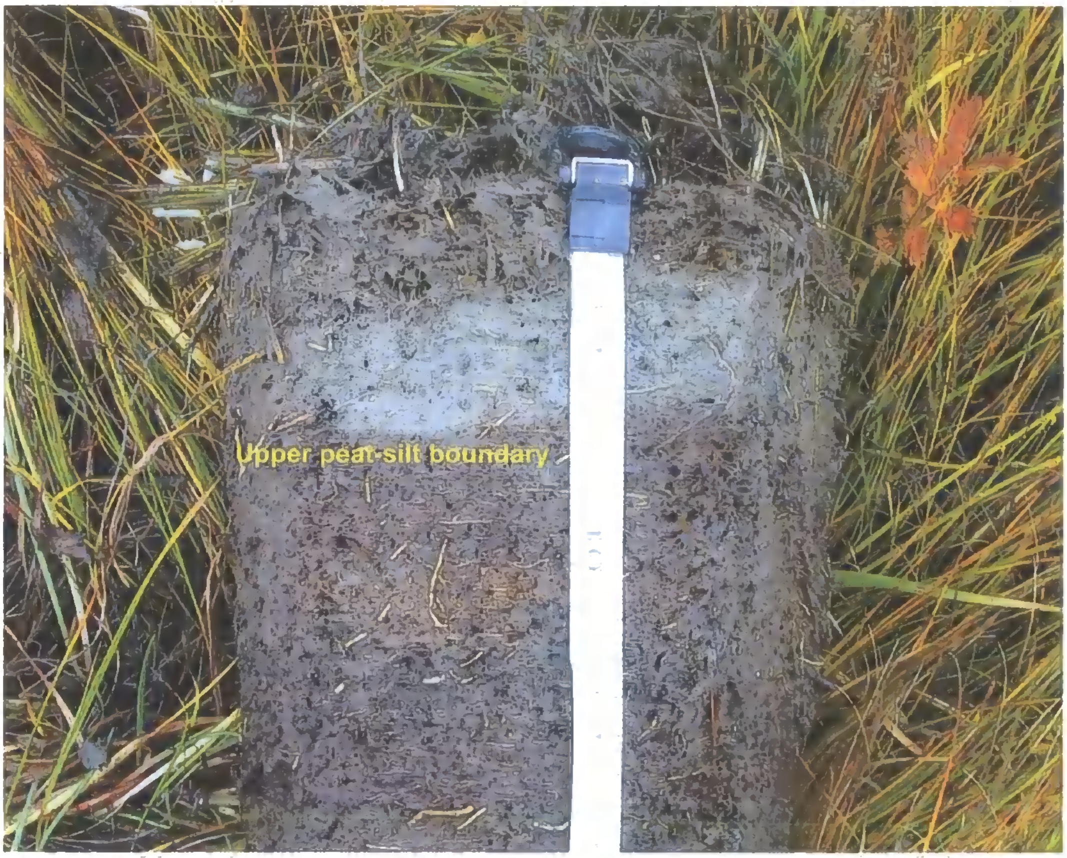

Figure 5.3

Lithology of Kenai 2000-7 showing the upper peat-silt boundary that represents co-seismic submergence during the 1964 earthquake. This sample was taken within 1 m of the monolith used for laboratory analyses, hence slightly different depth values

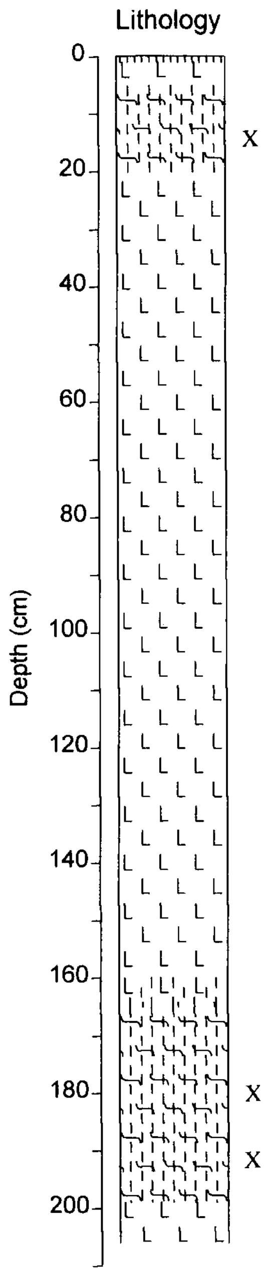

Depth (cm)	Description
0-1.5	Silty peat and modern root layer $Th^{0}3$, Ag1, Sh+ 3,0,2,2,-
1.5-5.5	Grey clay silt with herbaceous roots As1, Ag1, $Th^{1}2$ 2,0,2,0,0
5.5-21.5	Brown bryophyte herbaceous peat $Tb^{2}3$, $Th^{2}1$, Sh+, Dl+ 3,0,2,2,2 tephra @ 14 cm
21.5-160.5	Grey silt with occasional rootlets Ag4, Th^{3}+ 2,0,2,0,1
160.5-163.5	Grey silt with herbaceous rootlets Ag3, $Th^{2}1$ 2,0,2,0,0
163.5-165.5	Herbaceous peat with silt $Th^{2}2$, Sh1, Ag1 3,0,2,0,0
165.5-198.5	Mottled bryophyte herbaceous peat $Tb^{3}2$, $Th^{2}2$, Sh+ 3,2,2,1,0 Tephra @ 180 cm and 193 cm
198.5-206	Grey silt with rare herbaceous rootlets Ag4, Th+ 2,0,2,0,0

L L Silt | Herbaceous peat
X Tephra | Bryophyte peat

Figure 5.4

Detailed litho-stratigraphy of Kenai 2000-7

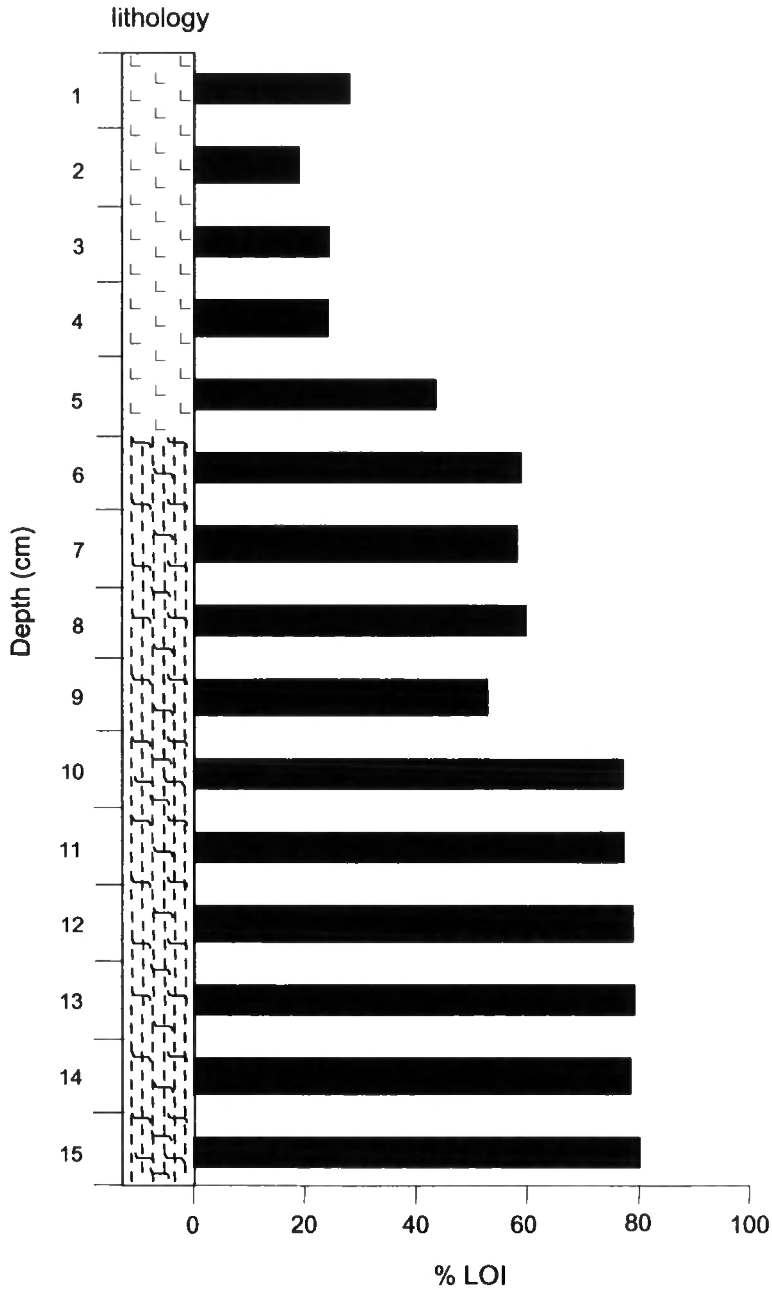

Figure 5.5

Loss on ignition (LOI) values for the upper part of Kenai 2000-7. Lithology symbols as figure 5.4

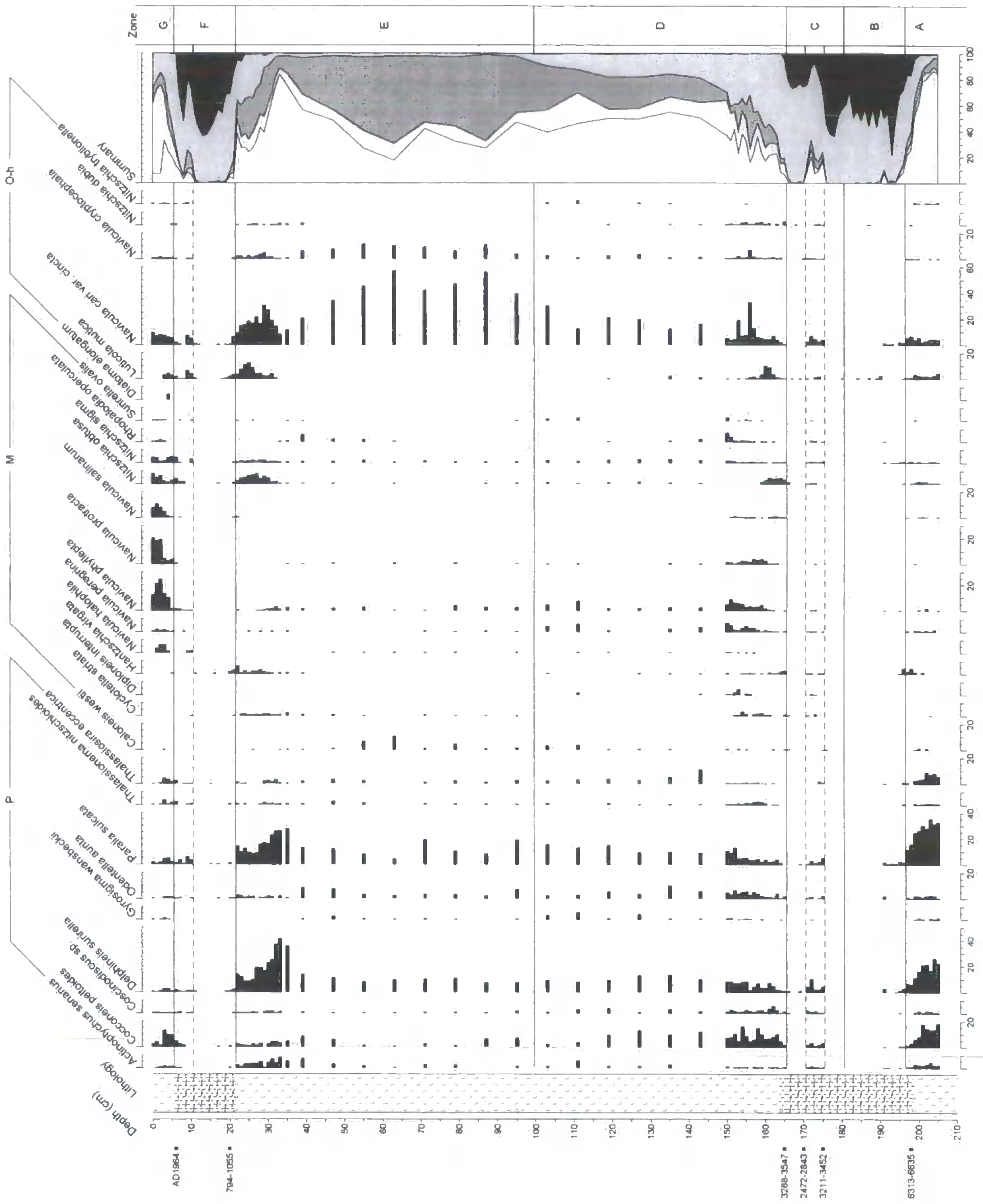

Figure 5.6a

Kenai 2000-7 diatom data (>2% total diatom valves) showing polyhalobian (P), mesohalobian (M) and oligohalobian-halophile (O-h) salinity classes, ordered left to right in summary graph with oligohalobian-indifferent (O-i) and halophobe (H)

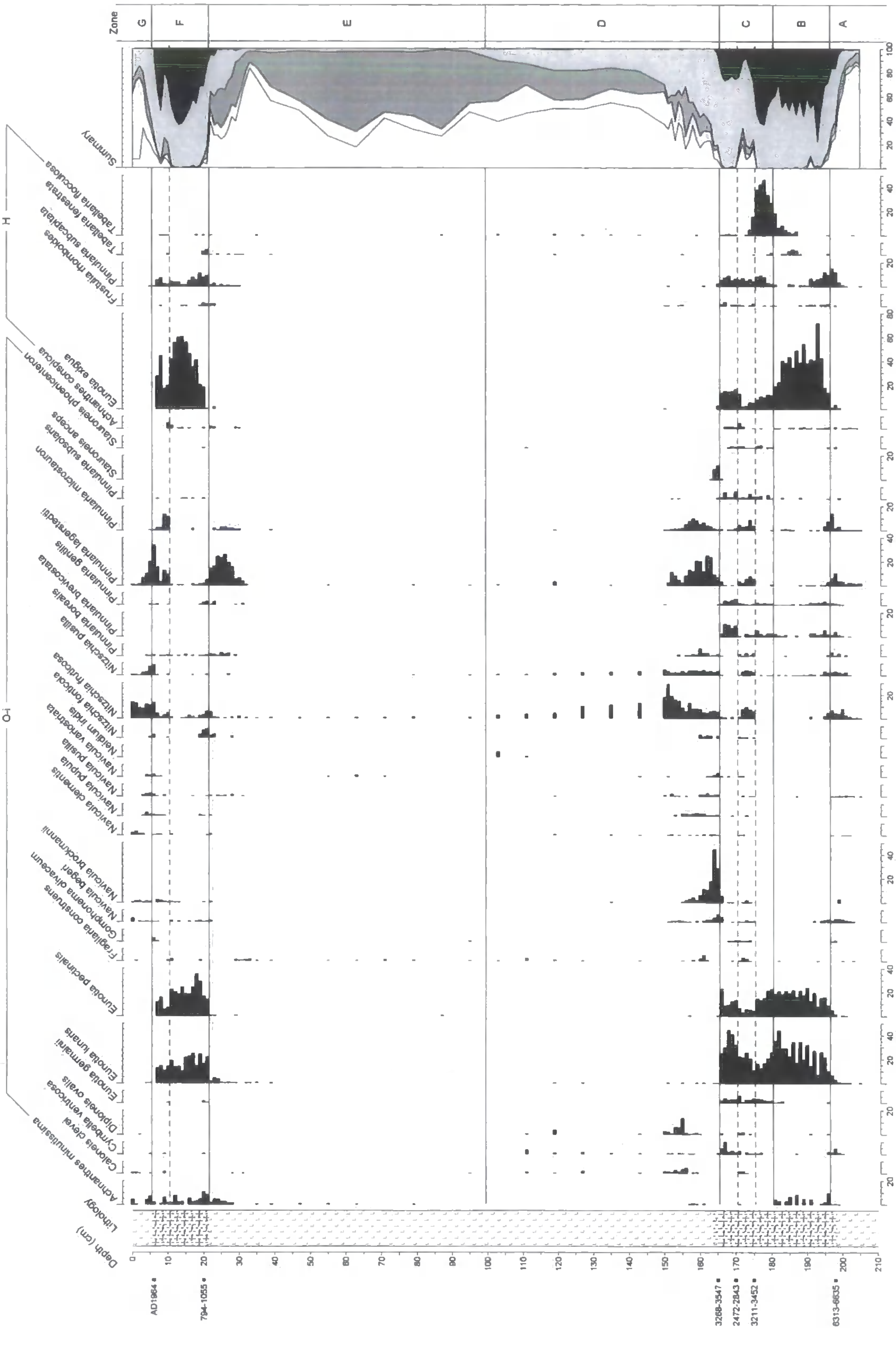

Figure 5.6b

Kenai 2000-7 diatom data (>2% total diatom valves) showing oligohalobian-indifferent (O-i) and halophobe (H) salinity classes, ordered left to right in summary graph after polyhalobian (P), mesohalobian (M) and oligohalobian-halophile (O-h)

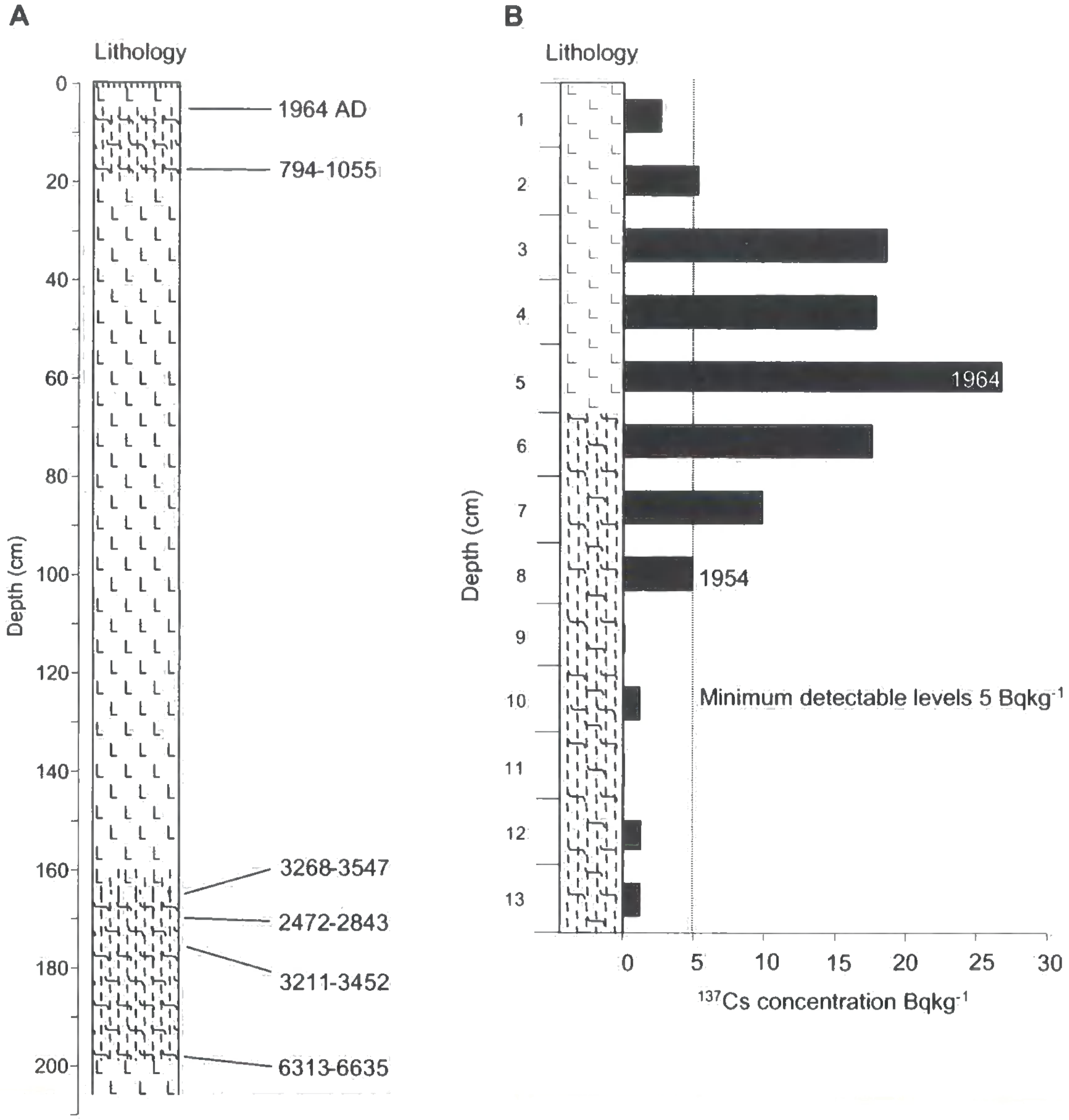

Figure 5.7

Chrono-stratigraphy of Kenai 2000-7 (a) radiocarbon results (cal yr BP) and (b) ^{137}Cs results

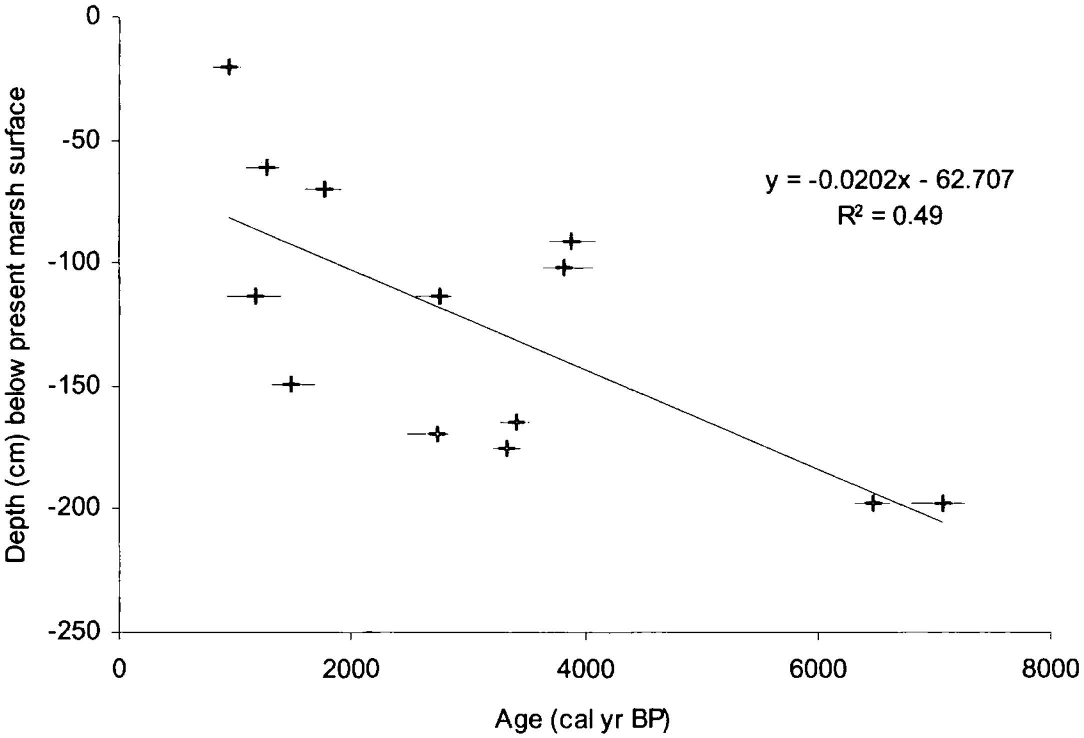

Figure 5.8

Radiocarbon dates for Kenai from this study (values in red) compared to re-calibrated dates of Combellick and Reger (1994, values in black) showing median age and 95% range.

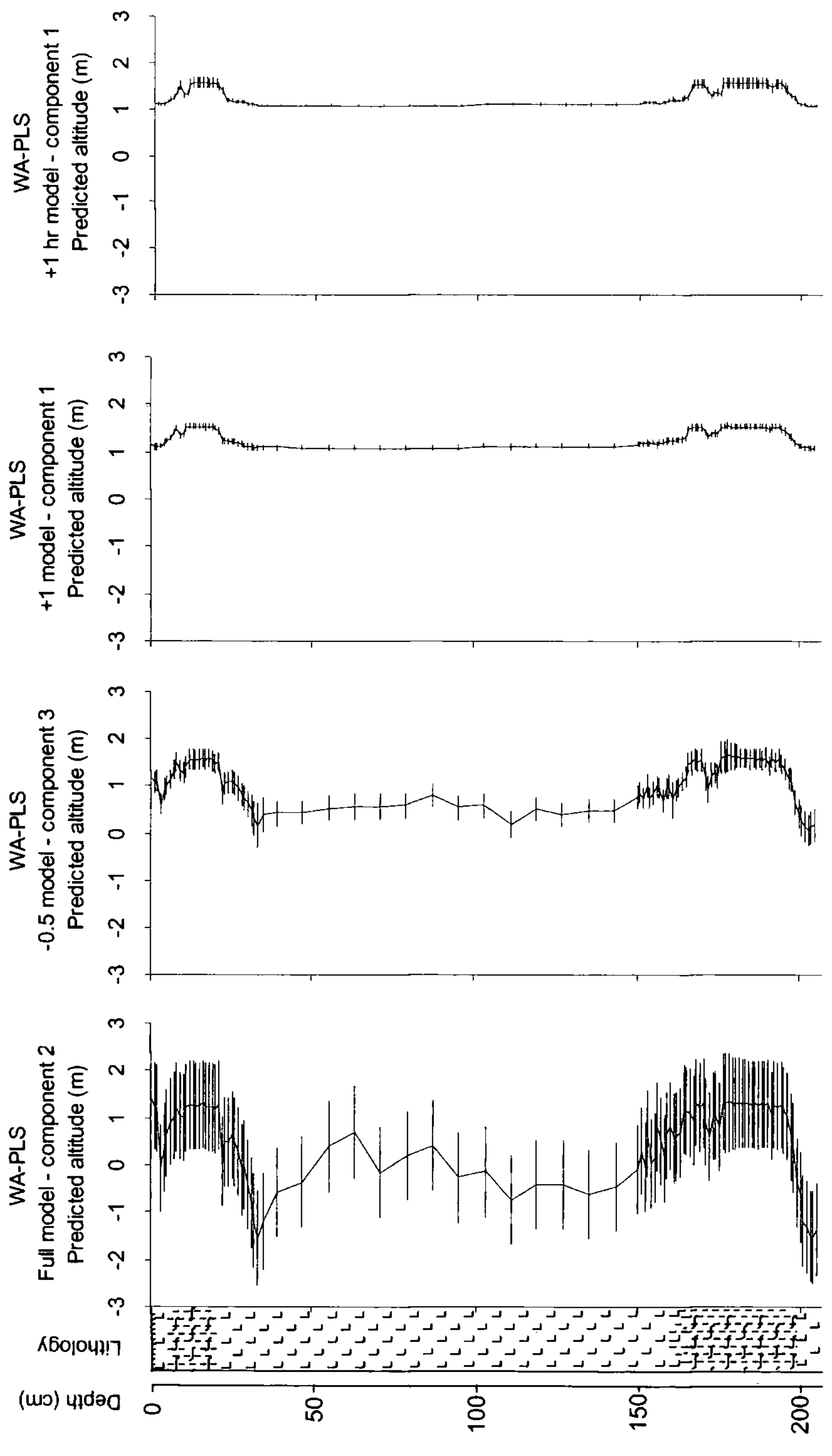

Figure 5.9

Calibration results for Kenai 2000-7 using the full model, samples above -0.5 m MHHW and samples above +1.0 m for both altitude (m) relative to MHHW and hours inundated per year (back calculated to altitude)

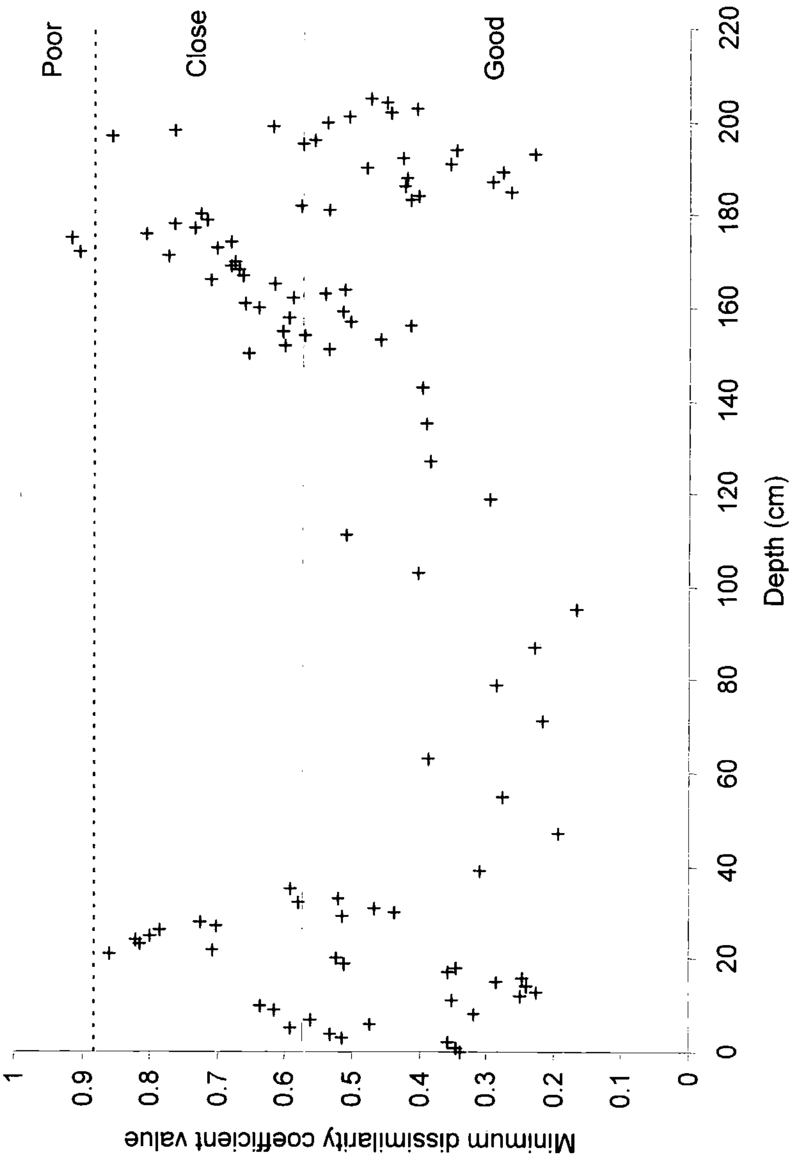

Figure 5.10

Minimum dissimilarity coefficient values from MAT for Kenai 2000-7

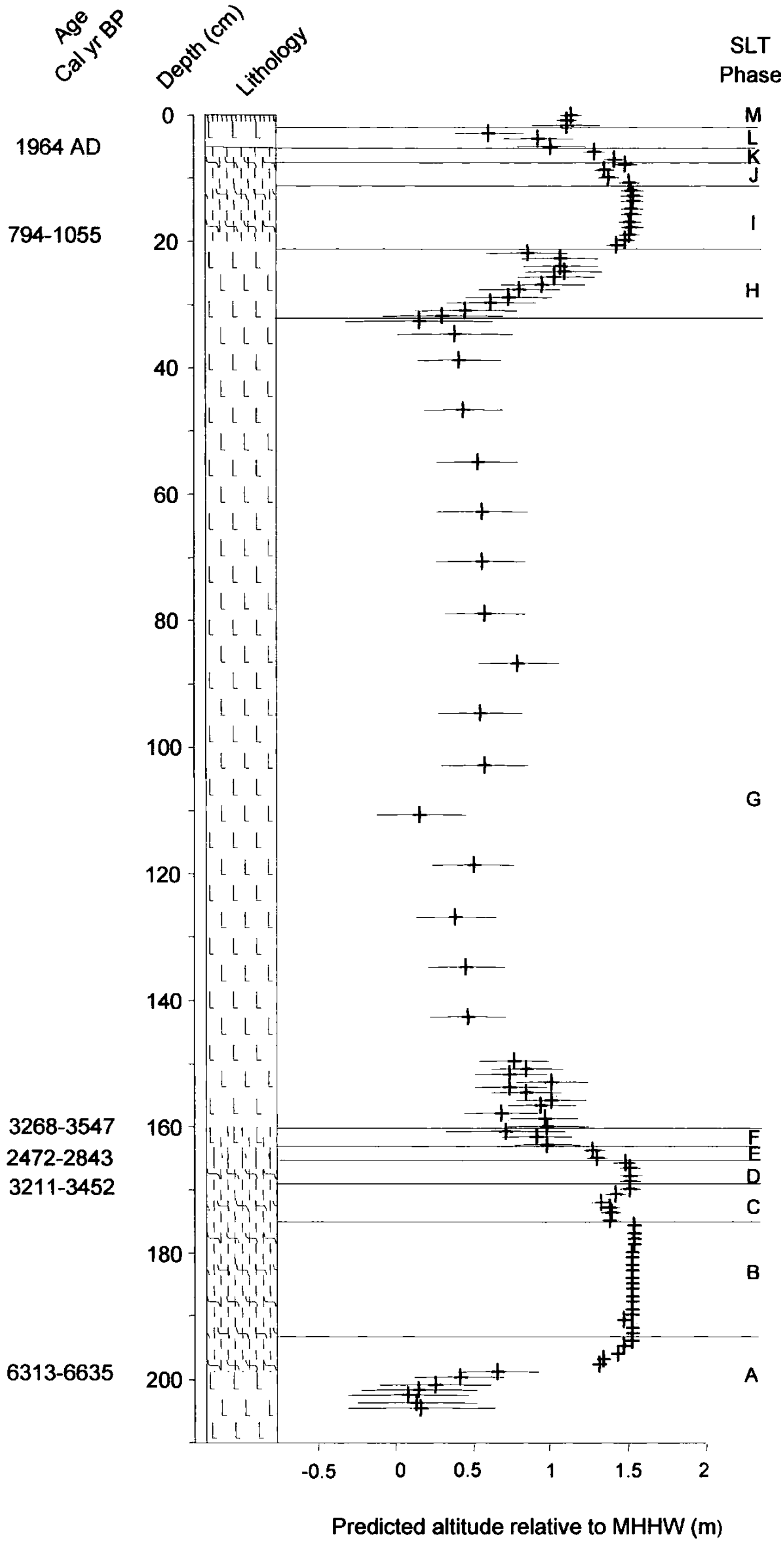

Figure 5.11

Reconstruction of relative sea-level change for Kenai 2000-7 using the best combination of models (table 5.2). Samples in red have 'poor' modern analogues

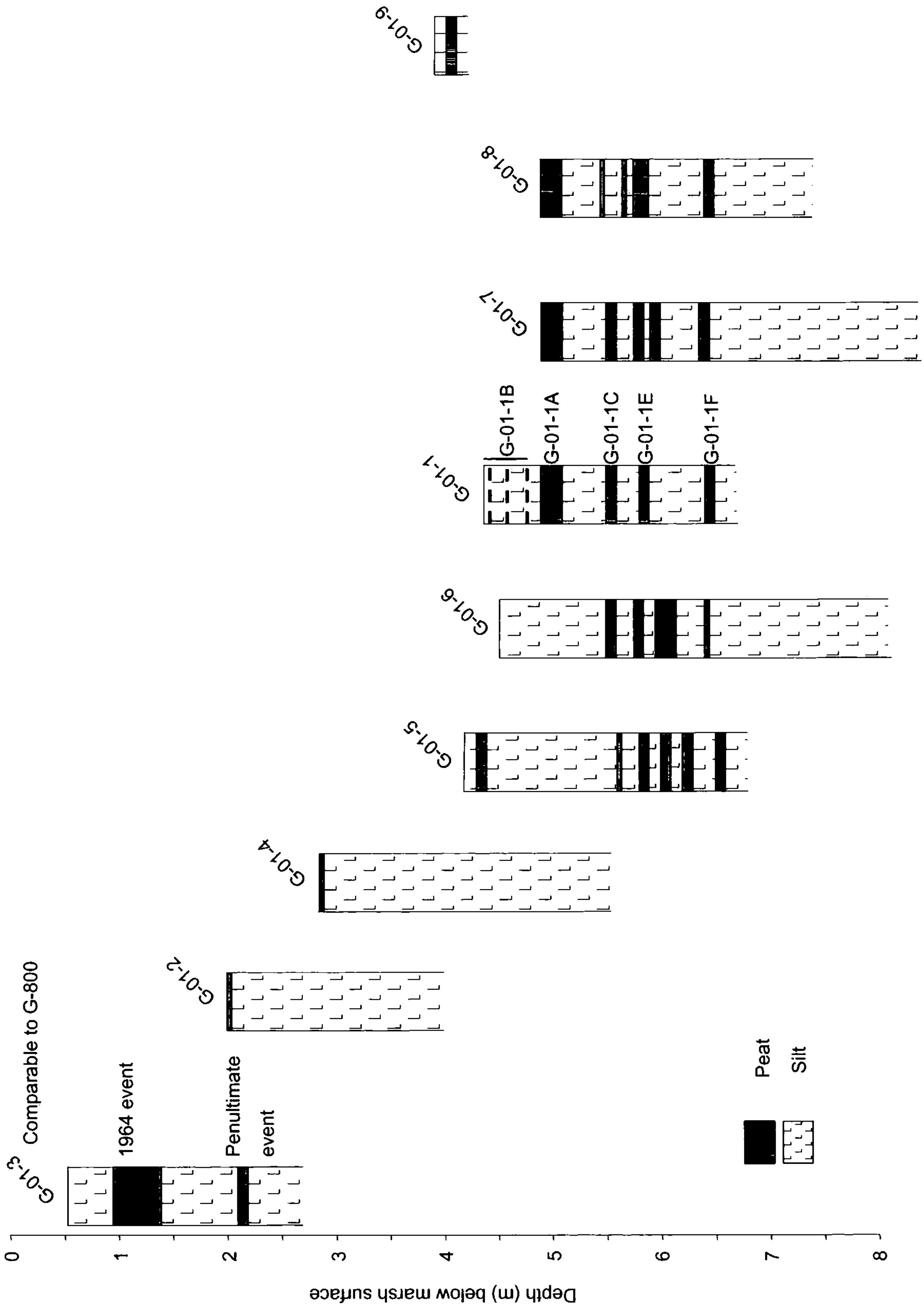

Figure 6.1

Summary litho-stratigraphy at Girdwood

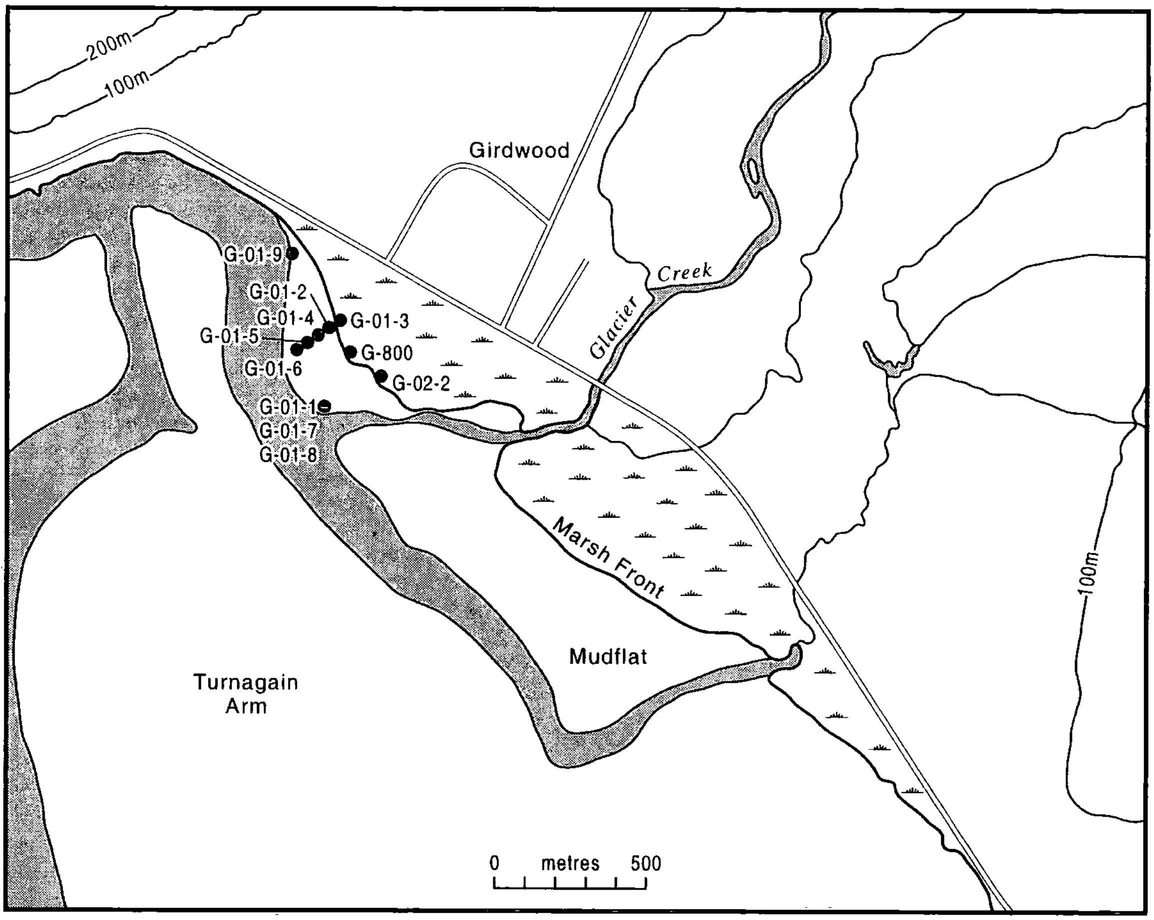

Figure 6.2

Location of sampling sites at Girdwood

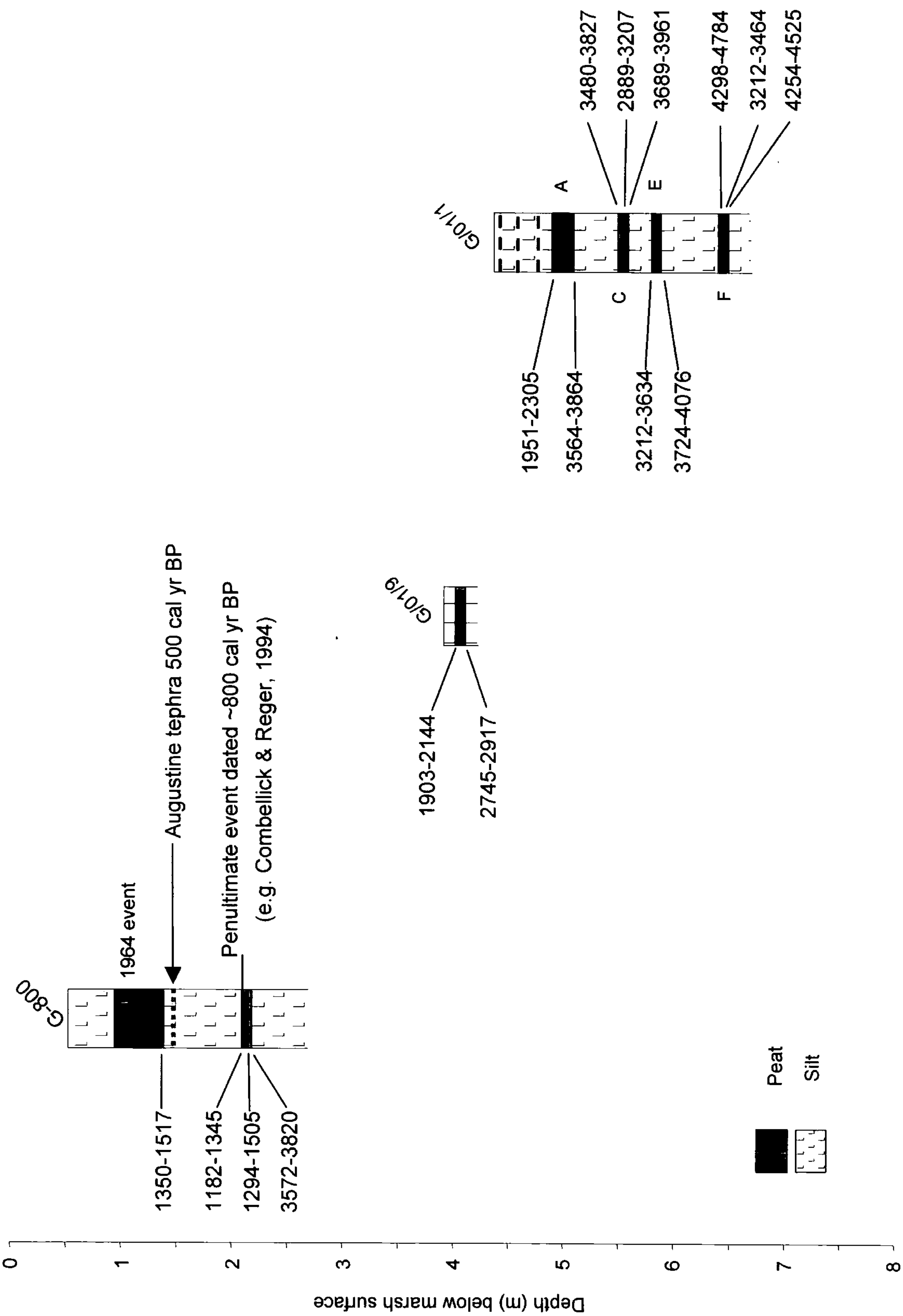

Figure 6.3

Chrono-stratigraphy of Girdwood G-800, G-01-1 and G-01-9 (cal yr BP)

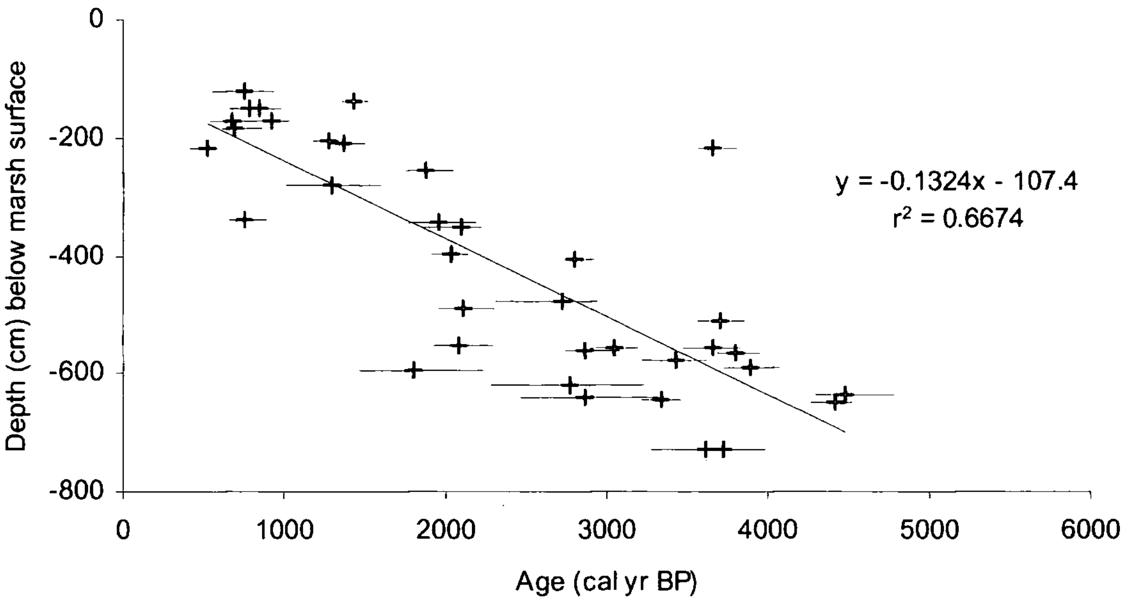

Figure 6.4

Radiocarbon dates for Girdwood from this study (values in red) compared to re-calibrated dates of Combellick and Reger (1994, values in black) showing median age and 95% range

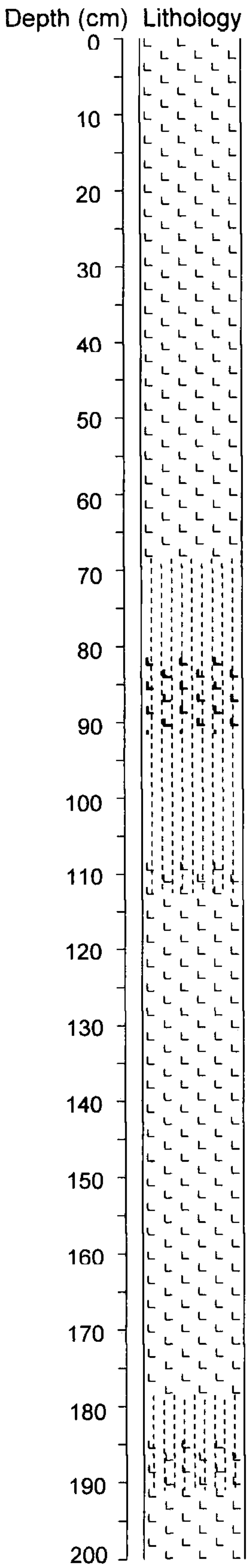

Depth (cm)	Description
0-30	Grey silt with herbaceous rootlets Ag3, As1, Th^1+ 2,0,2,0,-
30-55	Grey silt with herbaceous rootlets with slight sand increase Ag4, Th^2+, Ga++ 2,0,2,0,0
55-68.5	Grey silt with herbaceous rootlets and trace of sand Ag4, Th^2++, Ga+ 2,0,2,0,0
68.5-81.5	Brown herbaceous peat $Th^2$3, Sh1 3,0,2,+,4
81.5-91.5	Brown herbaceous peat with slight increase in silt content $Th^2$2, Sh1, Ag1 3,0,2,0,0
91.5-108.5	Brown herbaceous peat $Th^2$3, Sh1 3,0,2,+,0
108.5-112.5	Silty herbaceous peat $Th^2$3, Ag1 2,0,2,0,0
112.5-150	Grey silt with herbaceous rootlets Ag3, As1, Th^2+ 2,0,2,0,0
150-178.5	Grey silt with herbaceous rootlets with trace of sand Ag3, As1, Th^2++, Ga+ 2,0,2,0,0
178.5-184.5	Brown herbaceous peat, sharp upper contact $Th^3$2, Sh2 3,0,2,+,4
184.5-188.5	Silty peat with herbaceous rootlets $Th^3$2, Sh1, Ag1 2,0,2,0,0
188.5-194.5	Peaty silt Ag3, $Th^2$1 2,0,2,0,0
194.5-200	Grey silt with herbaceous rootlets Ag3, As1, Th^2+ 2,0,2,0,0 Core ends in this unit

L L Silt   I I I Herbaceous peat

Figure 6.5a

Detailed litho-stratigraphy of Girdwood G-800

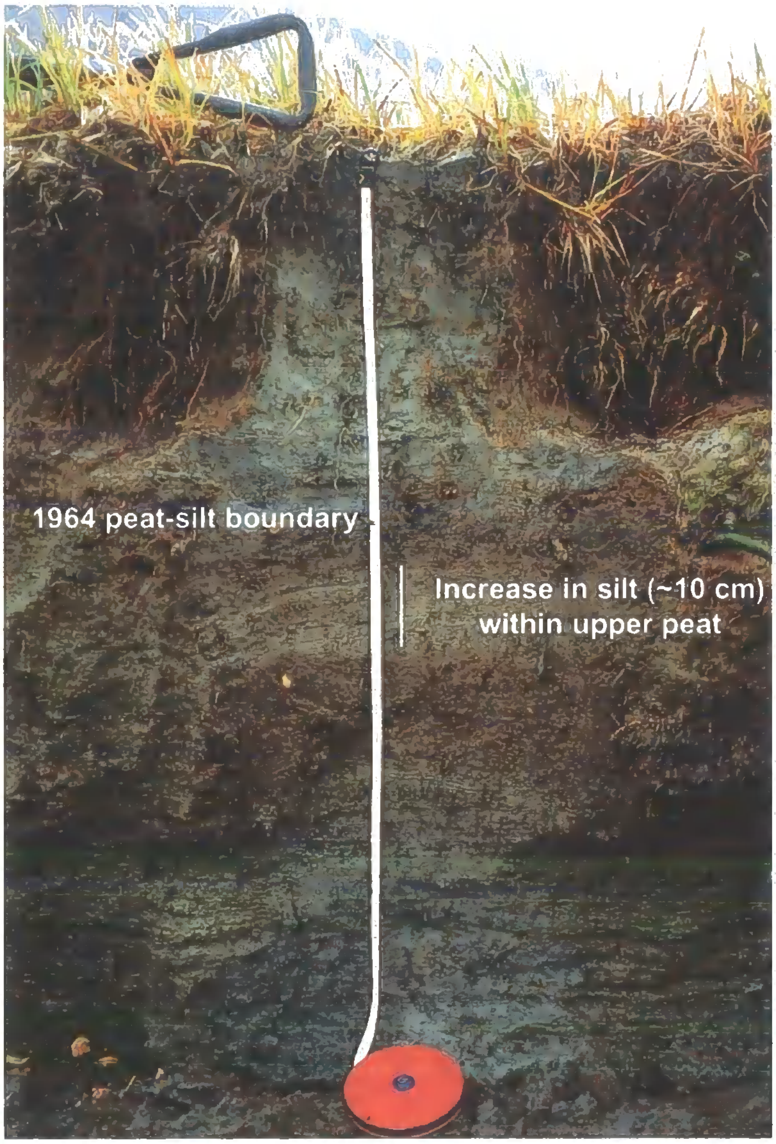

Figure 6.5b

Girdwood G-02-2 showing increase in silt content (~10 cm) within the upper peat layer. This section was not exposed during sampling in 2000 and 2001

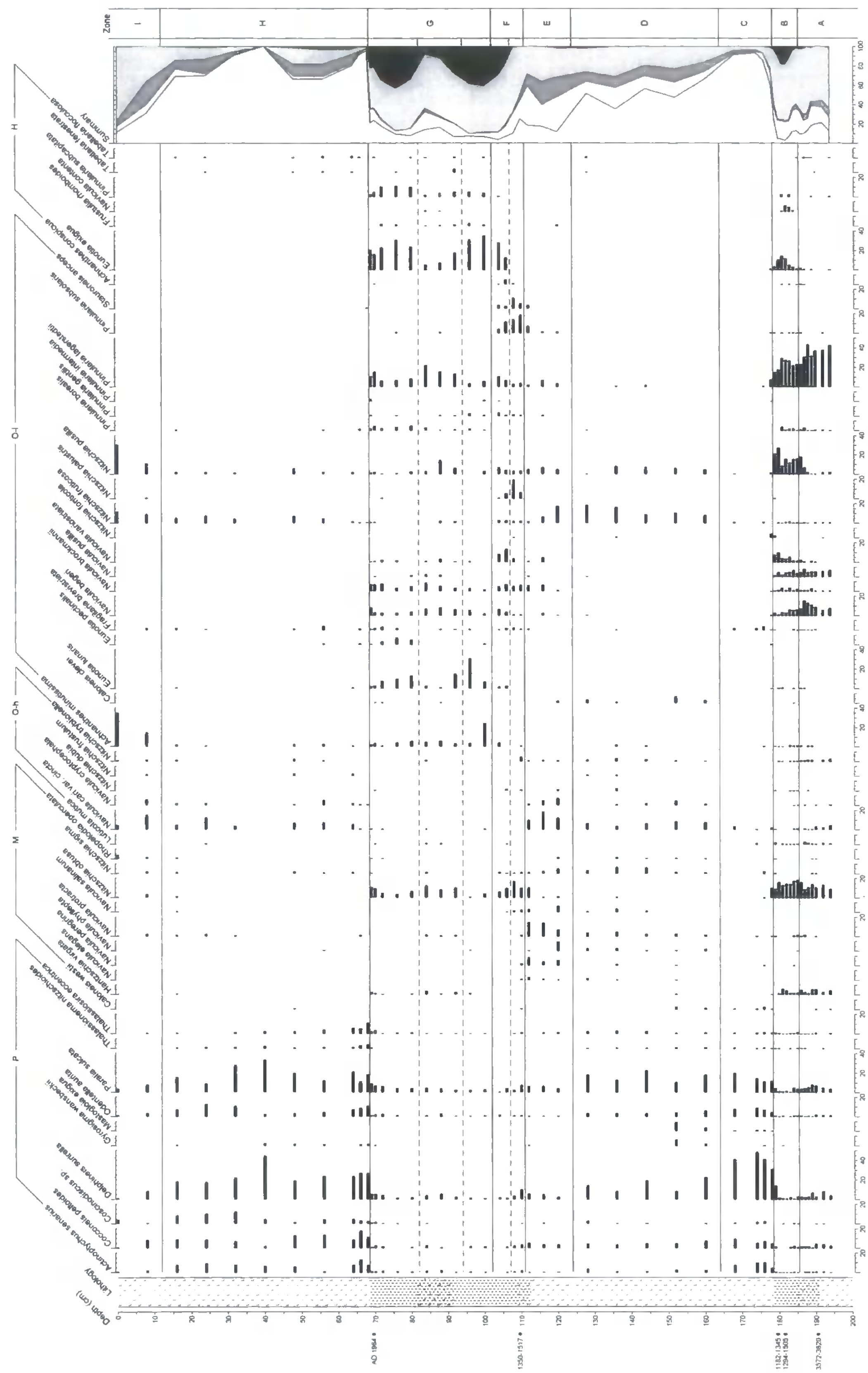

Figure 6.6

Girdwood G-800 diatom data (>2% total diatom valves). Summary salinity classes: polyhalobian (P), mesohalobian (M), oligohalobian-halophile (O-h), oligohalobian-indifferent (O-i), halophobe (H) ordered left to right in summary graph

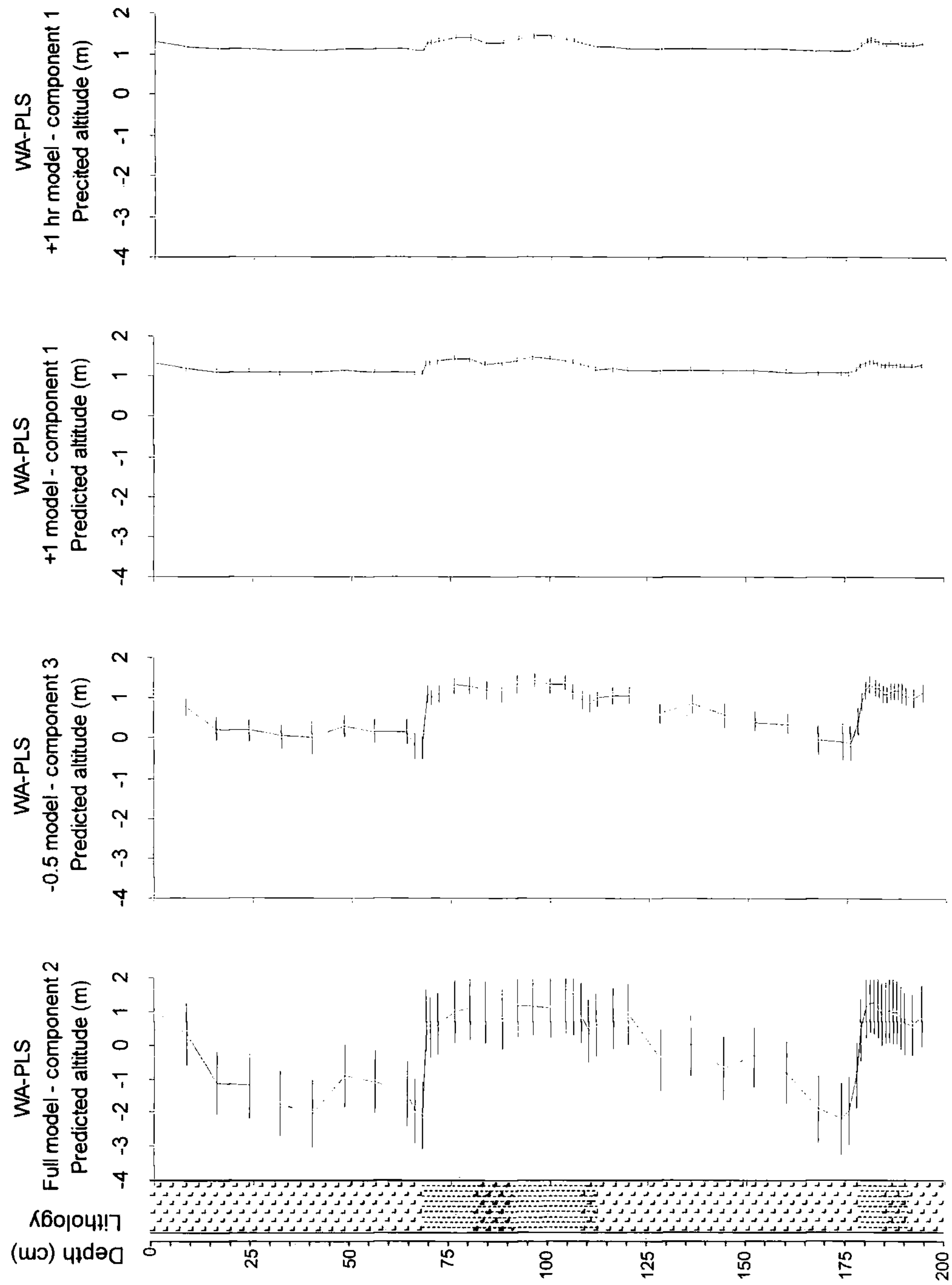

Figure 6.7

Calibration results for Girdwood G-800 using the full model, samples above -0.5 m MHHW and samples above +1.0 m for both altitude (m) relative to MHHW and hours inundated per year (back calculated to altitude)

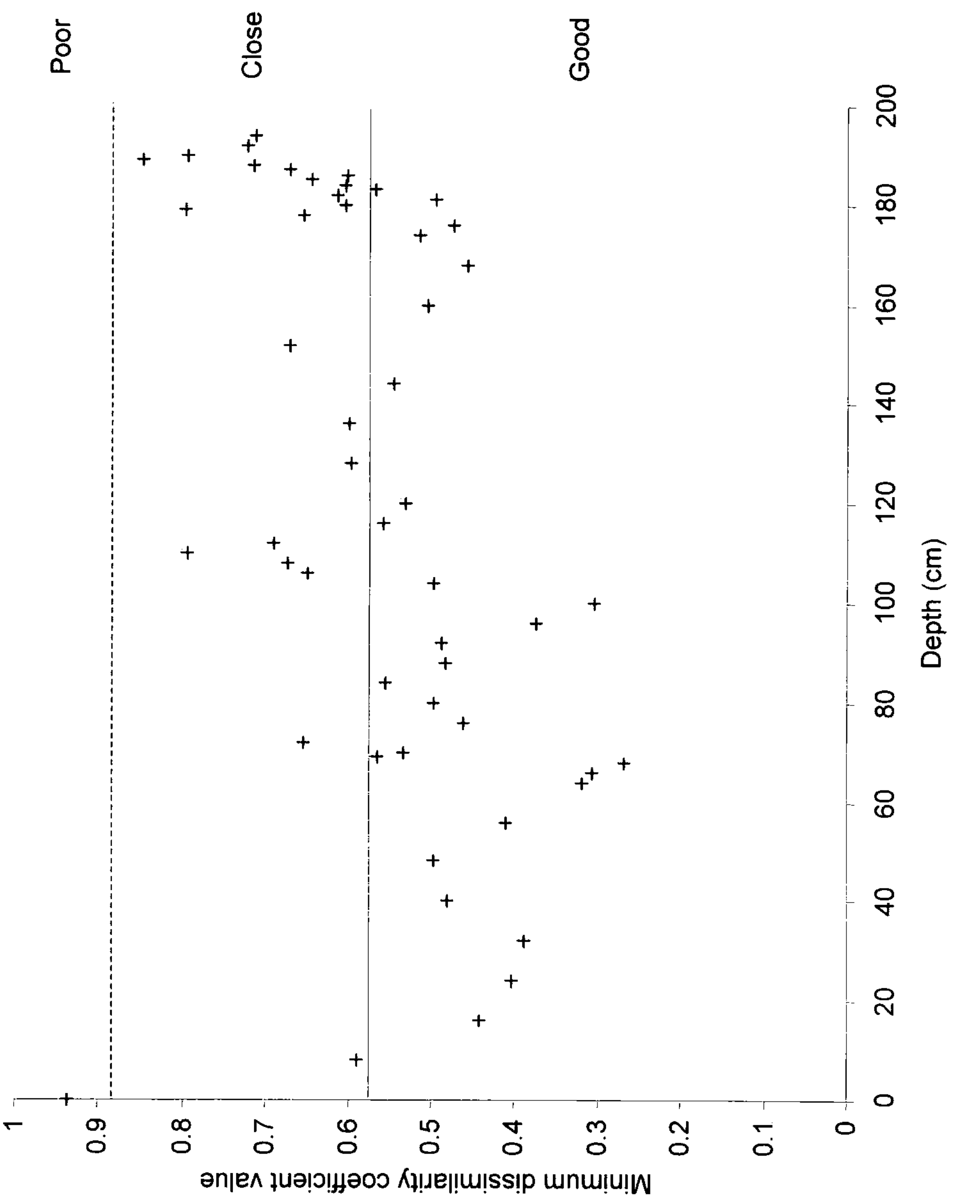

Figure 6.8

Minimum dissimilarity coefficient values from MAT for Girdwood G-800

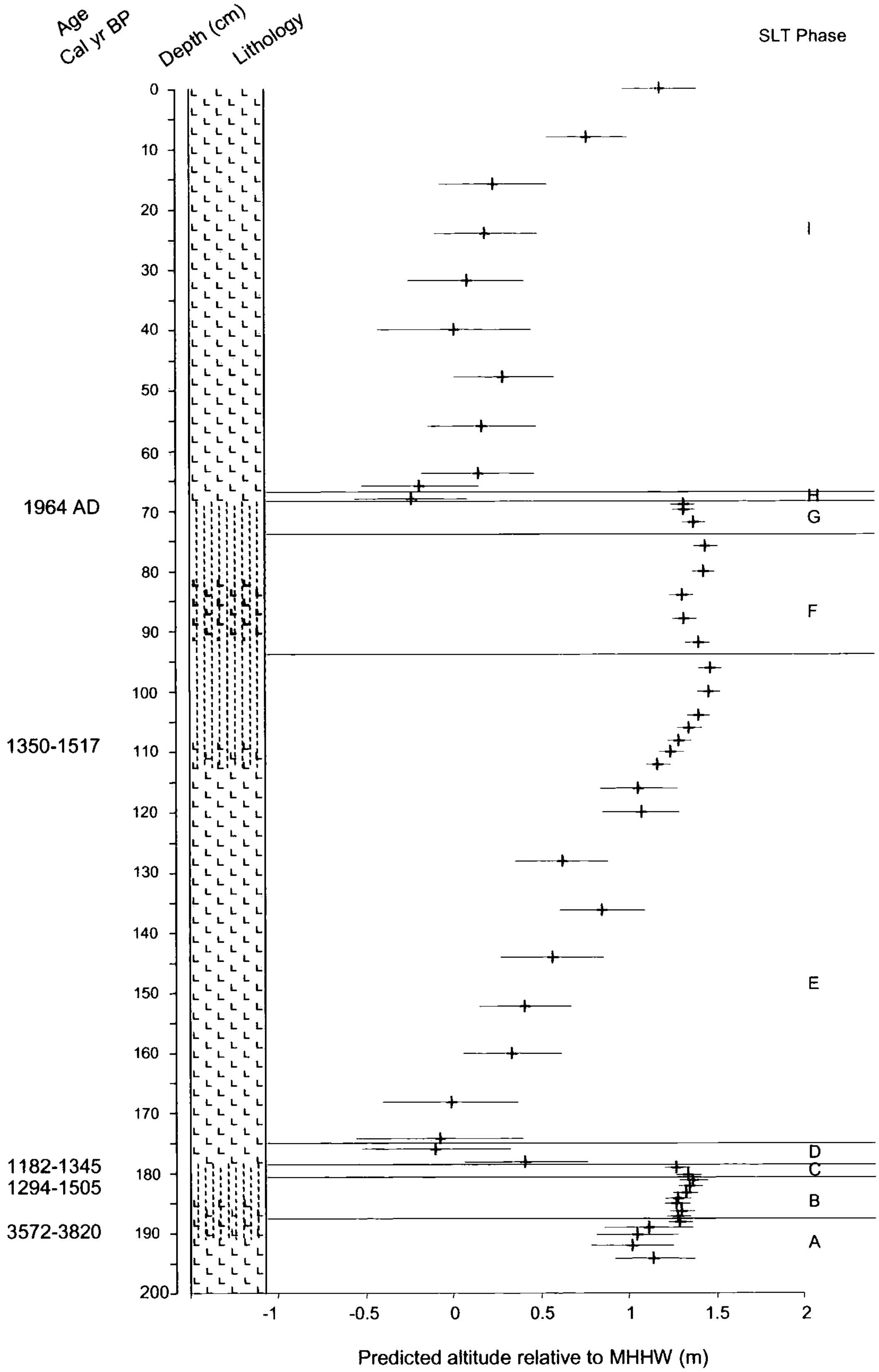

Figure 6.9

Reconstruction of relative sea-level change for Girdwood G-800 using the best combination of models (table 6.4). The sample in red has a 'poor' modern analogue

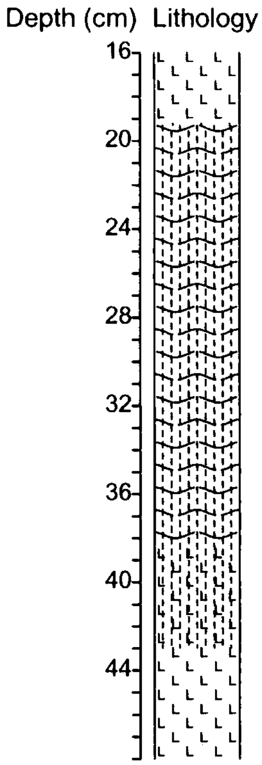

Depth (cm)	Description
0-19.5	Clay silt with occasional rootlets Ag3, As1, Th^2+ 2,0,2,0,-
19.5-38.5	Bryophyte peat with woody and herbaceous rootlets. Sharp upper boundary $Tb^2$3, $Th^2$1, Tl^2+ 3,1,2,2,4
38.5-43.5	Organic silty peat Ag1, As1, $Th^2$1, $Tb^2$1 2+,0,2,0,0
43.5-50	Clay silt with herbaceous rootlets Ag3, As1, Th^2++ 2,0,2,0,0

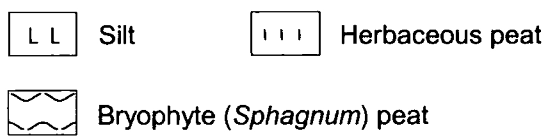

Figure 6.10

Detailed litho-stratigraphy of Girdwood G-01-1A

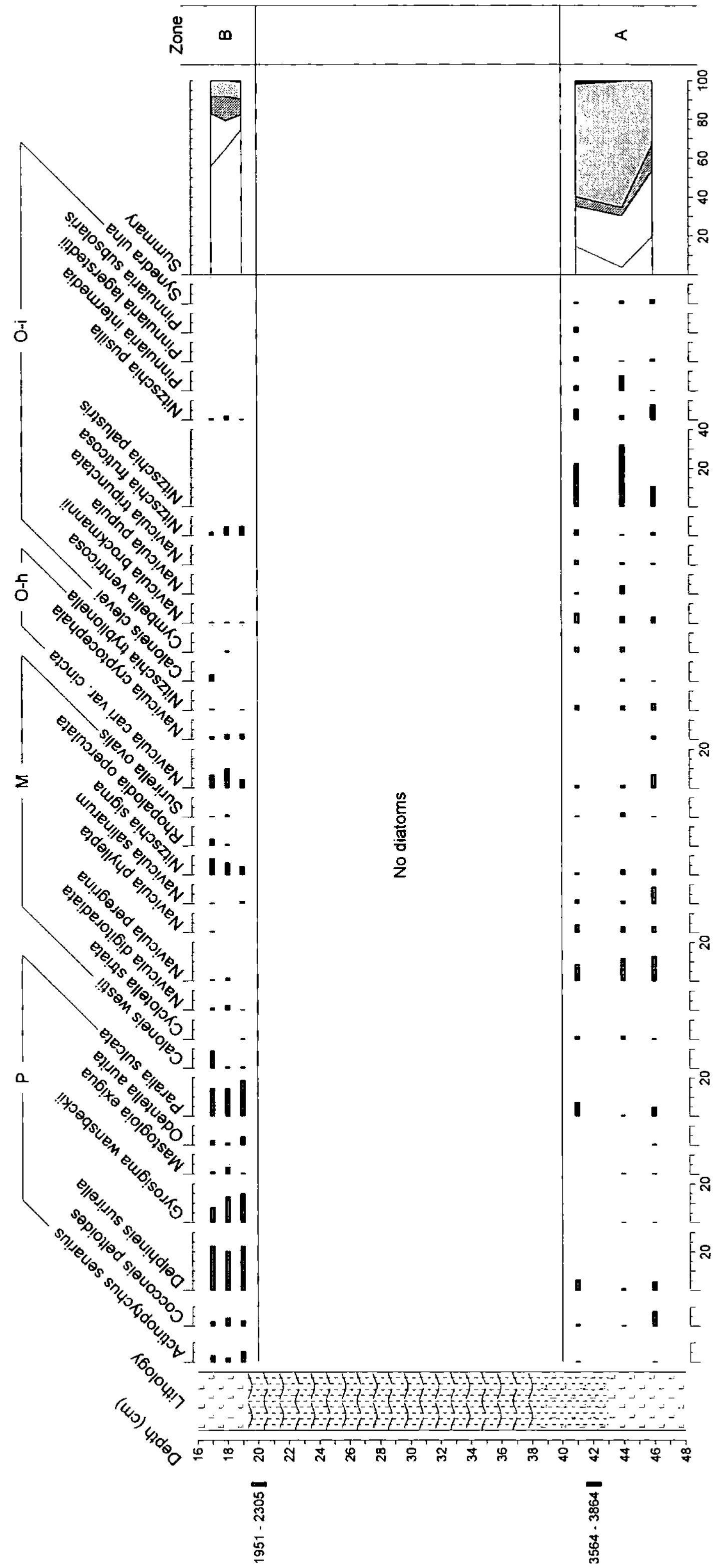

Figure 6.11a

Girdwood G-01-1A diatom data (>2% total diatom valves). Summary salinity classes: polyhalobian (P), mesohalobian (M), oligohalobian-halophile (O-h), oligohalobian-indifferent (O-i), halophobe (H) ordered left to right in summary graph

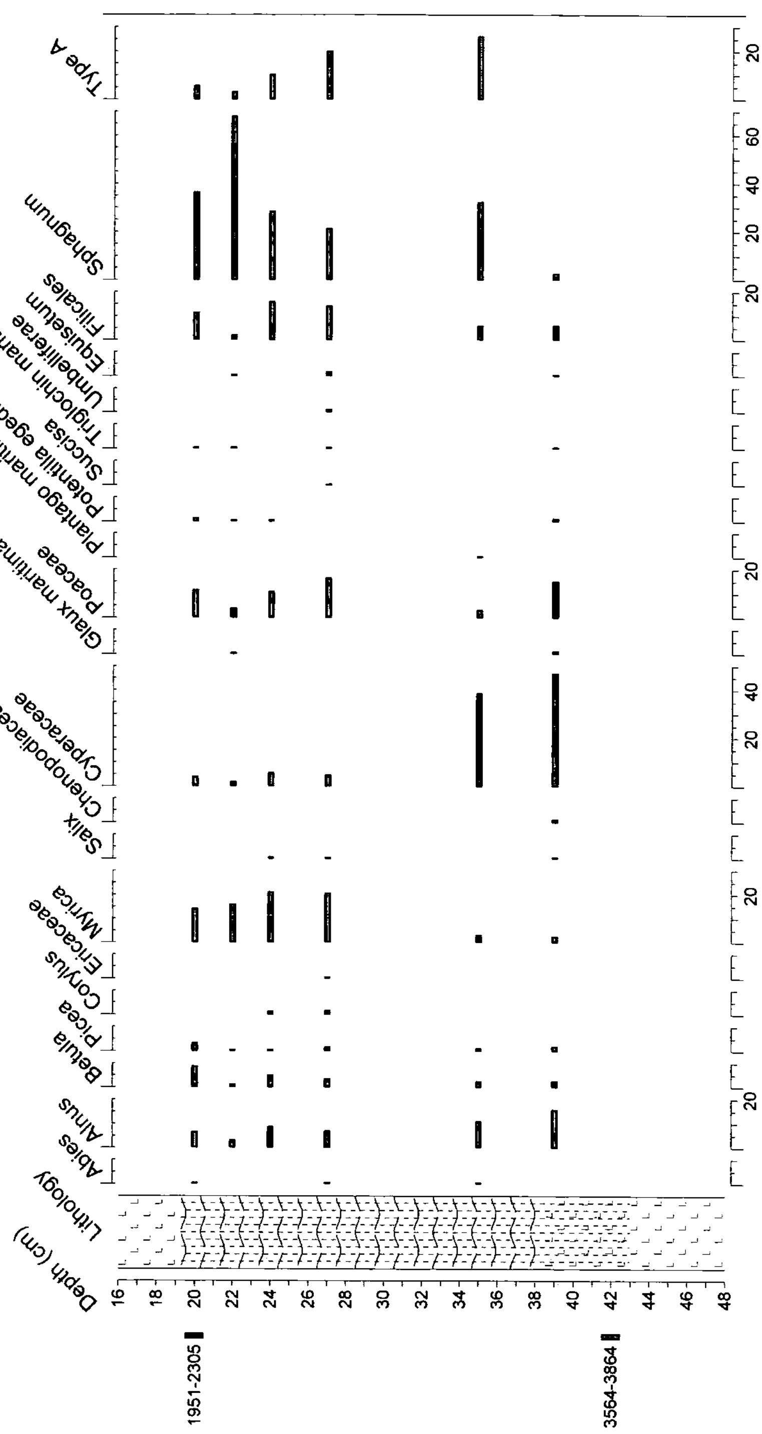

Figure 6.11b

Girdwood G-01-1A pollen data (>2% total pollen, counted by I.Shennan)

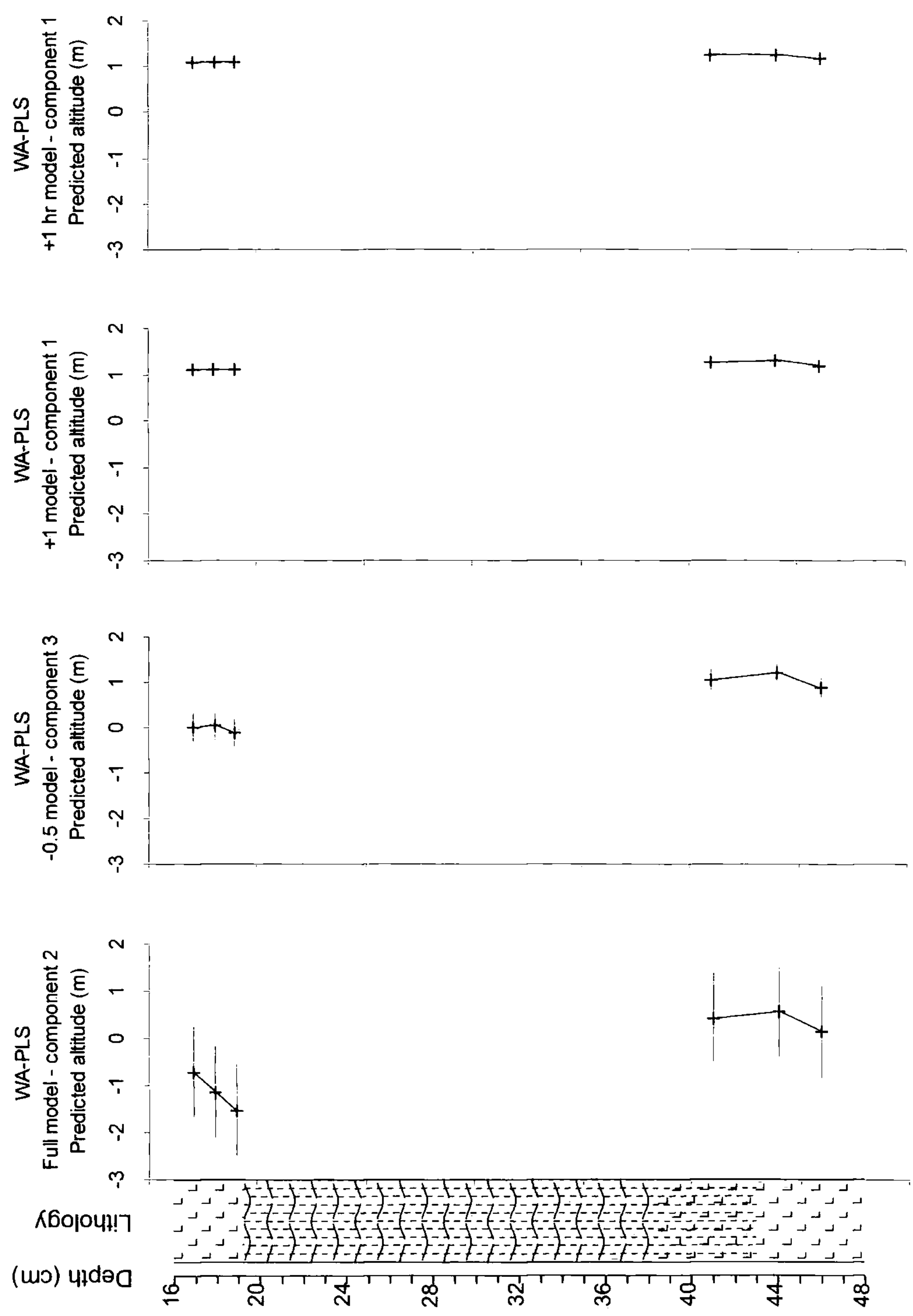

Figure 6.12

Calibration results for Girdwood G-01-1A using the full model, samples above -0.5 m MHHW and samples above +1.0 m for both altitude (m) relative to MHHW and hours inundated per year (back calculated to altitude)

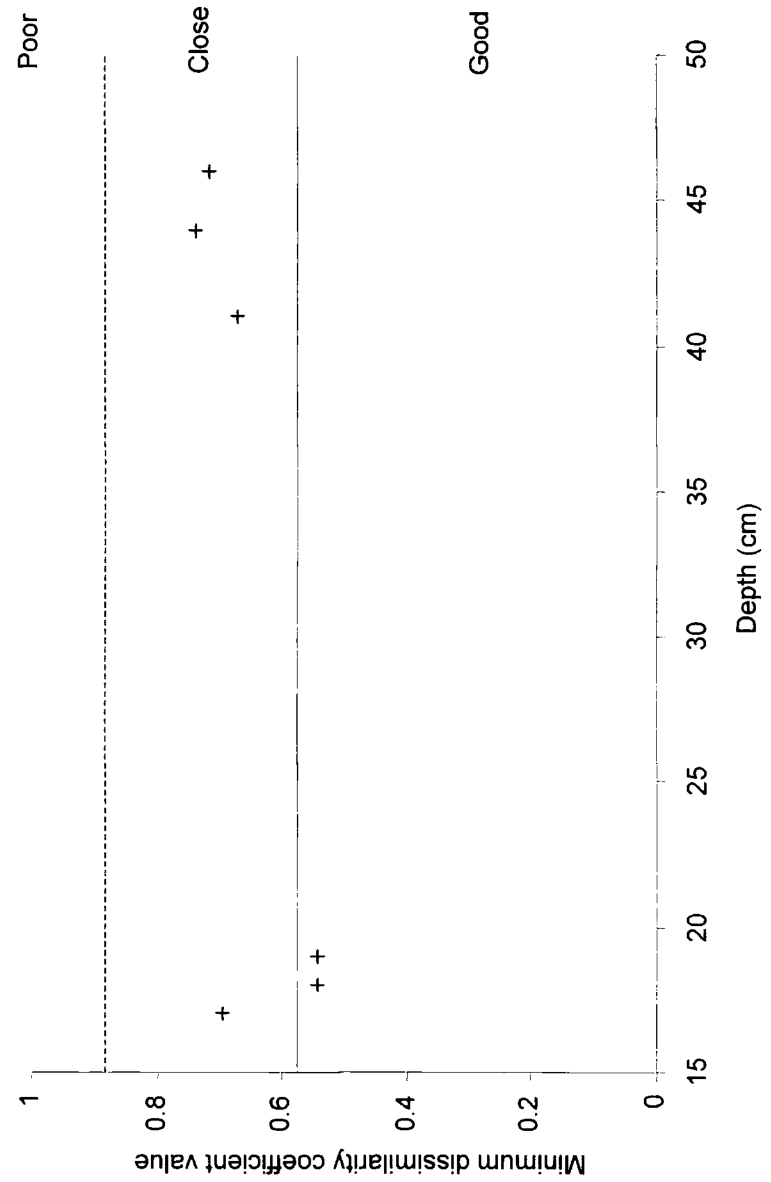

Figure 6.13

Minimum dissimilarity coefficient values from MAT for Girdwood G-01-1A

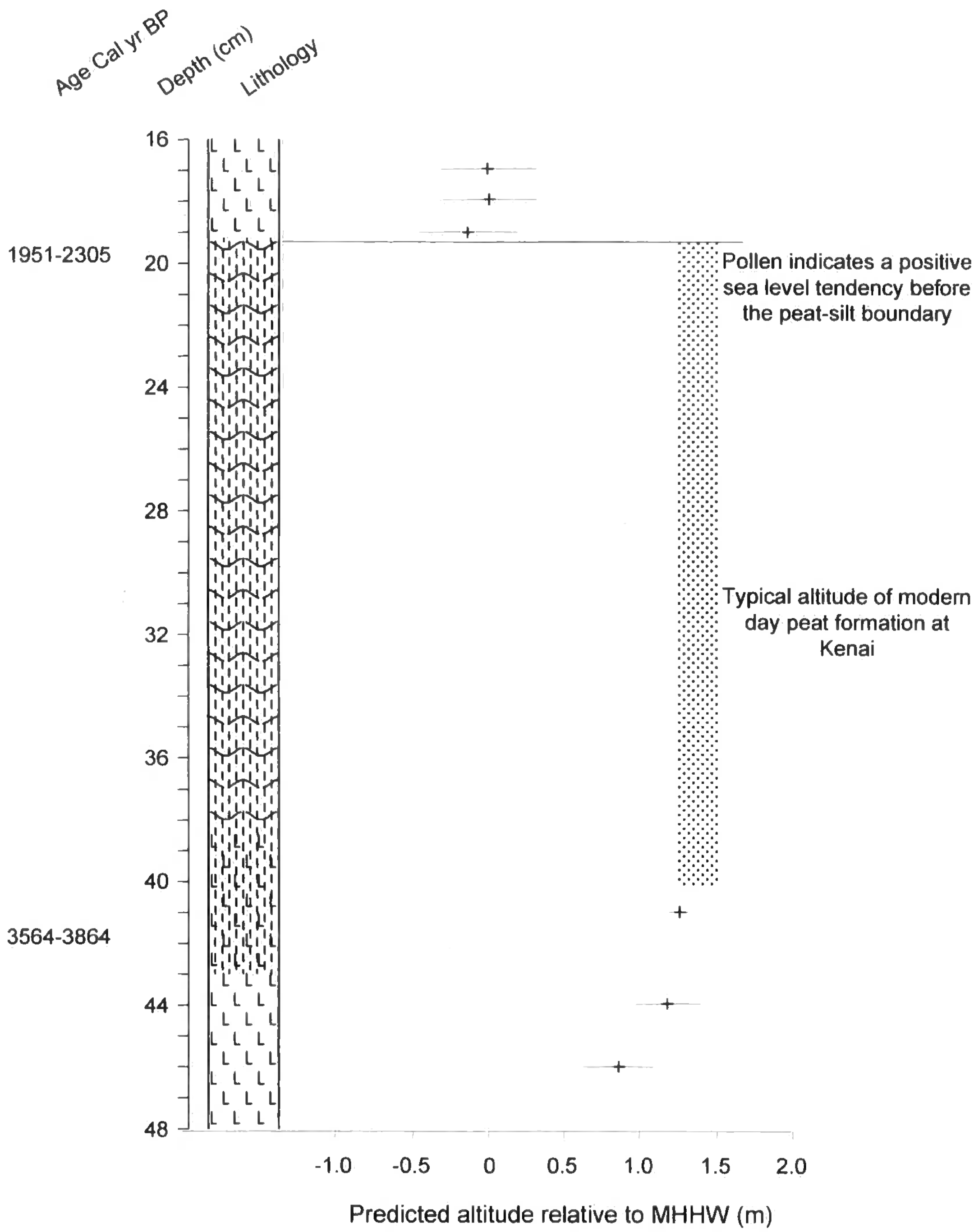

Figure 6.14

Reconstruction of relative sea-level change for Girdwood G-01-1A using the best combination of models (table 6.11). As diatoms are absent throughout the peat layer, pollen indicates it is well developed and probably formed between +1.35 and +1.57 m MHHW

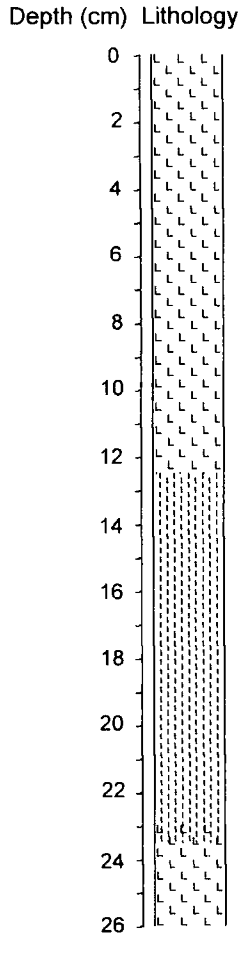

Depth (cm)	Description
0-2.5	Silt with herbaceous rootlets Ag4, Th+ 2,0,2,0,0
2.5-12.5	Grey silt Ag4 2,0,2,0,0
12.5-23.5	Peat with abundant herbaceous rootlets $Th^2 3$, Sh1, Ag+ 3,0,2,0,4
23.5-26	Silt with herbaceous rootlets Ag4, Th+ 2,0,2,0,0

L L Silt   I I I Herbaceous peat

Figure 6.15

Detailed litho-stratigraphy of Girdwood G-01-1C

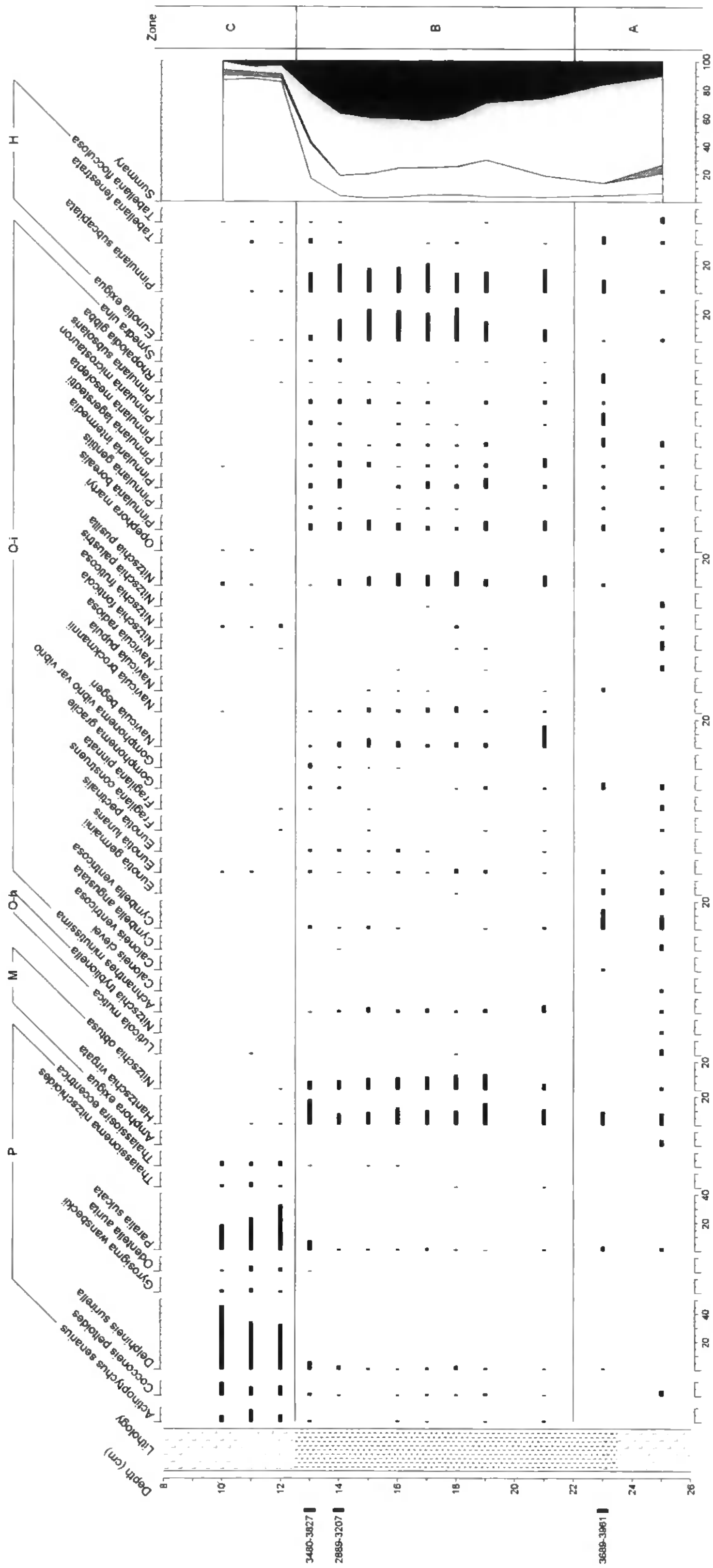

Figure 6.16

Girdwood G-01-1C diatom data (>2% total diatom valves). Summary salinity classes: polyhalobian (P), mesohalobian (M), oligohalobian-halophile (O-h), oligohalobian-indifferent (O-i), halophobe (H) ordered left to right in summary graph

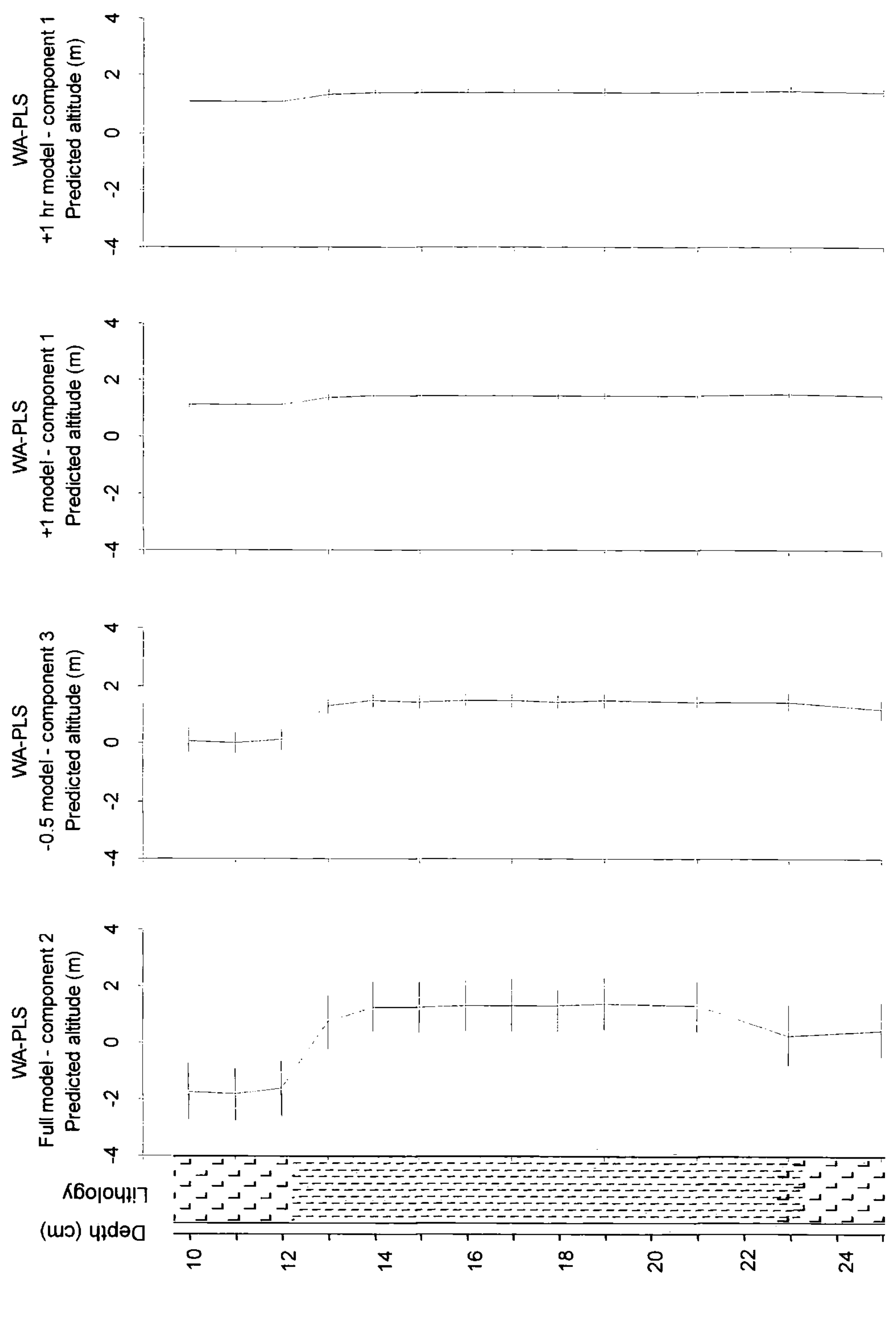

Figure 6.17

Calibration results for Girdwood G-01-1C using the full model, samples above -0.5 m MHHW and samples above +1.0 m for both altitude (m) relative to MHHW and hours inundated per year (back calculated to altitude)

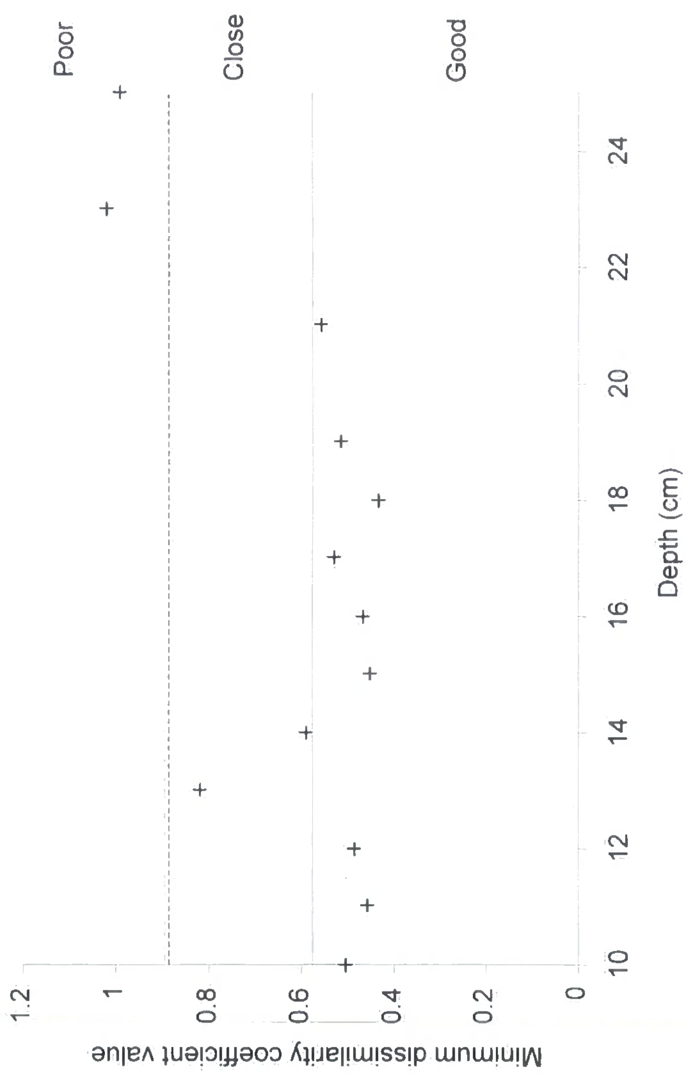

Figure 6.18

Minimum dissimilarity coefficient values from MAT for Girdwood G-01-1C

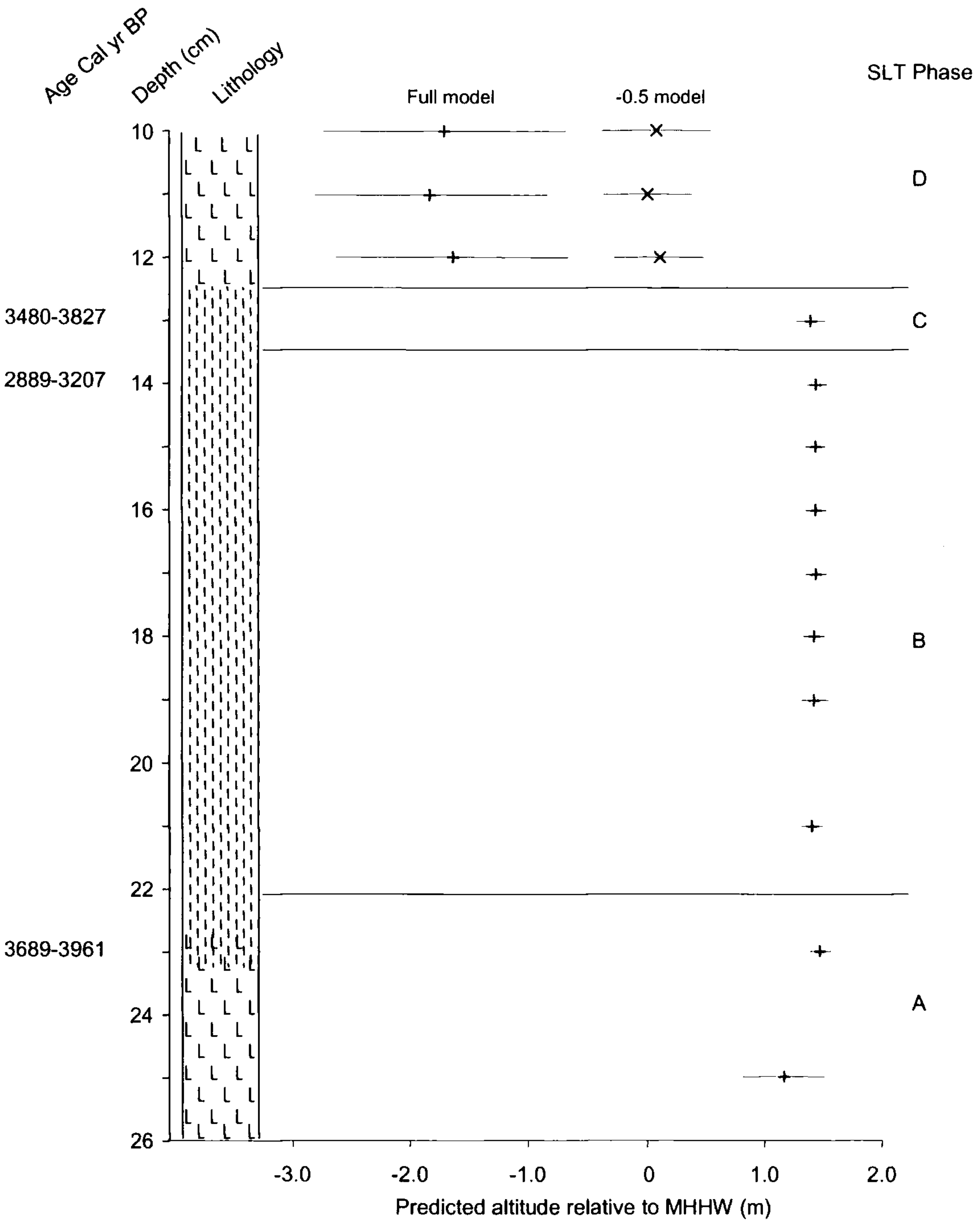

Figure 6.19

Reconstruction of relative sea-level change for Girdwood G-01-1C using the best combination of models (table 6.15). Samples in red have 'poor' modern analogues and it illustrates the difference in using the full and -0.5 m models when estimating the altitude of silt units

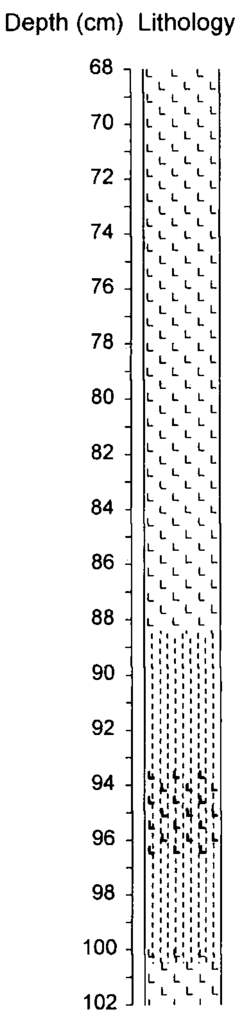

Depth (cm)	Description
68-88.5	Grey silt with herbaceous rootlets Ag4, Th^3+ 2,0,2,0,0
88.5-100.5	Herbaceous peat with sharp upper contact. Increase in silt content between 93.5 to 96.5 cm $Th^3$3, Sh1, Ag++ 3,0,2,0,4
100.5-102	Grey silt with herbaceous rootlets Ag4, Th+ 2,0,2,0,0

Silt   Herbaceous peat

Figure 6.20

Detailed litho-stratigraphy of Girdwood G-01-1E

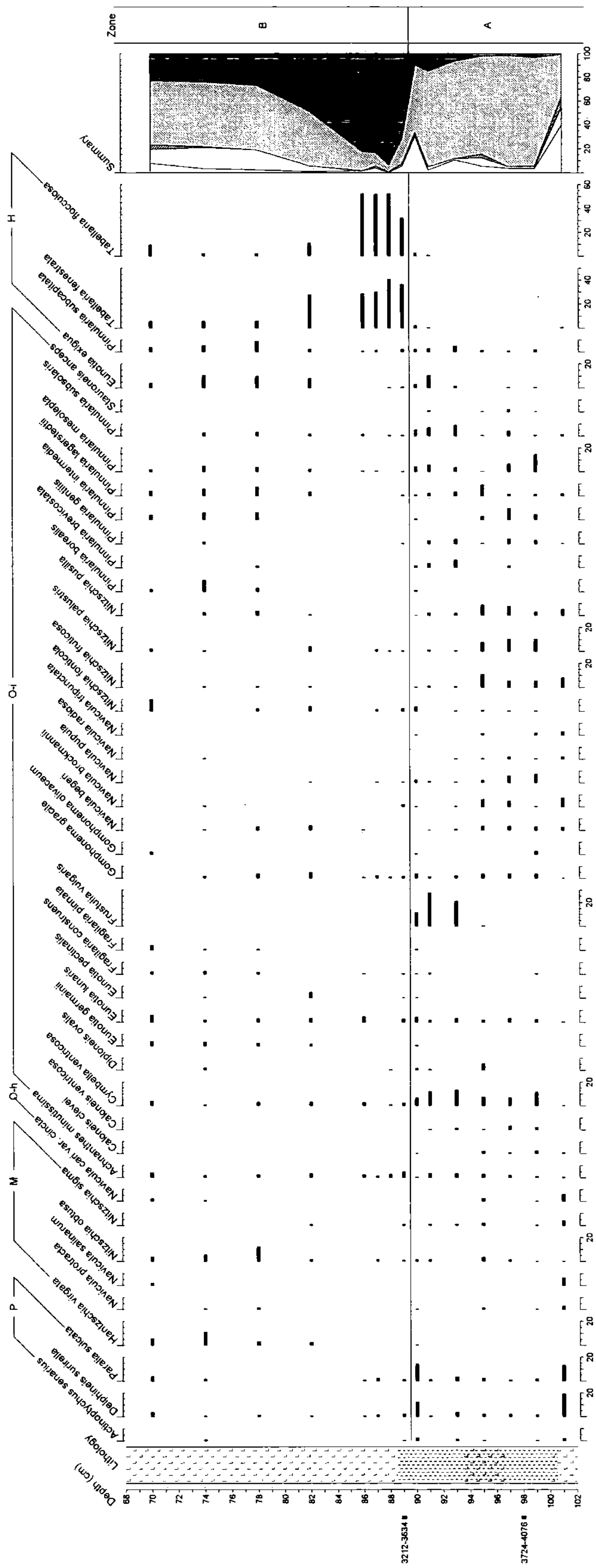

Figure 6.21

Girdwood G-01-1E diatom data (>2% total diatom valves). Summary salinity classes: polyhalobian (P), mesohalobian (M), oligohalobian-halophile (O-h), oligohalobian-indifferent (O-i), halophobe (H) ordered left to right in summary graph

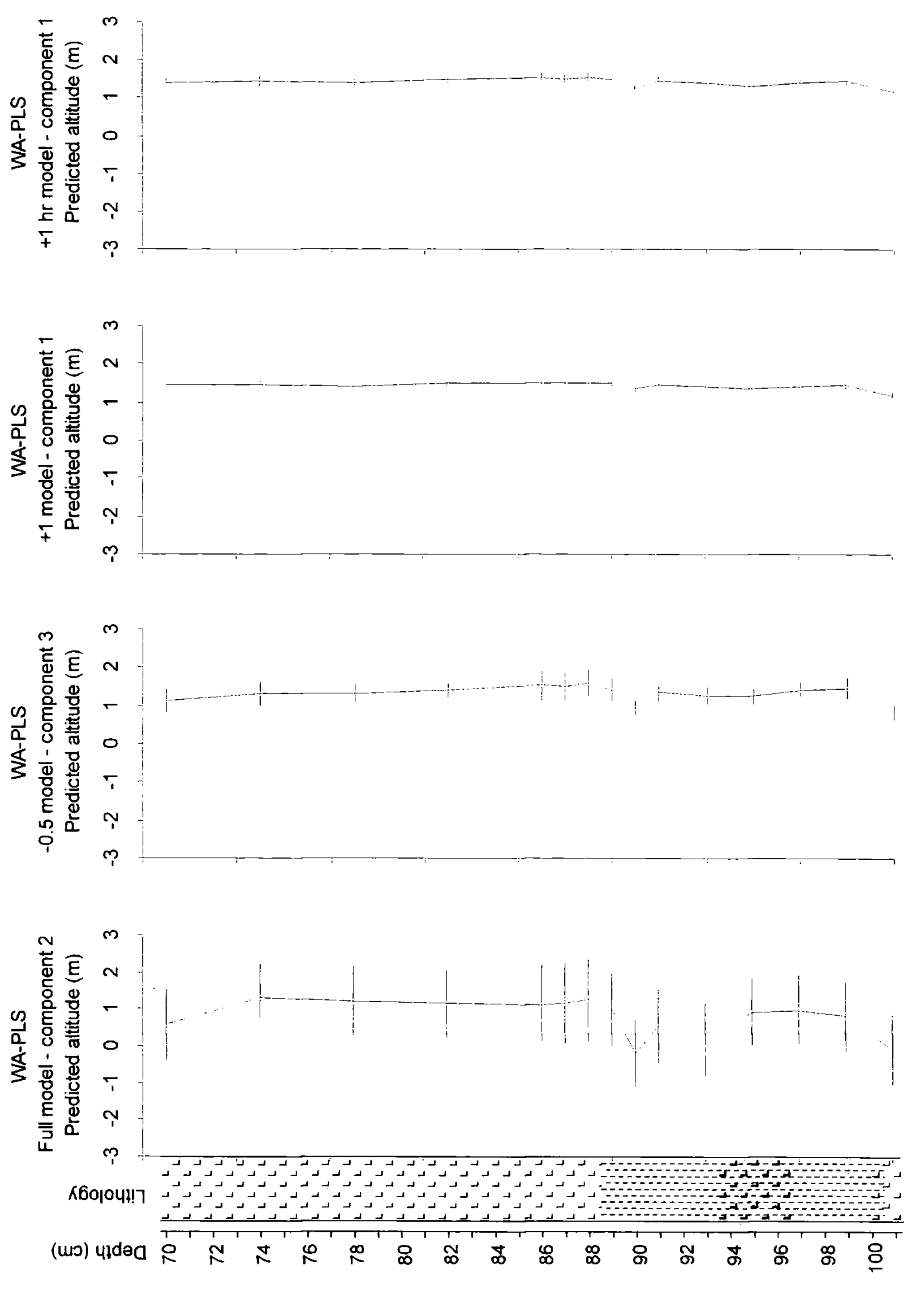

Figure 6.22

Calibration results for Girdwood G-01-1E using the full model, samples above -0.5 m MHHW and samples above +1.0 m for both altitude (m) relative to MHHW and hours inundated per year (back calculated to altitude)

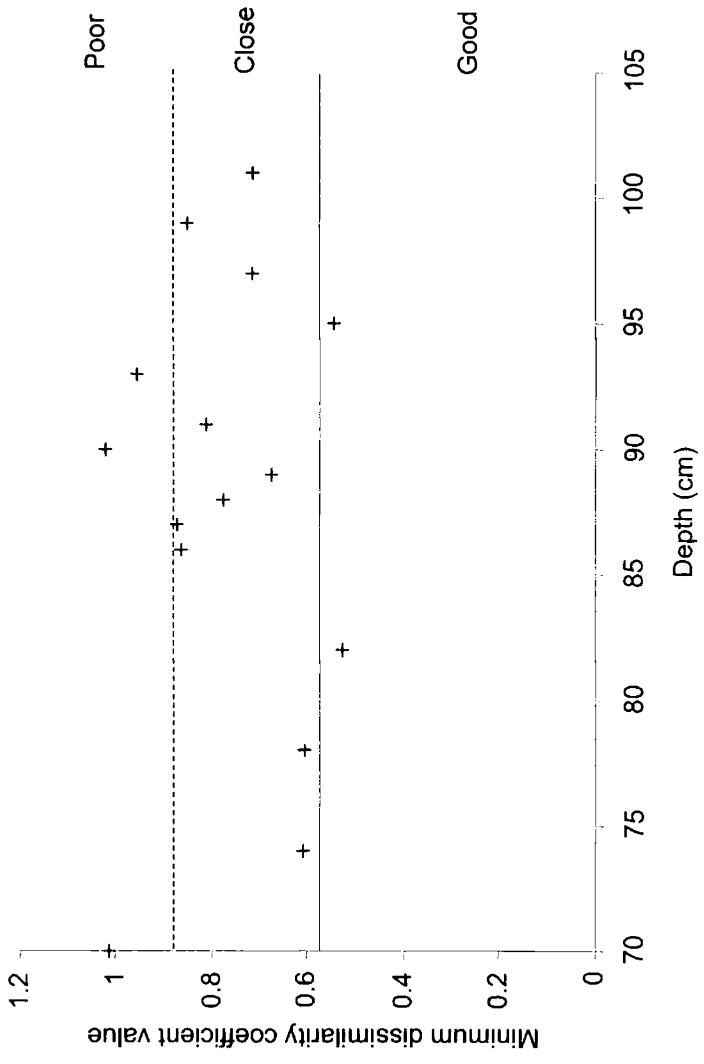

Figure 6.23

Minimum dissimilarity coefficient values from MAT for Girdwood G-01-1E

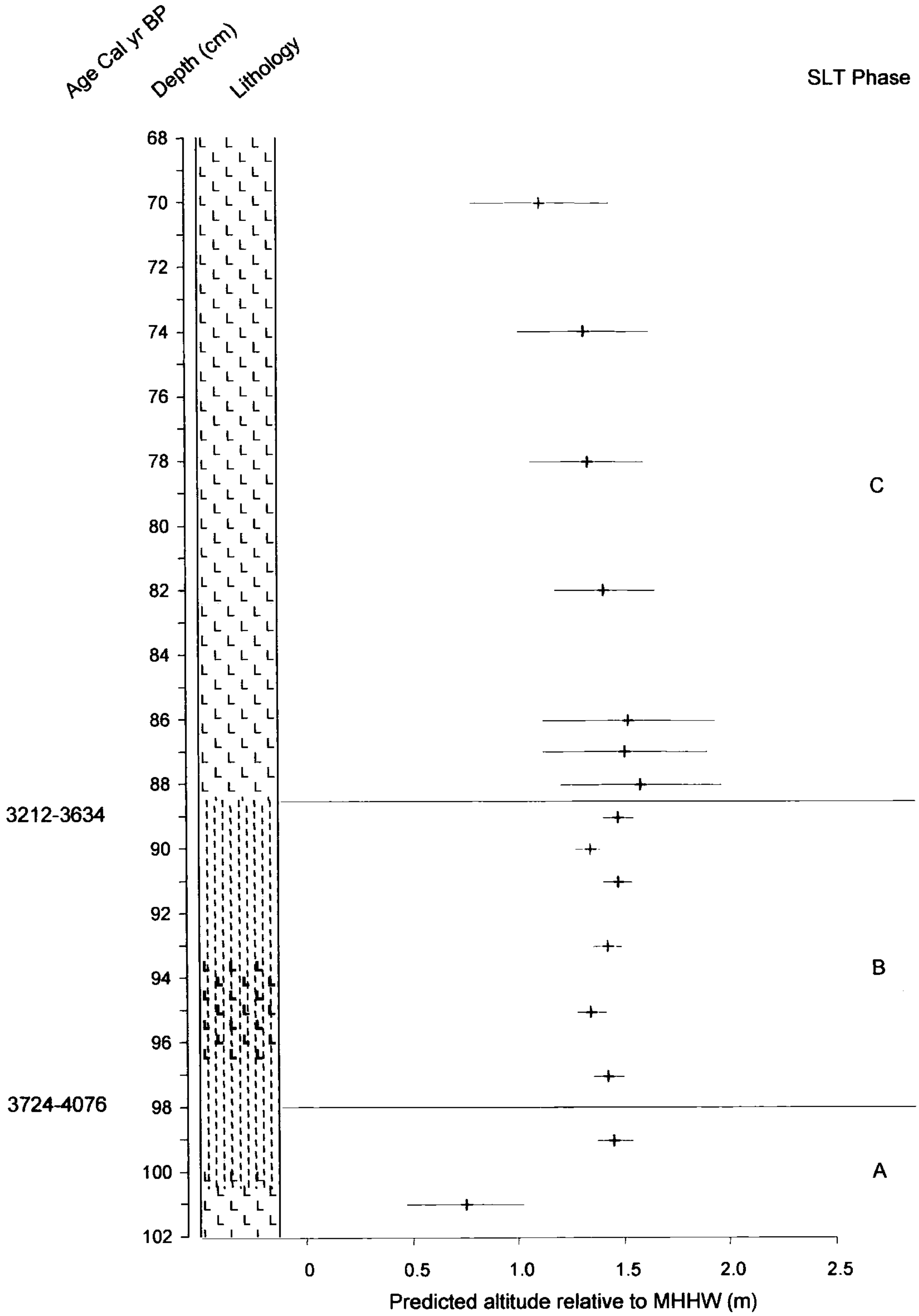

Figure 6.24

Reconstruction of relative sea-level change for Girdwood G-01-1E using the best combination of models (table 6.20). Samples in red have 'poor' modern analogues

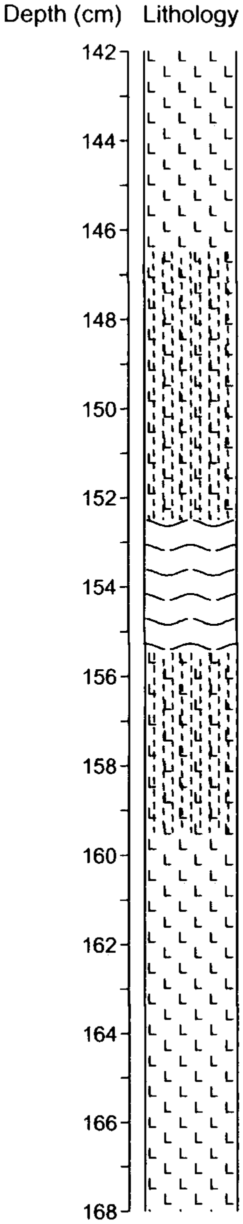

Depth (cm)	Description
142-146.5	Grey silt with herbaceous rootlets Ag4, Th+ 2,0,2,0,0
146.5-152.5	Silty peat. Sharp Upper contact $Th^2/Tb^2 2$, Ag2 3,0,2,0,4
152.5-155.5	Bryophyte peat. Transitional to silty peat above and below $Tb^3 4$ 3,1,2,2,0
155.5-159.5	Silty peat $Th^2/Tb^2 2$, Ag2 3,0,2,0,0
159.5-168	Grey silt with herbaceous rootlets Ag4, Th+ 2,0,2,0,0

Silt

Herbaceous peat

Bryophyte (*Sphagnum*) peat

Figure 6.25

Detailed litho-stratigraphy of Girdwood G-01-1F

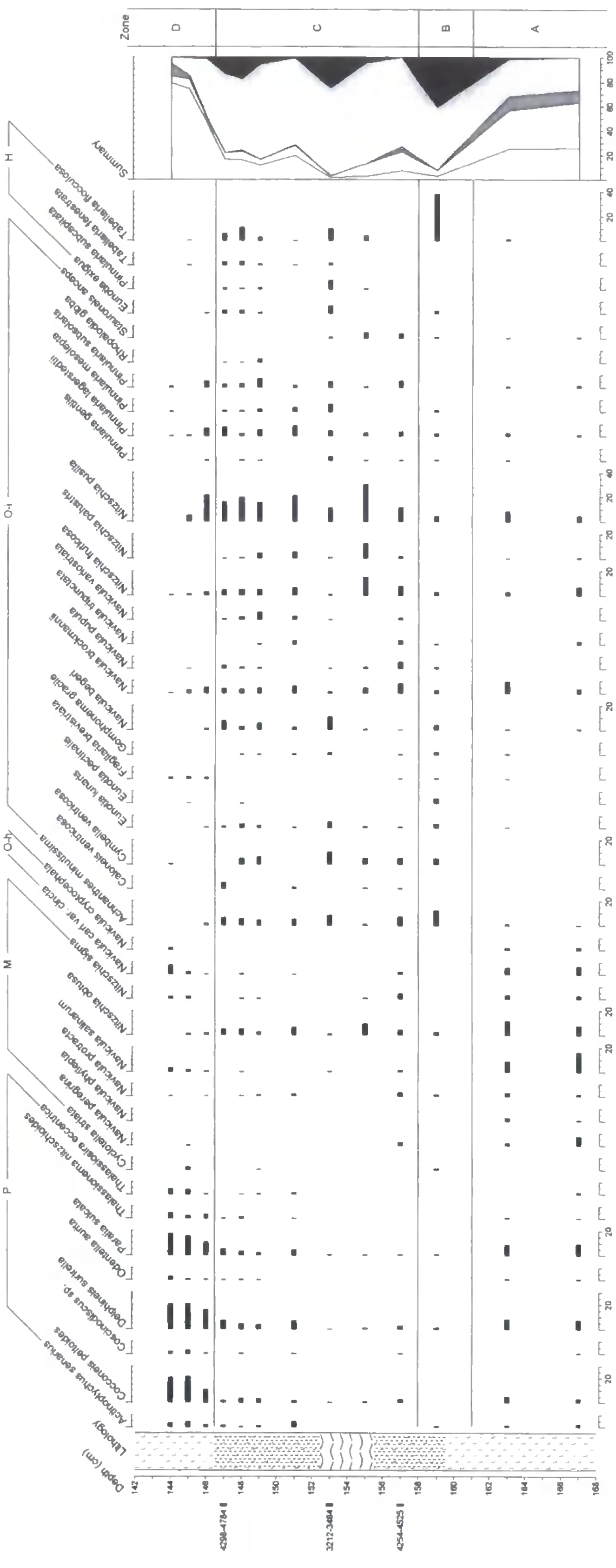

Figure 6.26

Girdwood G-01-1F diatom data (>2% total diatom valves). Summary salinity classes: polyhalobian (P), mesohalobian (M), oligohalobian-halophile (O-h), oligohalobian-indifferent (O-i), halophobe (H) ordered left to right in summary graph

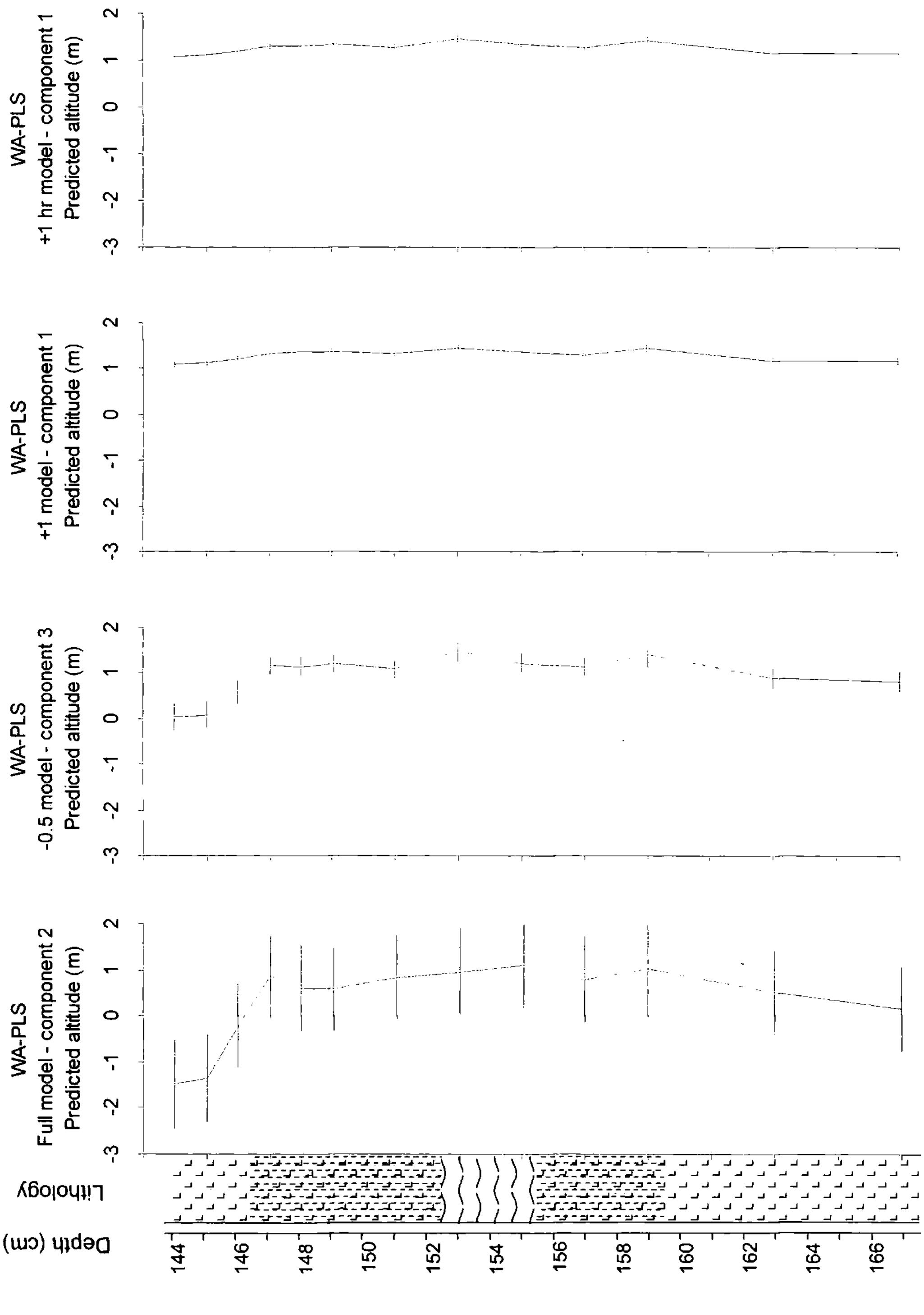

Figure 6.27

Calibration results for Girdwood G-01-1F using the full model, samples above -0.5 m MHHW and samples above +1.0 m for both altitude (m) relative to MHHW and hours inundated per year (back calculated to altitude)

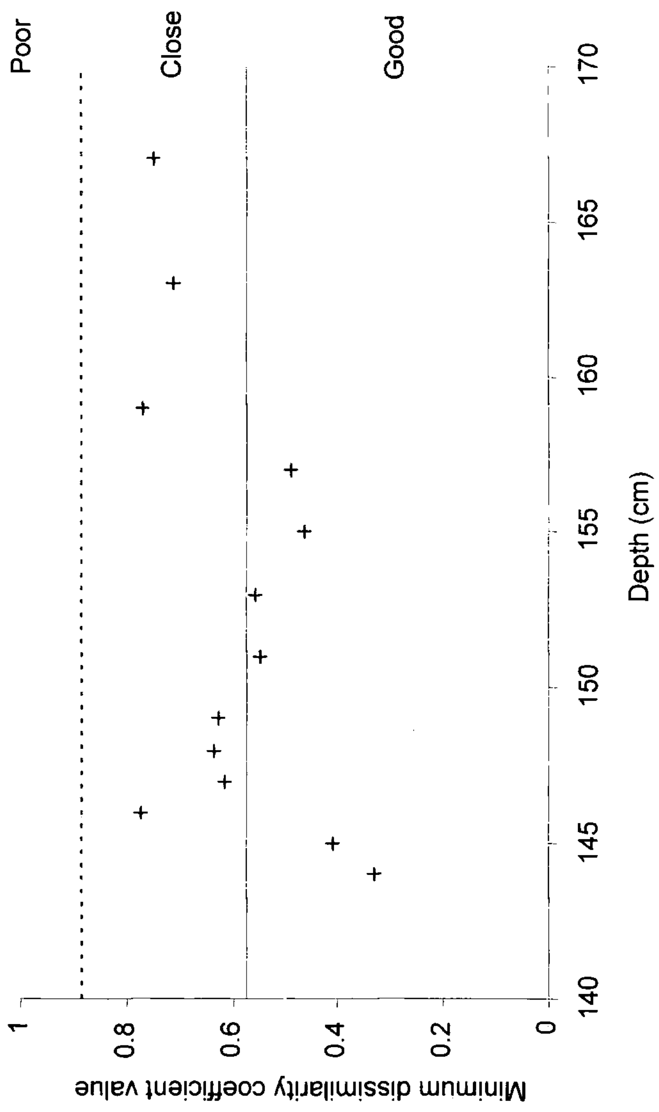

Figure 6.28

Minimum dissimilarity coefficient values from MAT for Girdwood G-01-1F

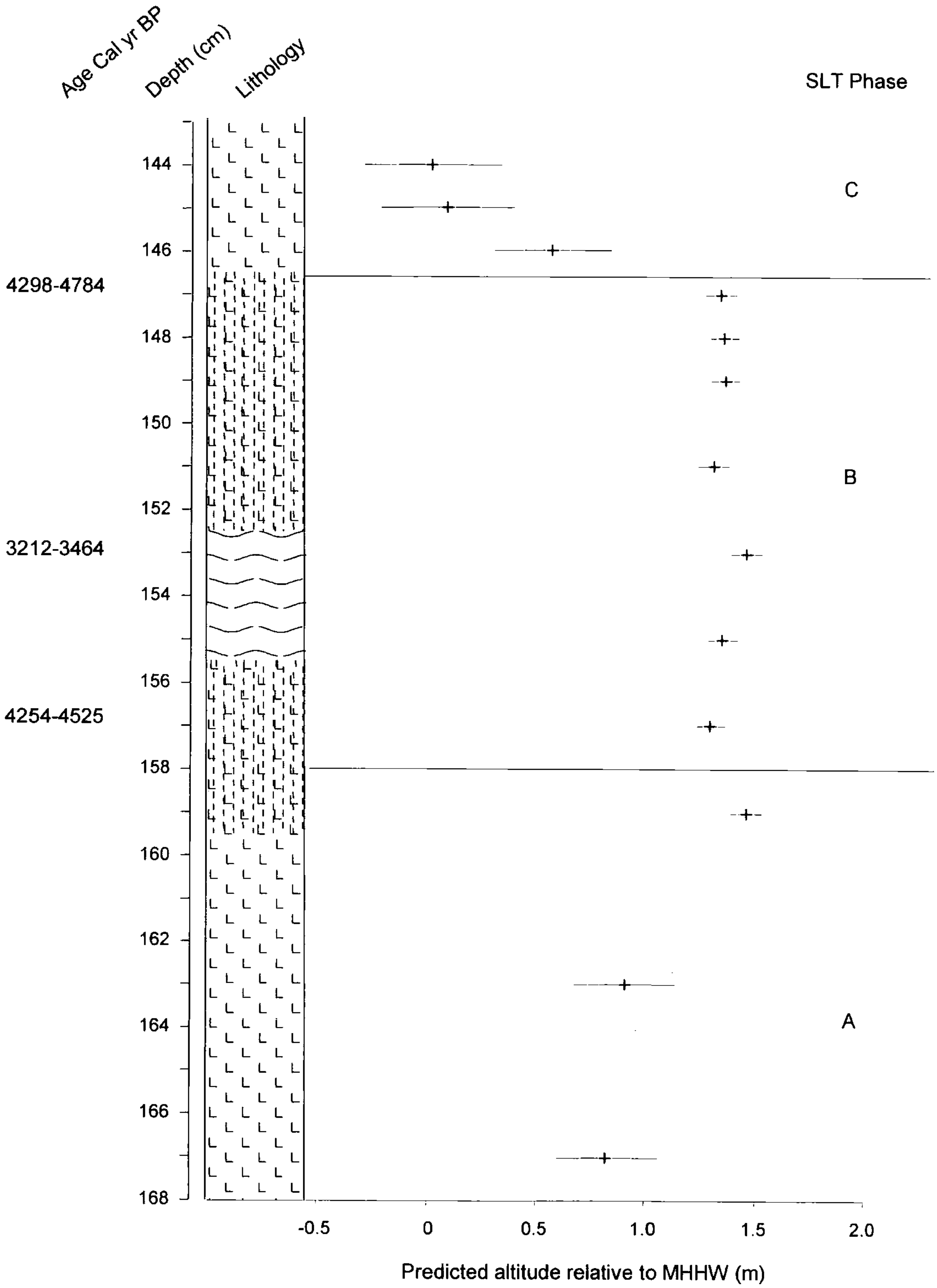

Figure 6.29

Reconstruction of relative sea-level change for Girdwood G-01-1F using the best combination of models (table 6.25)

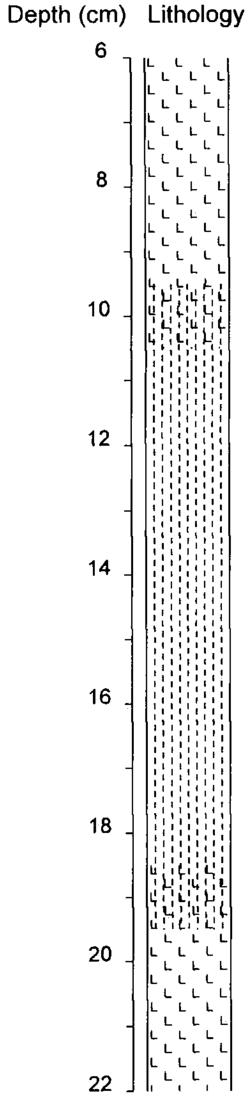

Depth (cm)	Description
6-9.5	Silt with herbaceous rootlets Ag4, As+, Th^2+ 2,0,2,0,0
9.5-10.5	Silty herbaceous peat $Th^2$3, Ag1 3,0,2,0,4
10.5-18.5	Herbaceous peat $Th^2$3, Sh1 3,0,2,0,0
18.5-19.5	Silty herbaceous peat $Th^2$3, Ag1 3,0,2,0,0
19.5-22	Silt with herbaceous rootlets Ag4, As+, Th^2+ 2,0,2,0,0

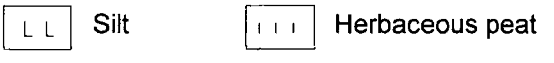

Figure 6.30

Detailed litho-stratigraphy of Girdwood G-01-9

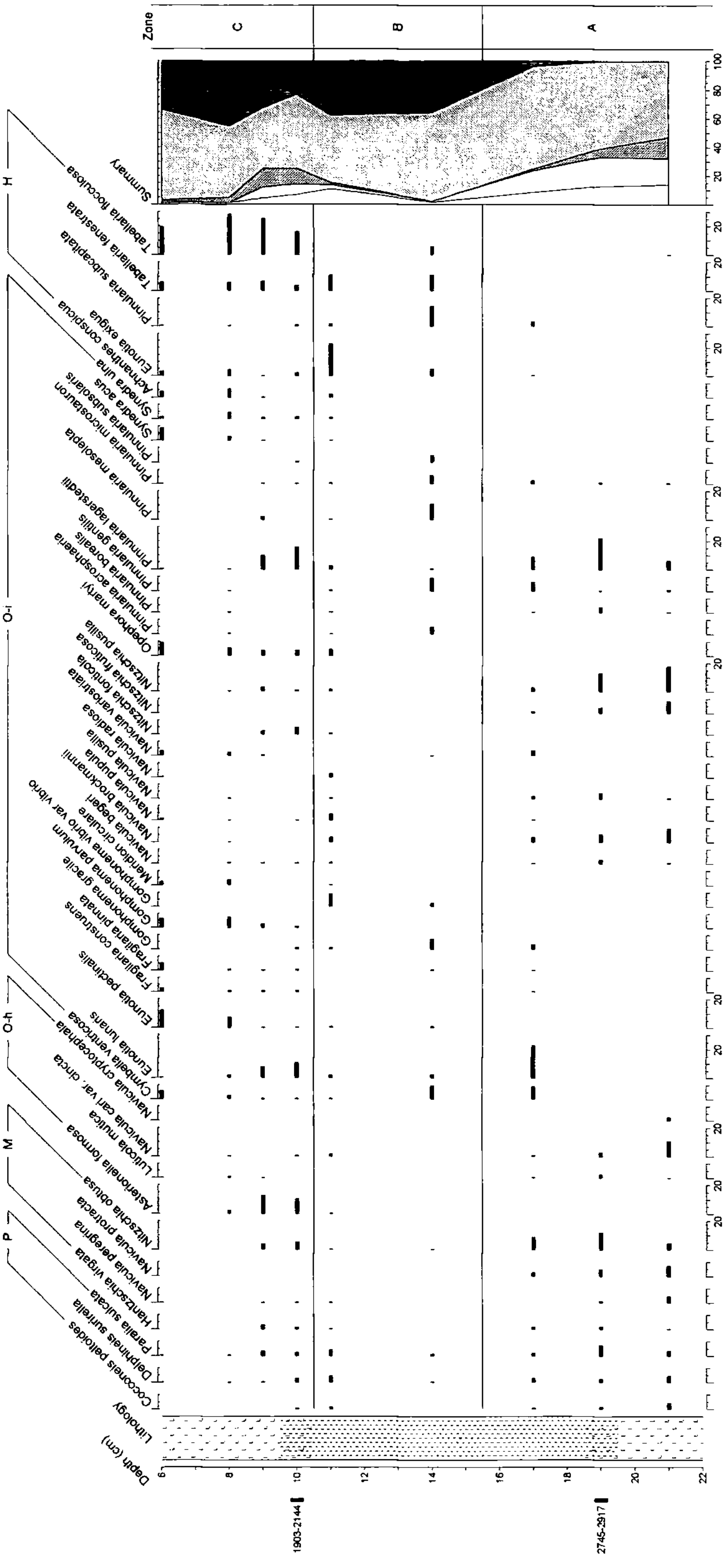

Figure 6.31

Girdwood G-01-9 diatom data (>2% total diatom valves). Summary salinity classes: polyhalobian (P), mesohalobian (M), oligohalobian-halophile (O-h), oligohalobian-indifferent (O-i), halophobe (H) ordered left to right in summary graph

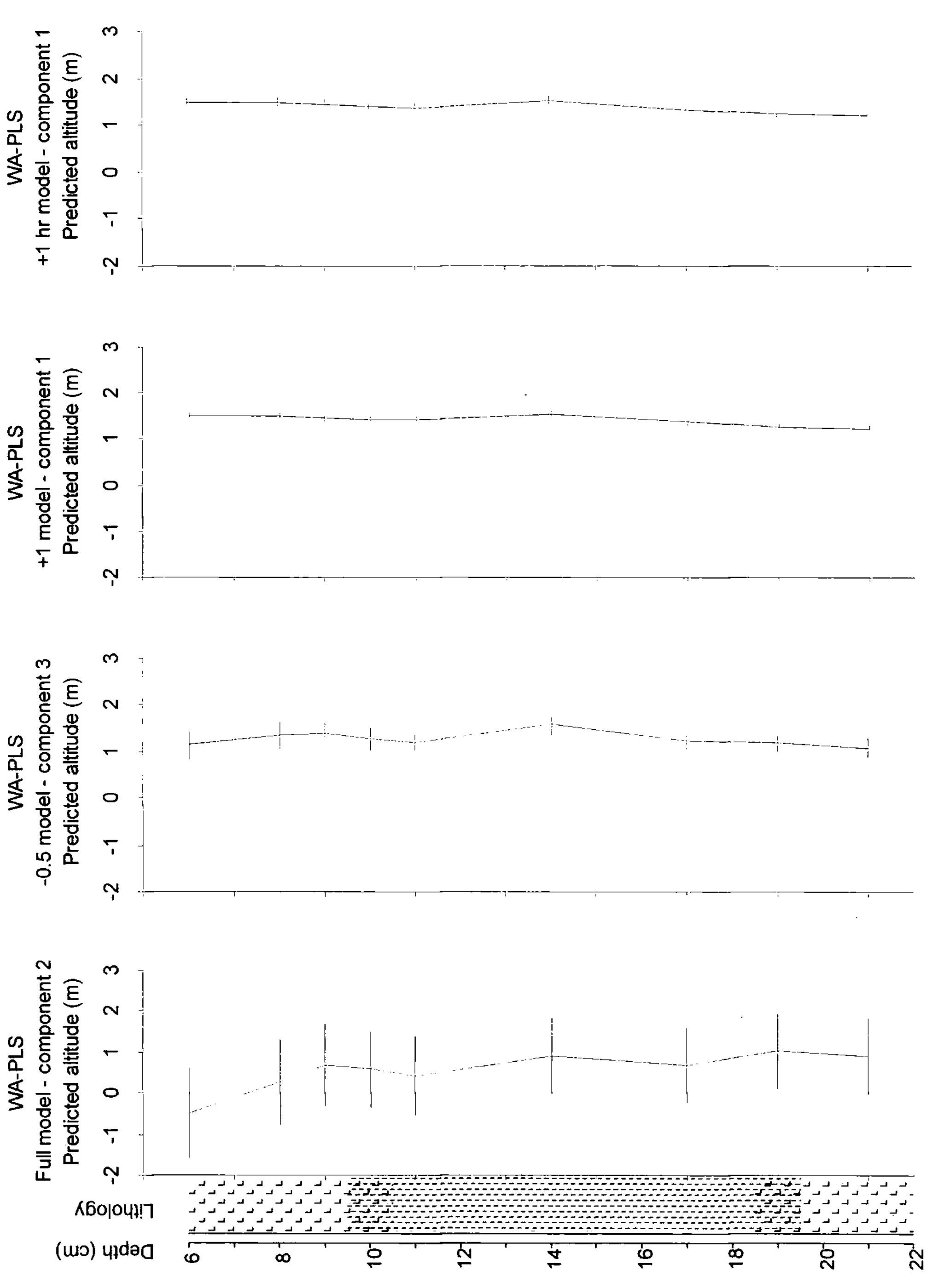

Figure 6.32

Calibration results for Girdwood G-01-9 using the full model, samples above -0.5 m MHHW and samples above +1.0 m for both altitude (m) relative to MHHW and hours inundated per year (back calculated to altitude)

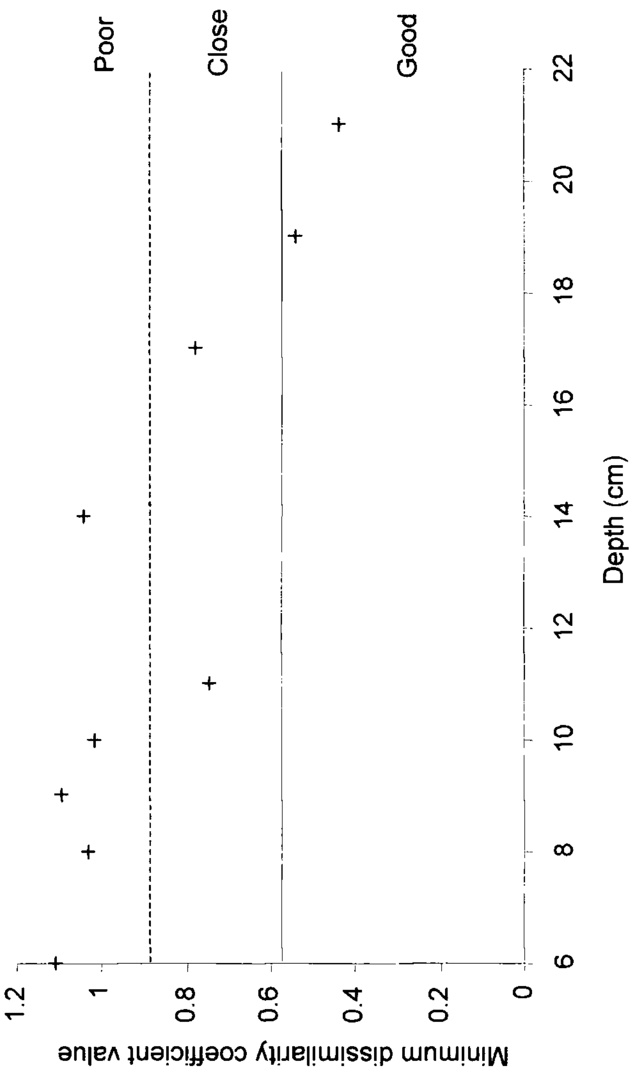

Figure 6.33

Minimum dissimilarity coefficient values from MAT for Girdwood G-01-9

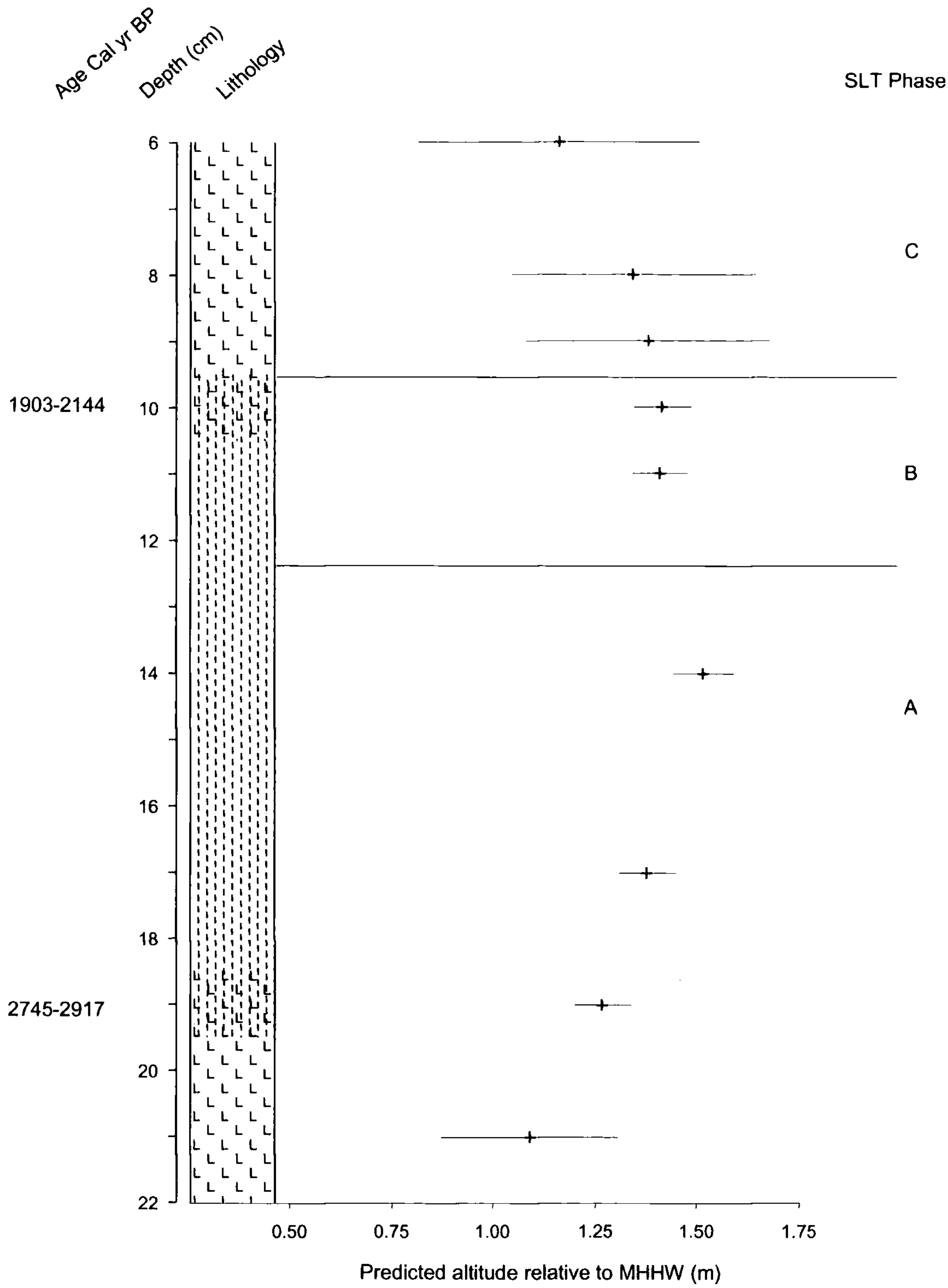

Figure 6.34

Reconstruction of relative sea-level change for Girdwood G-01-9 using the best combination of models (table 6.30). Samples in red have 'poor' modern analogues

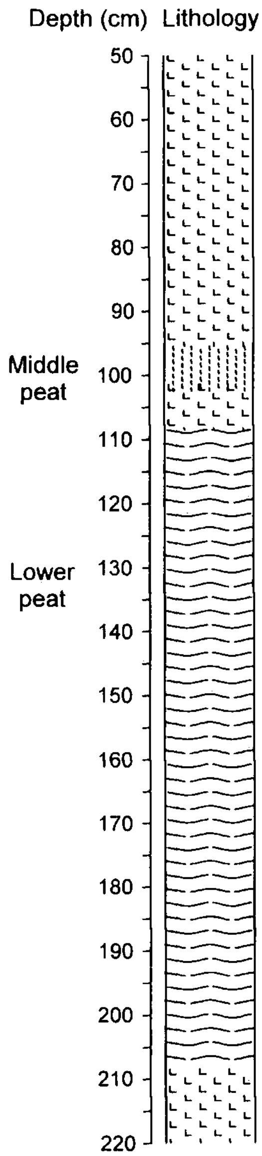

Depth (cm)	Description
54-67.5	Clay silt with rare plant fragments Ag3, As1 2,0,2,0,-
67.5-95.5	Grey clay silt with herbaceous rootlets and organic matter Ag3, As1, Th+ 2,0,2,0,0
95.5-102.5	Fibrous peat with some silt. Distinct upper boundary $Th^3 2$, Sh2 3,0,2,0,4
102.5-108.5	Clay silt with rootlets Ag3, As1, Th+ 2,0,2,0,0
108.5-208.5	Bryophyte Peat with distinct tephras and wood layers throughout. Tephras @ 111, 134-138, 157-160, 163-164, 183-187. Wood @100-105, 138 and 185. $Tb^3 4$ 3,1,2,0,4
208.5-216	Compacted clay with fine rootlets Ag4, Th+ 2,0,2,0,0

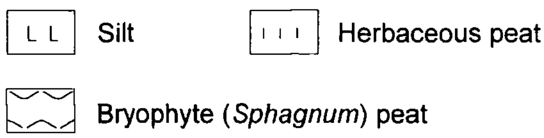

Figure 7.1a

Detailed litho-stratigraphy of the lower and middle peat layers at Kasilof (KS-01-1)

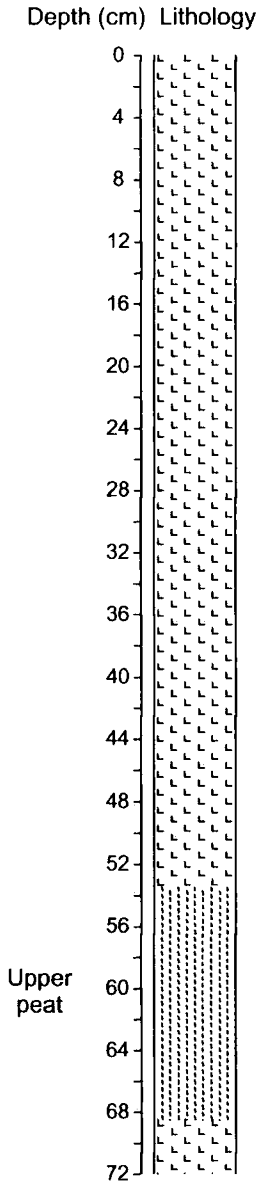

Depth (cm)	Description
0-53.5	Clay silt with rootlets Ag3, As1, Th+ 2,0,2,0,-
53.5-68.5	Herbaceous peat with sharp upper boundary Tephra @ 62 and 67 cm $Th^3$2, Sh2 3,0,2,0,4
68.5-75	Grey clay silt with herbaceous rootlets (less towards base) Ag3, As1, Th+ 2,0,2,0,2

L L Silt

Herbaceous peat

Figure 7.1b

Detailed litho-stratigraphy of the upper peat layer at Kasilof (KS-3)

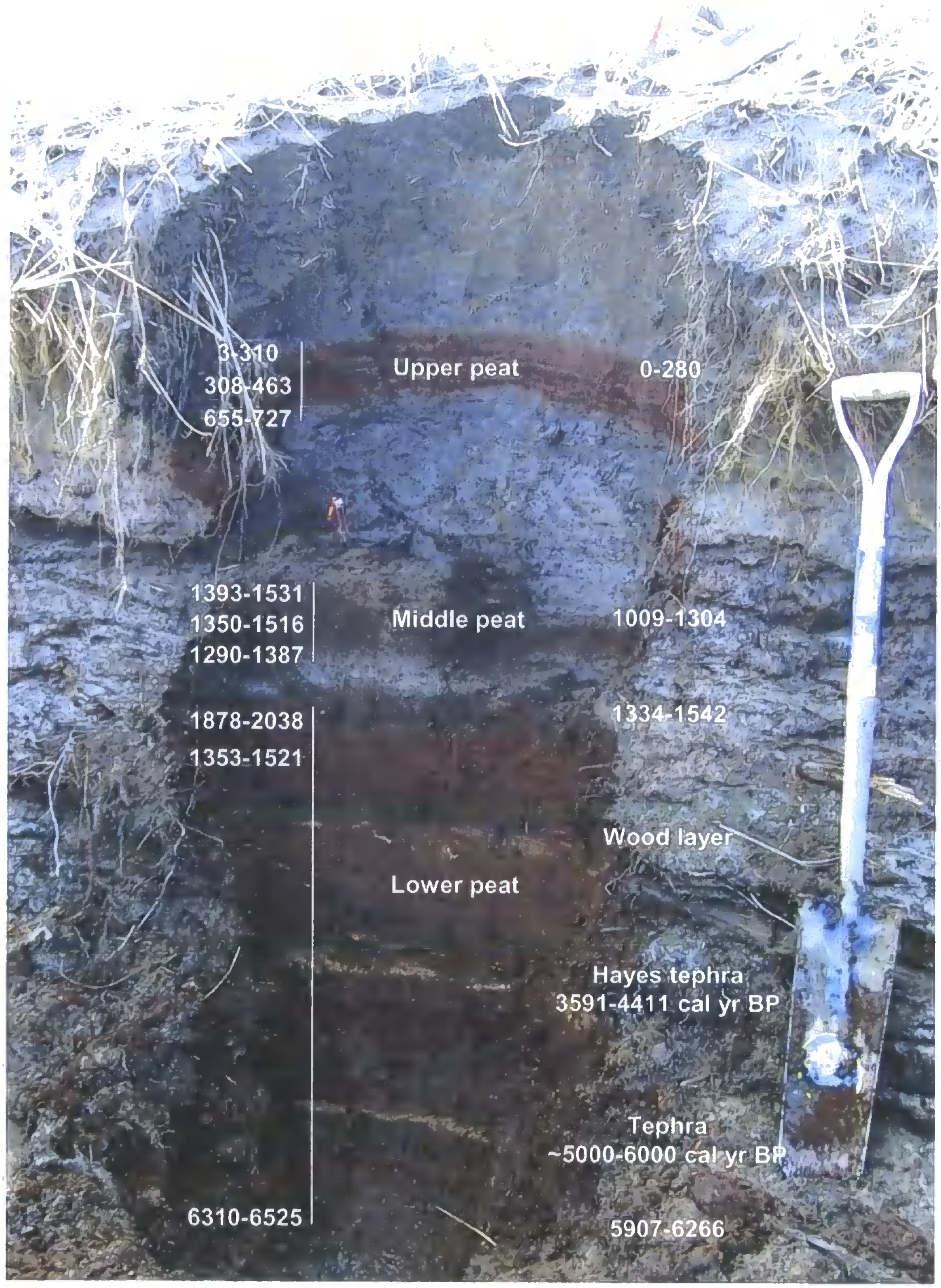

Figure 7.2

Chrono-stratigraphy of Kasilof. All dates are cal yr BP with those on the left from this thesis and those on the right re-calibrated from Combellick and Reger (1994)

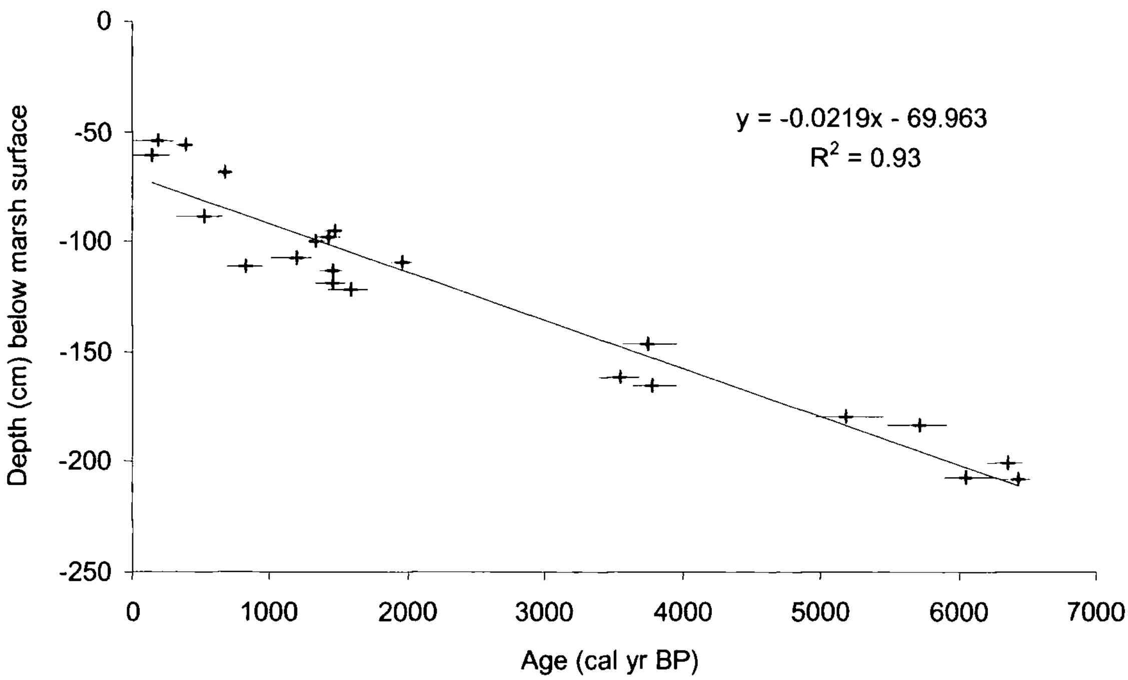

Figure 7.3

Radiocarbon dates for Kasilof from this study (values in red) compared to re-calibrated dates of Combellick and Reger (1994, values in black) showing median age and 95% range

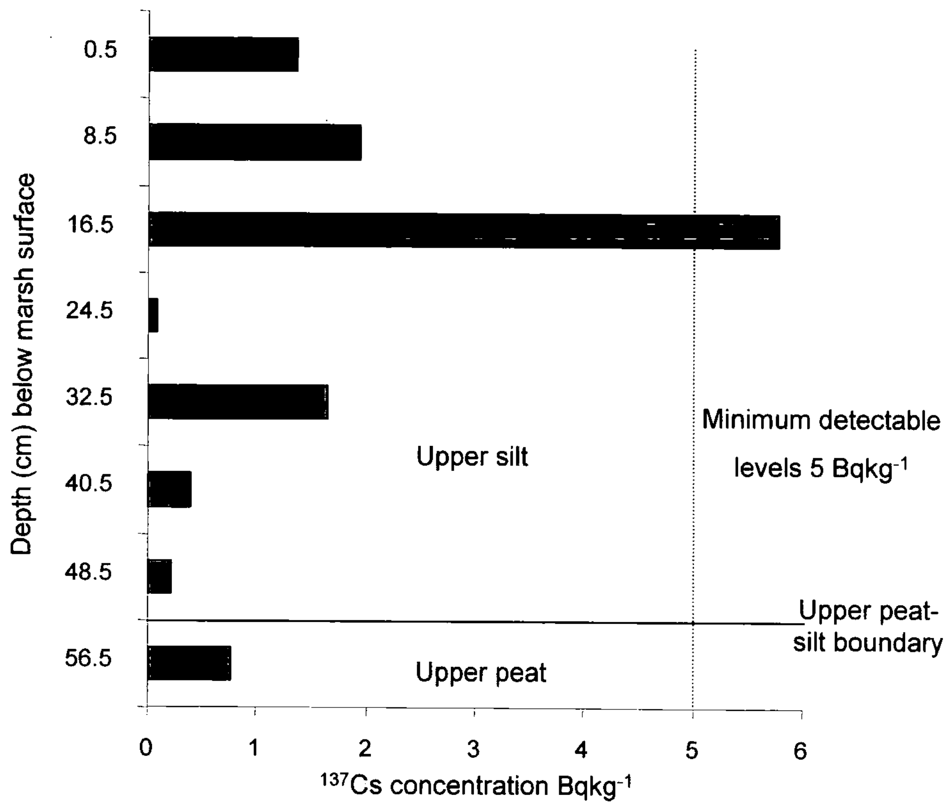

Figure 7.4

^{137}Cs results for the upper part of KS-3

Figure 7.5

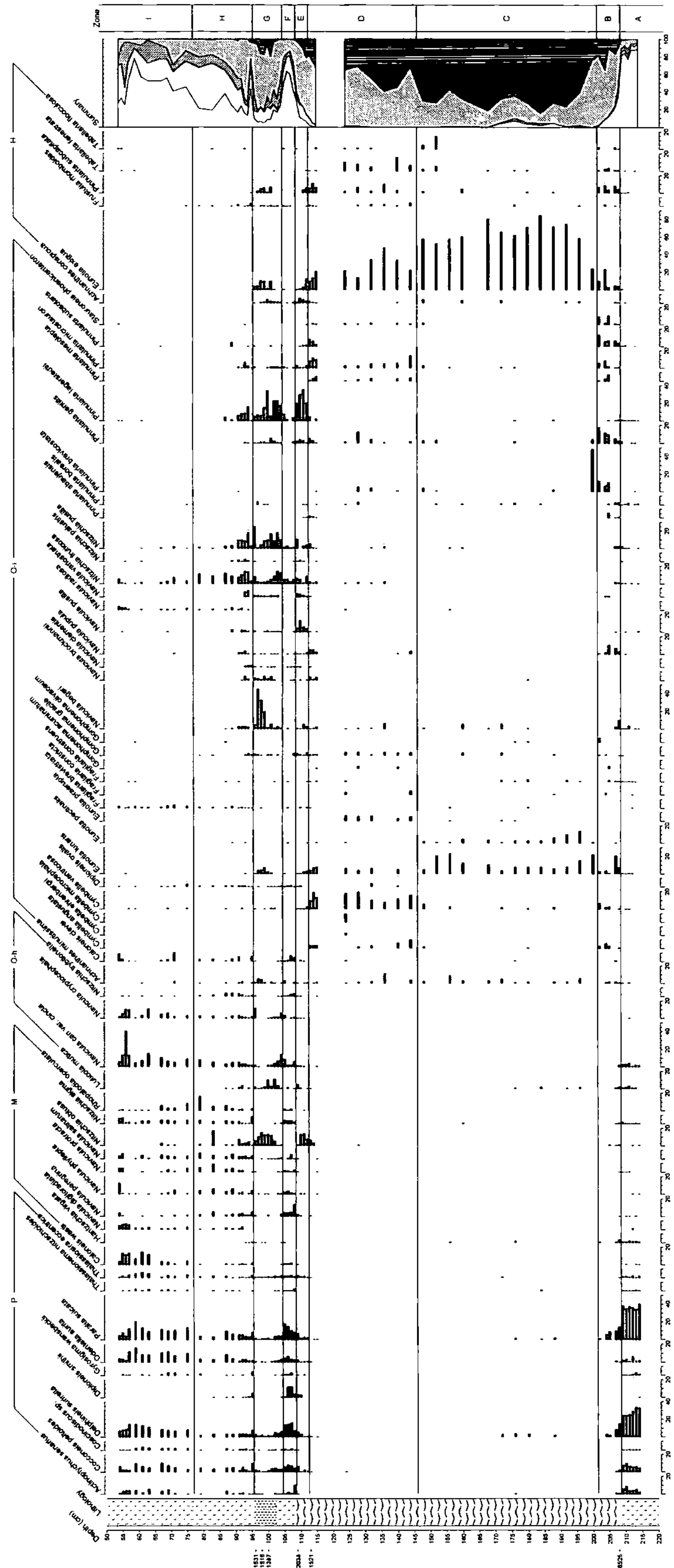

Kasilof KS-01-1 diatom data (>2% total diatom valves). Summary salinity classes: polyhalobian (P), mesohalobian (M), oligohalobian-halophile (O-h), oligohalobian-indifferent (O-i), halophobe (H) ordered left to right in summary graph

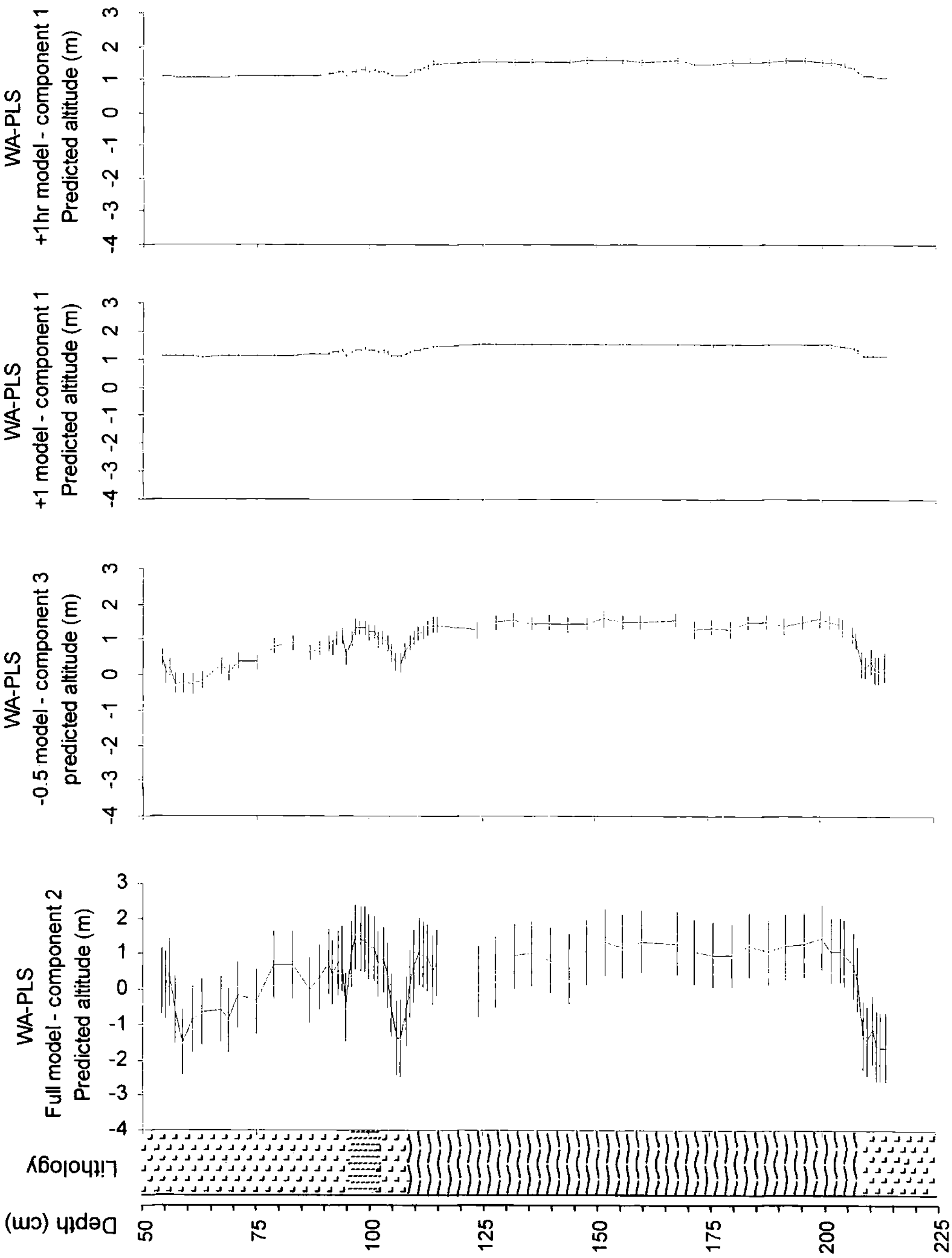

Figure 7.6

Calibration results for Kasilof KS-01-1 using the full model, samples above -0.5 m MHHW and samples above +1.0 m for both altitude (m) relative to MHHW and hours inundated per year (back calculated to altitude)

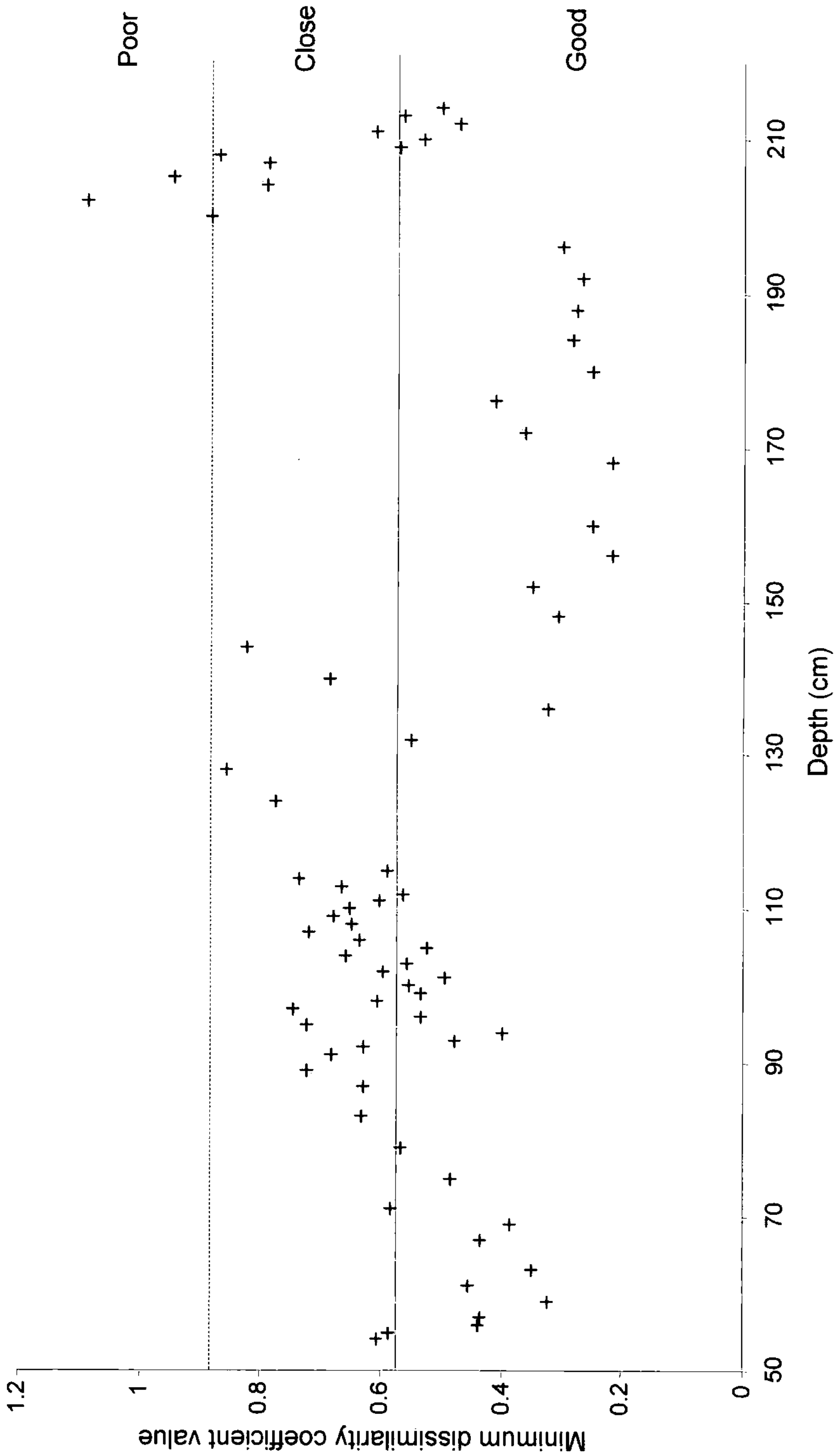

Figure 7.7

Minimum dissimilarity coefficient values from MAT for Kasilof KS-01-1

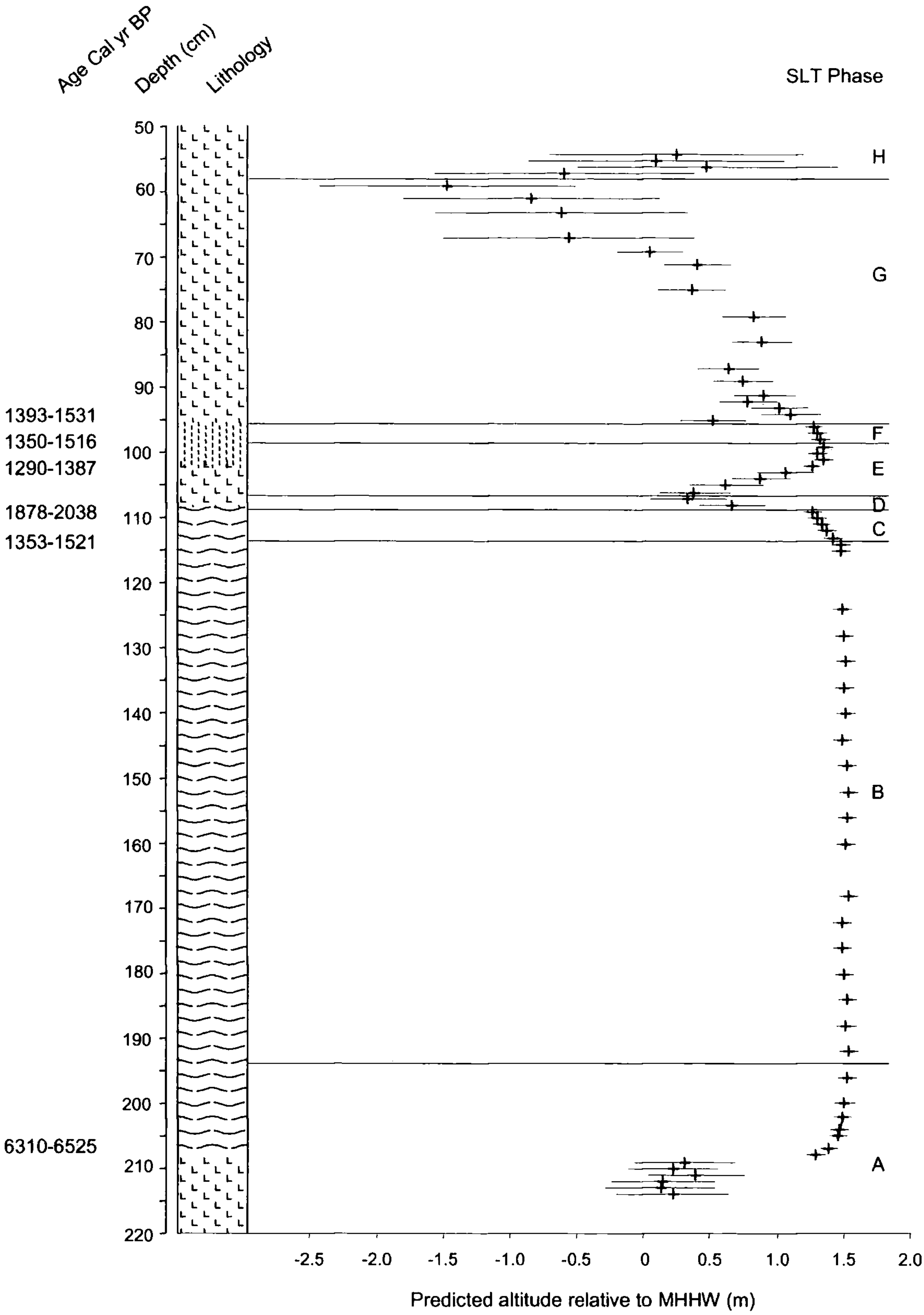

Figure 7.8

Reconstruction of relative sea-level change for Kasilof KS-01-1 using the best combination of models (table 7.4). Samples in red have 'poor' modern analogues

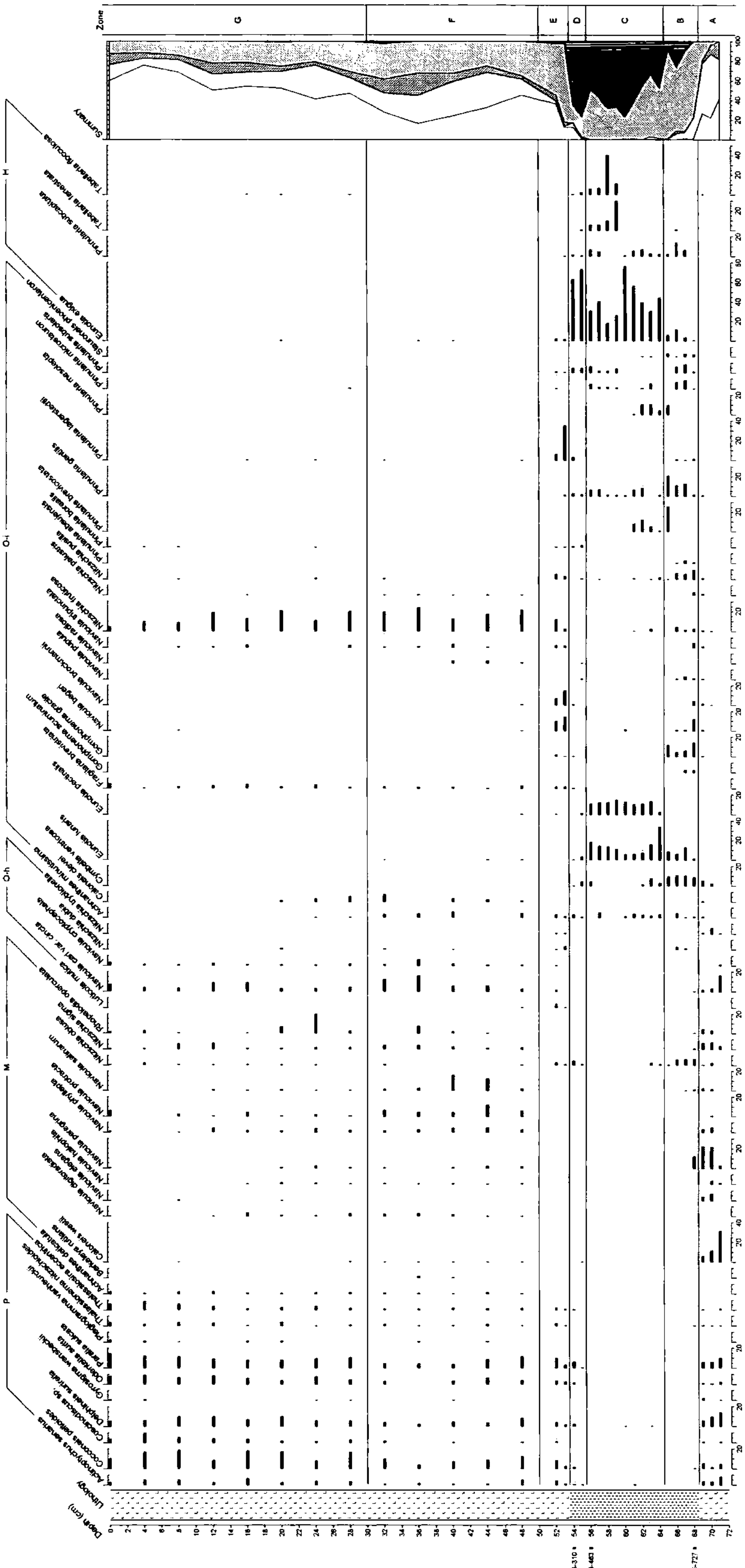

Figure 7.9

Kasilof KS-3 diatom data (>2% total diatom valves). Summary salinity classes: polyhalobian (P), mesohalobian (M), oligohalobian-halophile (O-h), oligohalobian-indifferent (O-i), halophobe (H) ordered left to right in summary graph

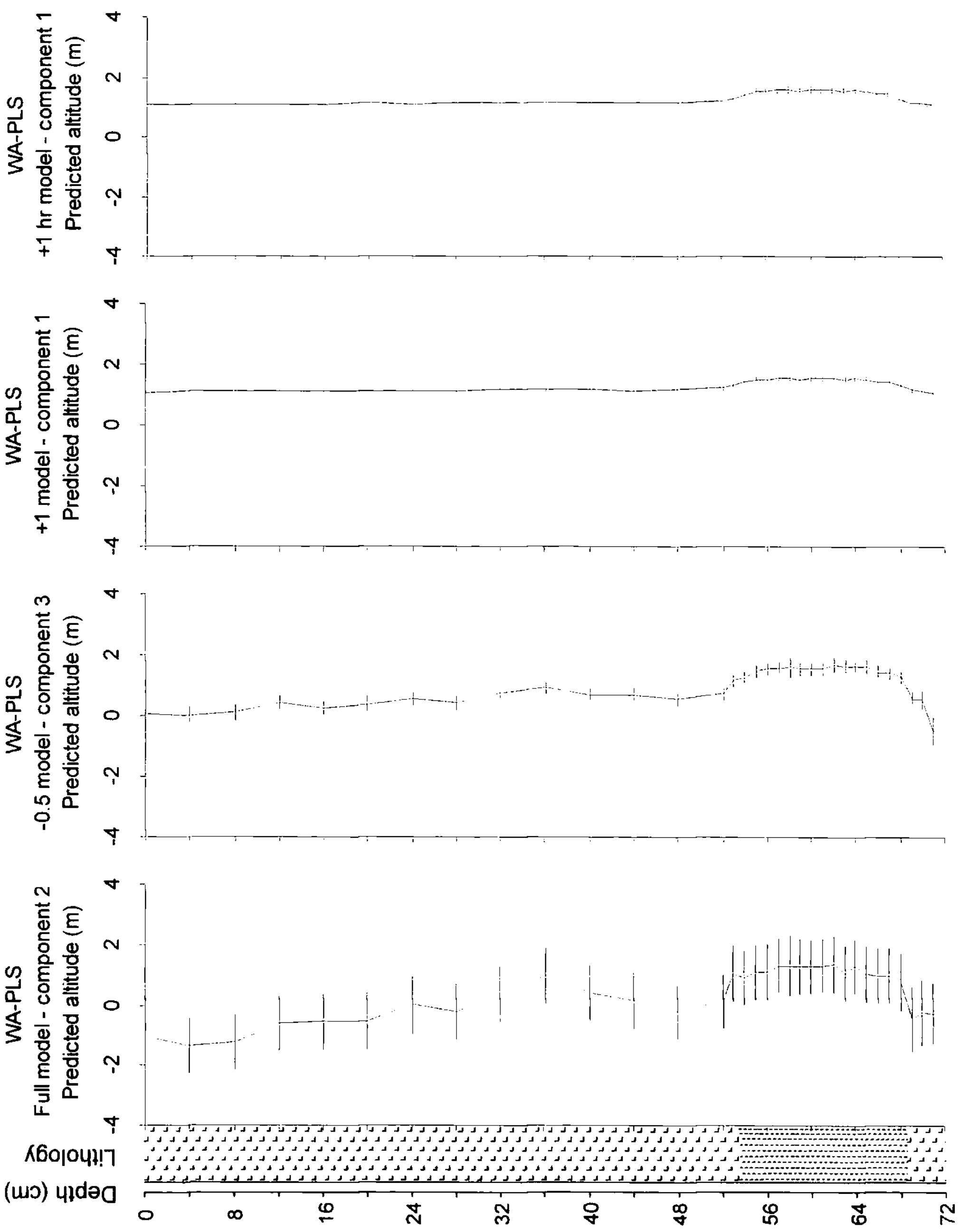

Figure 7.10

Calibration results for Kasilof KS-3 using the full model, samples above -0.5 m MHHW and samples above +1.0 m for both altitude (m) relative to MHHW and hours inundated per year (back calculated to altitude)

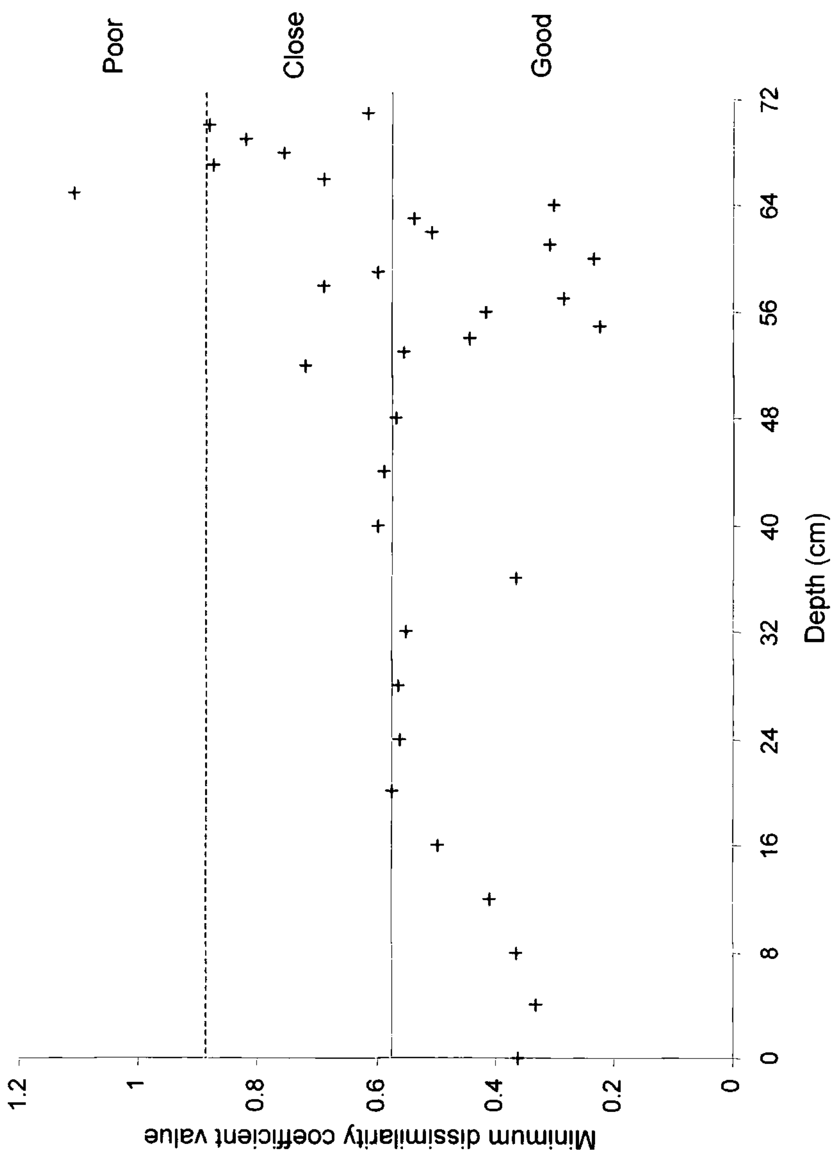

Figure 7.11

Minimum dissimilarity coefficient values from MAT for Kasilof KS-3

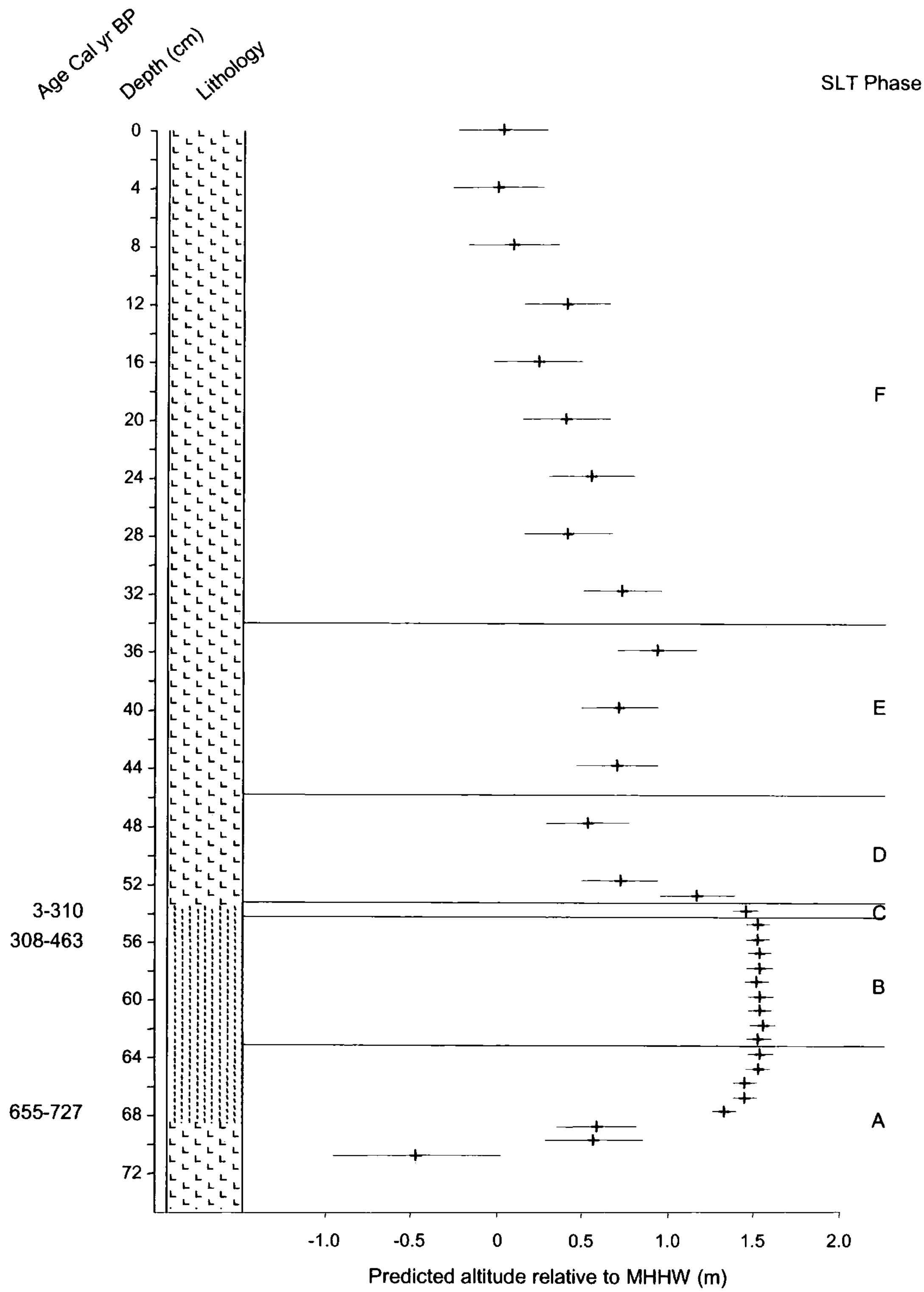

Figure 7.12

Reconstruction of relative sea-level change for Kasilof KS-3 using the best combination of models (table 7.9). The sample in red has a 'poor' modern analogue

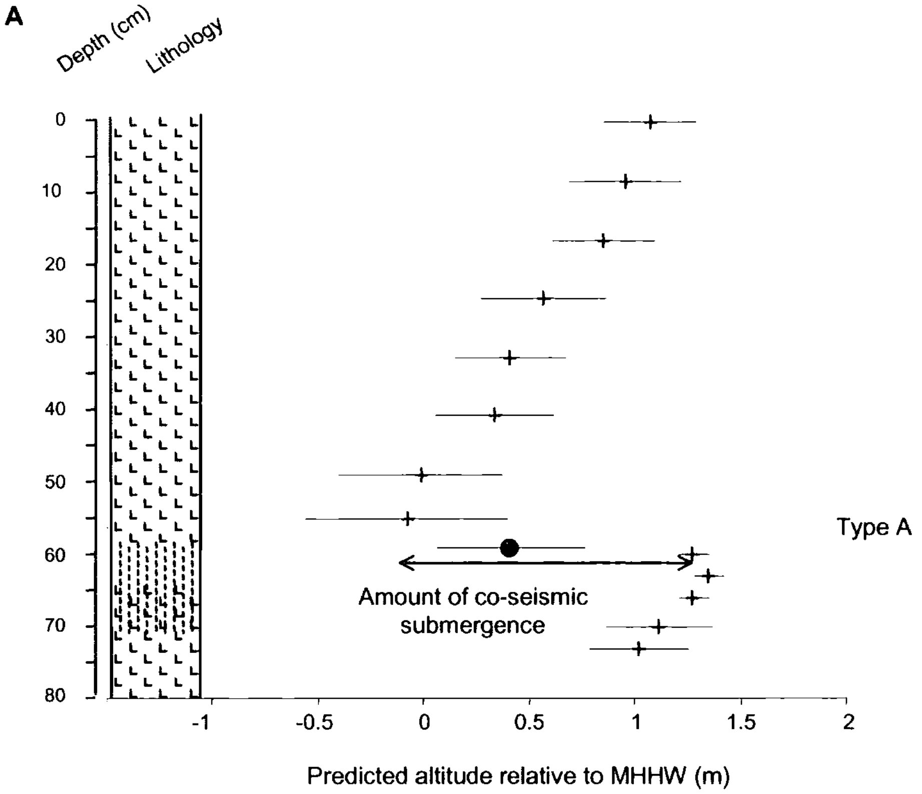

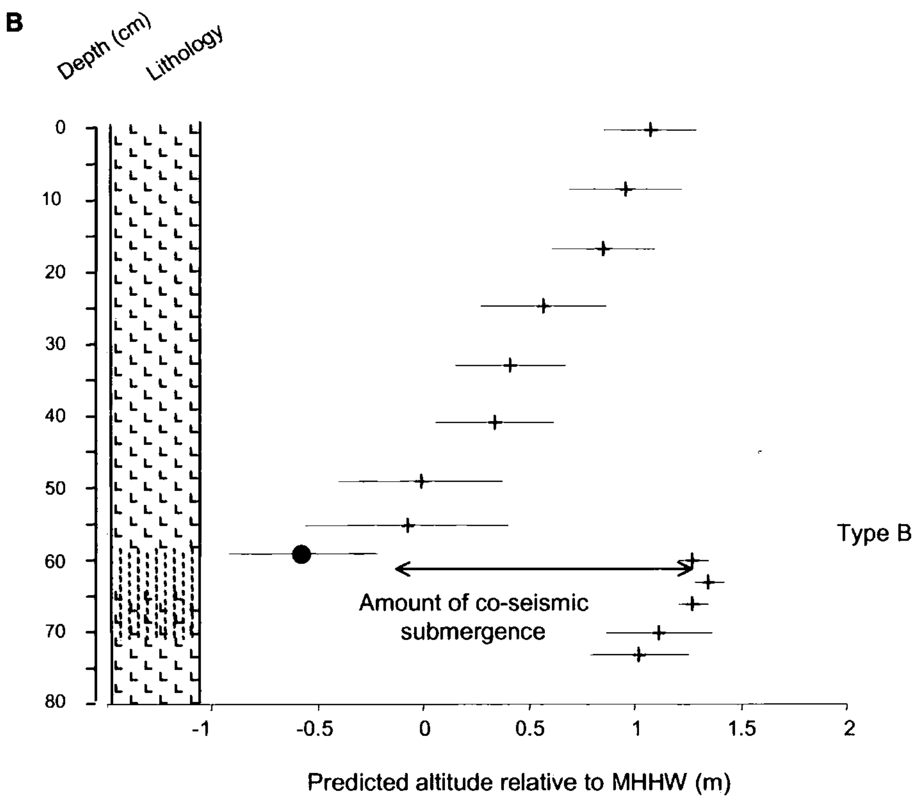

Figure 8.1

Models of reconstructed relative sea-level change showing effects of different types of reworked sediment (solid circle) following co-seismic submergence

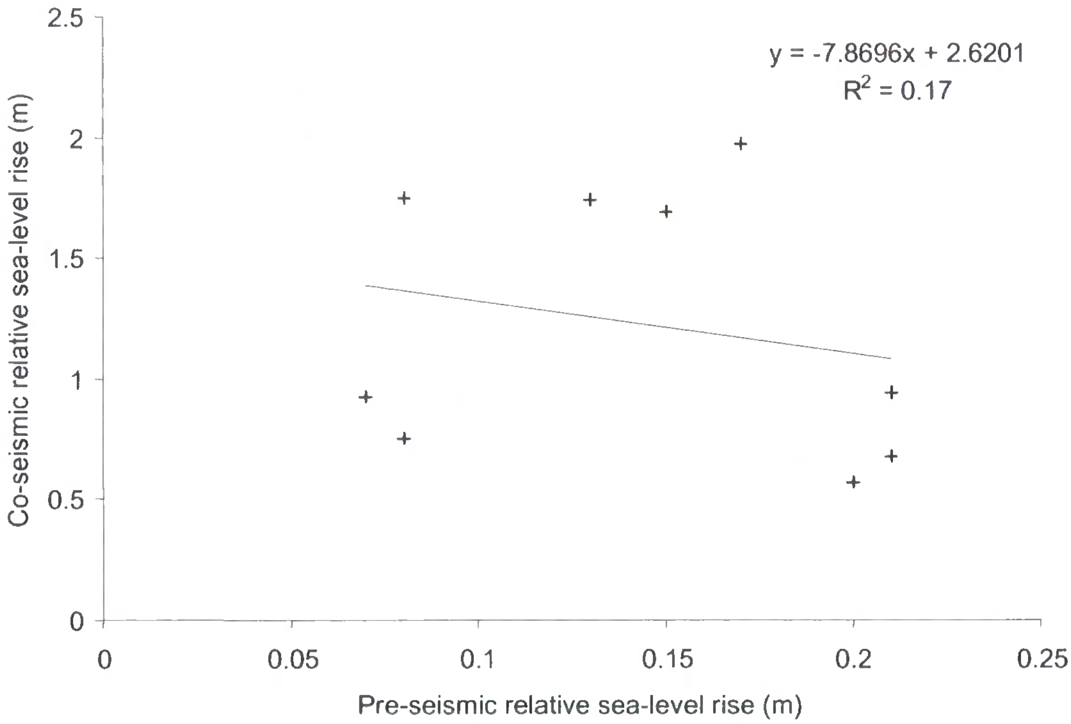

Figure 8.2

Relationship between the magnitude of pre-seismic and co-seismic relative sea-level rise for the nine EDC events with a quantified estimate of the pre-seismic sea-level rise (table 8.1)

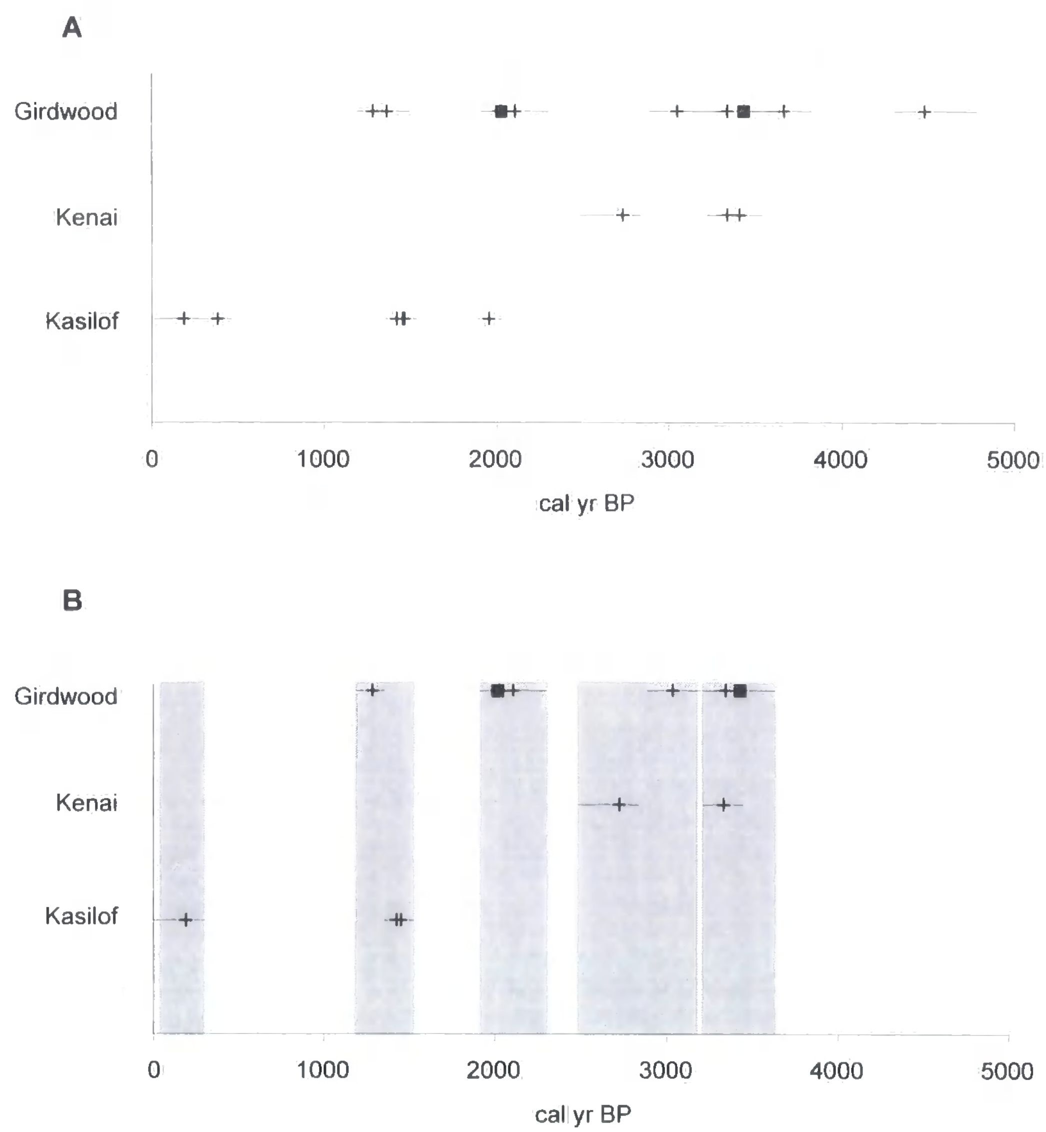

Figure 8.3

Possible pre-1964 periods of co-seismic submergence using AMS dates from this thesis

A: All ages from the top of peat layers and start of any pre-seismic signal at each site

B: Best estimate for each peat-silt boundary by comparing the stratigraphic order of all radiocarbon dates. Shaded areas represent possible co-seismic periods (table 8.2)

Both graphs show median ages and 95% ranges for both certain and possible EDC related events (table 8.1). Solid squares represent peats at Girdwood with freshwater diatoms characterising the overlying silt

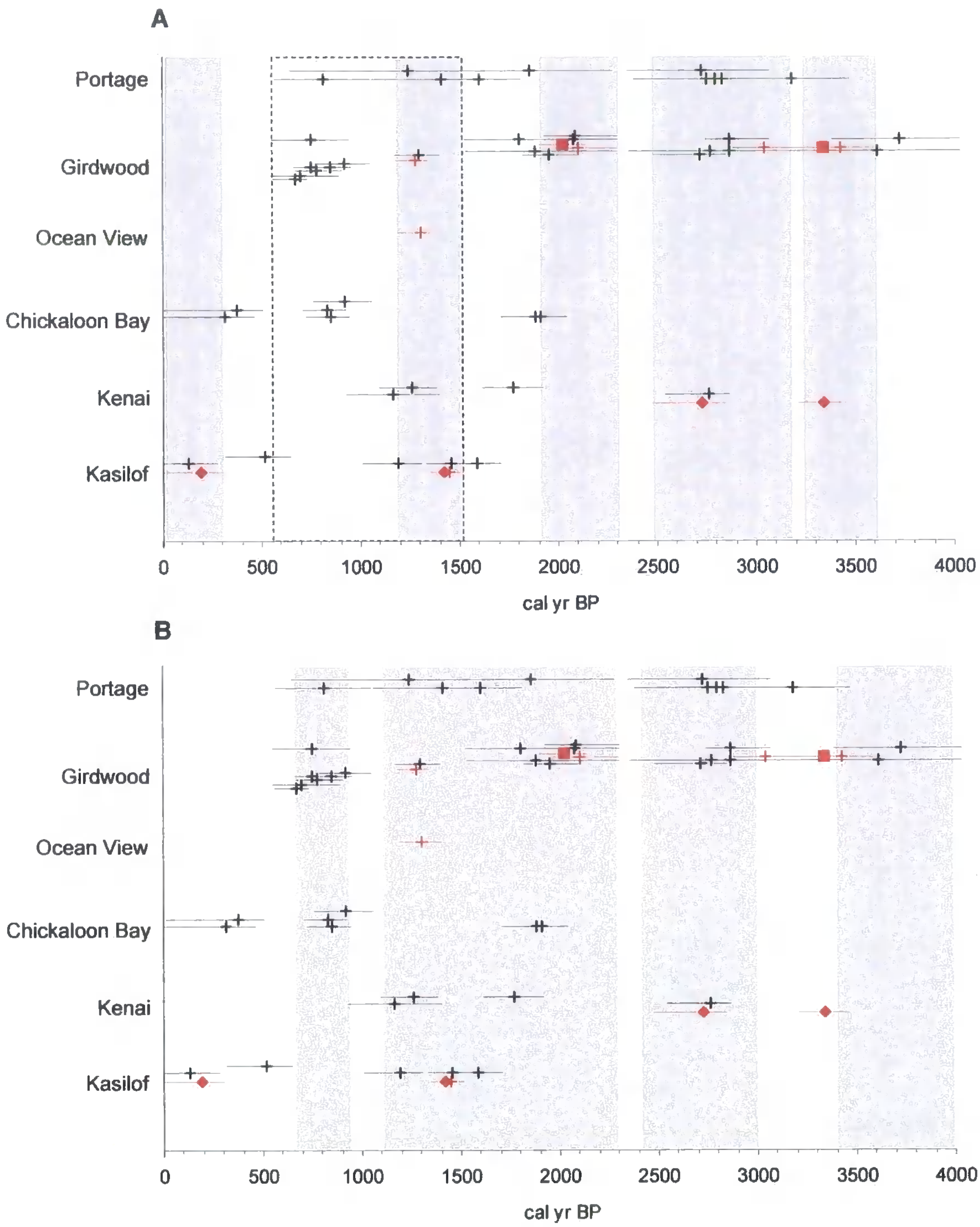

Figure 8.4

Radiocarbon dates from sites around the Cook Inlet, from this thesis (in red) and elsewhere (see text). Symbols indicate the median age and 95% range. For dates from this study, red vertical lines represent the median age of definite co-seismic events, red diamonds possible co-seismic events and red squares probable non-seismic events (table 8.1). Shaded boxes in **A** show possible pre-1964 co-seismic periods based on radiocarbon dates from this study (table 8.2) and in **B** the 4 main periods of co-seismic submergence suggested by Combellick (1994). For explanation of the dashed box see text

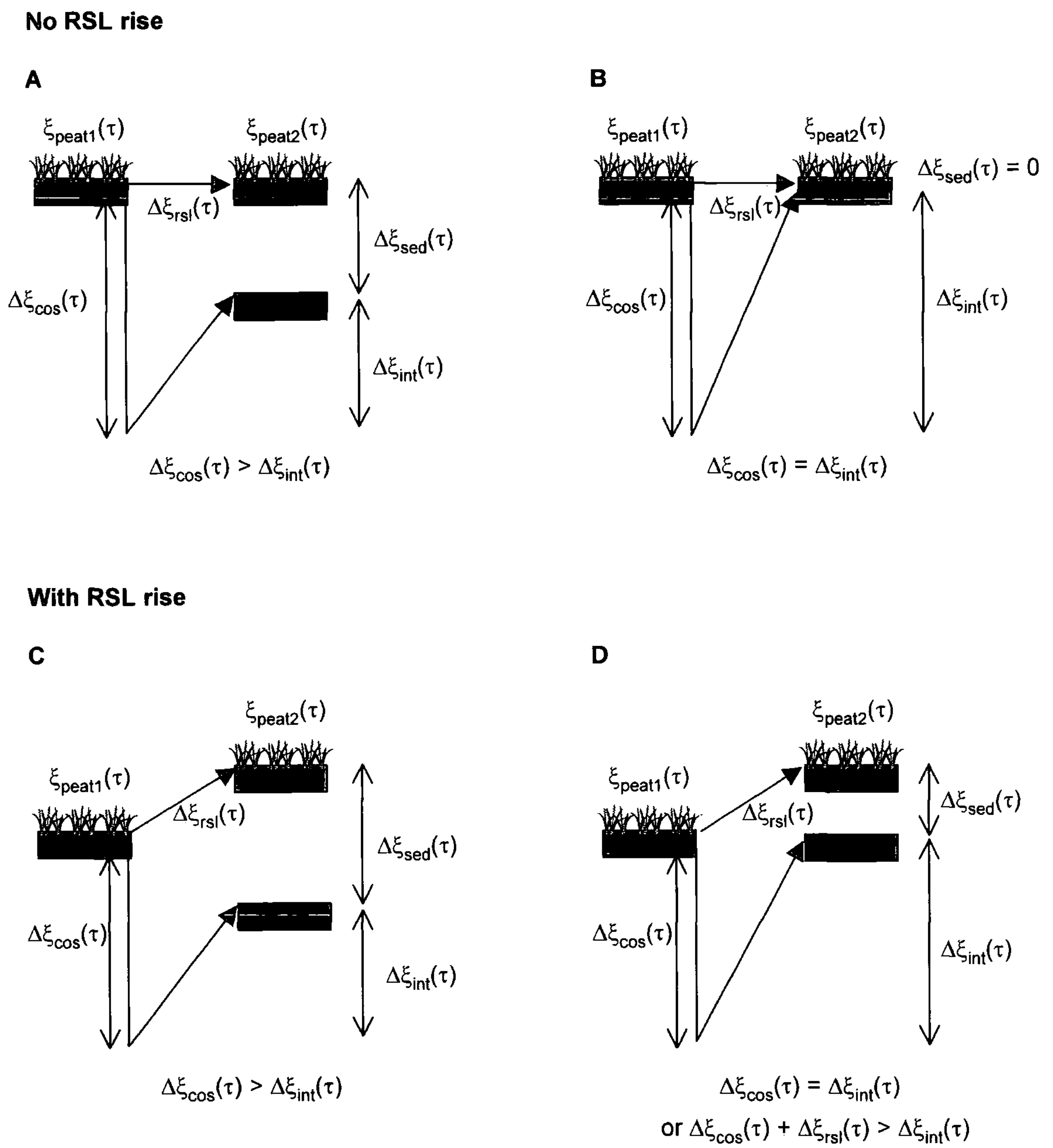

$\Delta\xi_{int}(\tau)$ = post- and inter-seismic uplift

$\Delta\xi_{rsl}(\tau)$ = non-seismic sea-level change over the time period in question

$\Delta\xi_{cos}(\tau)$ = co-seismic submergence accompanying an earthquake

$\Delta\xi_{sed}(\tau)$ = sedimentation between the tops of two peat layers

$\xi_{peat1}(\tau)$ = formation height of the top of the first buried peat

$\xi_{peat2}(\tau)$ = formation height of the top of the second buried peat

Figure 8.5

Schematic models of co-seismic submergence, post- and inter-seismic uplift, sediment accumulation and marsh peat burial with no background relative sea-level rise (**A** and **B**) and with background relative sea-level rise (**C** and **D**)

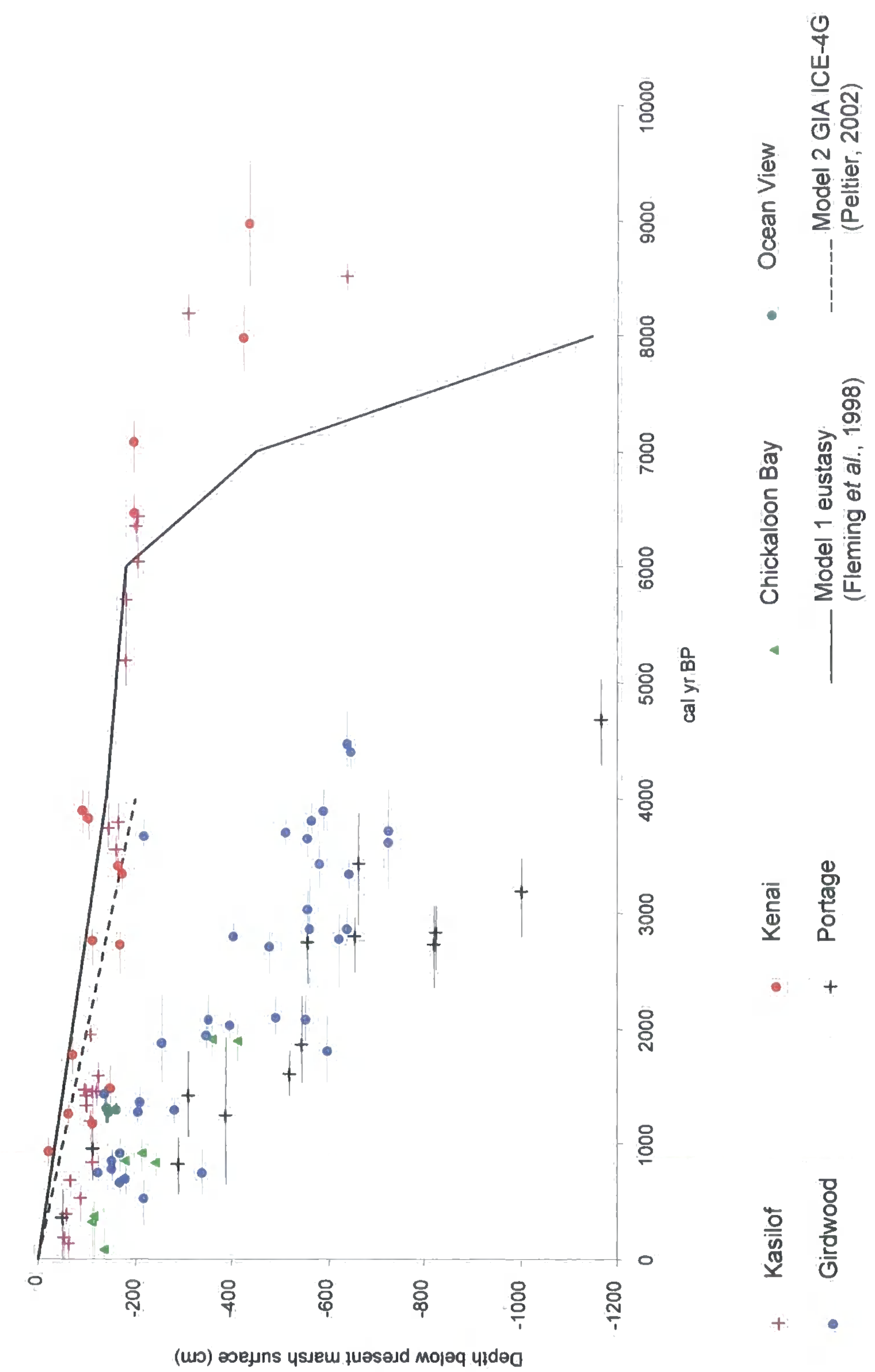

Figure 8.6

Relationship between age of peat layers and depth below present marsh surface at different sites around the Cook Inlet compared to eustatic and GIA models